Spektroskopia gamma na wiązce

Paweł J. Napiorkowski

Plan

- Terminologia
- Eksperyment w fizyce jądrowej
- Reakcje jądrowe
- Stany wzbudzone w jądrach atomowych - schemat poziomów
- Czasy życia stanów jądrowych - struktura jądra atomowego
- Wzbudzenia kulombowskie - mikroskop jądrowy

Terminologia

Terminologia

- **Spektroskopia**

Terminologia

- **Spektroskopia**

  ➡nauka o powstawaniu i interpretacji widm powstających w wyniku oddziaływań wszelkich rodzajów promieniowania na materię (*Wikipedia*)

Terminologia

- **Spektroskopia**

  ➡nauka o powstawaniu i interpretacji widm powstających w wyniku oddziaływań wszelkich rodzajów promieniowania na materię (*Wikipedia*)

  ➡study of the absorption and emission of light and other radiation by matter, as related to the dependence of these processes on the wavelength of the radiation (*Brittanica*)

Terminologia

- **Spektroskopia**

  ➡nauka o powstawaniu i interpretacji widm powstających w wyniku oddziaływań wszelkich rodzajów promieniowania na materię (*Wikipedia*)

  ➡study of the absorption and emission of light and other radiation by matter, as related to the dependence of these processes on the wavelength of the radiation (*Brittanica*)

  ➡to dziedzina nauki, która obejmuje metody badania materii przy wykorzystaniu zjawiska promieniowania

Terminologia

- **Spektroskopia**

  ➡nauka o powstawaniu i interpretacji widm powstających w wyniku oddziaływań wszelkich rodzajów promieniowania na materię (*Wikipedia*)

  ➡study of the absorption and emission of light and other radiation by matter, as related to the dependence of these processes on the wavelength of the radiation (*Brittanica*)

  ➡to dziedzina nauki, która obejmuje metody badania materii przy wykorzystaniu zjawiska promieniowania

- **Widmo**

Terminologia

- **Spektroskopia**

  ➡nauka o powstawaniu i interpretacji widm powstających w wyniku oddziaływań wszelkich rodzajów promieniowania na materię (*Wikipedia*)

  ➡study of the absorption and emission of light and other radiation by matter, as related to the dependence of these processes on the wavelength of the radiation (*Brittanica*)

  ➡to dziedzina nauki, która obejmuje metody badania materii przy wykorzystaniu zjawiska promieniowania

- **Widmo**

  ➡zarejestrowany obraz promieniowania rozłożonego na poszczególne częstości, długości fal lub energie (*Wikipedia*).

Terminologii c.d.

- **Spektroskopia gamma**

  ➡sztuka badania jąder atomowych przez interpretację liczby i energii kwantów gamma (fotonów) emitowanych przez nie.

- **Na wiązce (on-line)**

  ➡bezpośrednia obserwacja procesów wywołanych przez zainicjowaną reakcję jądrową

  ➡w odróżnieniu od spektroskopii off-line - badanie promieniowania będącego następstwem procesów zachodzących w jądrze atomowym

Eksperyment w fizyce jądrowej

Eksperyment w fizyce jądrowej

- Pomiar impulsu elektrycznego:

Eksperyment w fizyce jądrowej

- Pomiar impulsu elektrycznego:

  ➡amplituda

Eksperyment w fizyce jądrowej

- Pomiar impulsu elektrycznego:
  - ➡amplituda
  - ➡przebieg w czasie - Pulse Shape Analysis

Eksperyment w fizyce jądrowej

- Pomiar impulsu elektrycznego:
  - ➡amplituda
  - ➡przebieg w czasie - Pulse Shape Analysis
- Oddziaływanie kwantu gamma z materią w detektorze:

Eksperyment w fizyce jądrowej

- Pomiar impulsu elektrycznego:
  - ➡amplituda
  - ➡przebieg w czasie - Pulse Shape Analysis
- Oddziaływanie kwantu gamma z materią w detektorze:
  - ➡Energia kwantu gamma

Eksperyment w fizyce jądrowej

- Pomiar impulsu elektrycznego:
  - ➡amplituda
  - ➡przebieg w czasie - Pulse Shape Analysis
- Oddziaływanie kwantu gamma z materią w detektorze:
  - ➡Energia kwantu gamma
  - ➡Czas oddziaływania (w sensie t_0 a nie Δt)

Eksperyment w fizyce jądrowej

- Pomiar impulsu elektrycznego:
  - ➡amplituda
  - ➡przebieg w czasie - Pulse Shape Analysis
- Oddziaływanie kwantu gamma z materią w detektorze:
  - ➡Energia kwantu gamma
  - ➡Czas oddziaływania (w sensie t_0 a nie Δt)
  - ➡Miejsce oddziaływania (PSA)

Eksperyment w fizyce jądrowej

- Pomiar impulsu elektrycznego:
  - ➡amplituda
  - ➡przebieg w czasie - Pulse Shape Analysis
- Oddziaływanie kwantu gamma z materią w detektorze:
  - ➡Energia kwantu gamma
  - ➡Czas oddziaływania (w sensie t_0 a nie Δt)
  - ➡Miejsce oddziaływania (PSA)
- Stworzenie specyficznych warunków emisji i rejestracji kwantów gamma.

Reakcje jądrowe

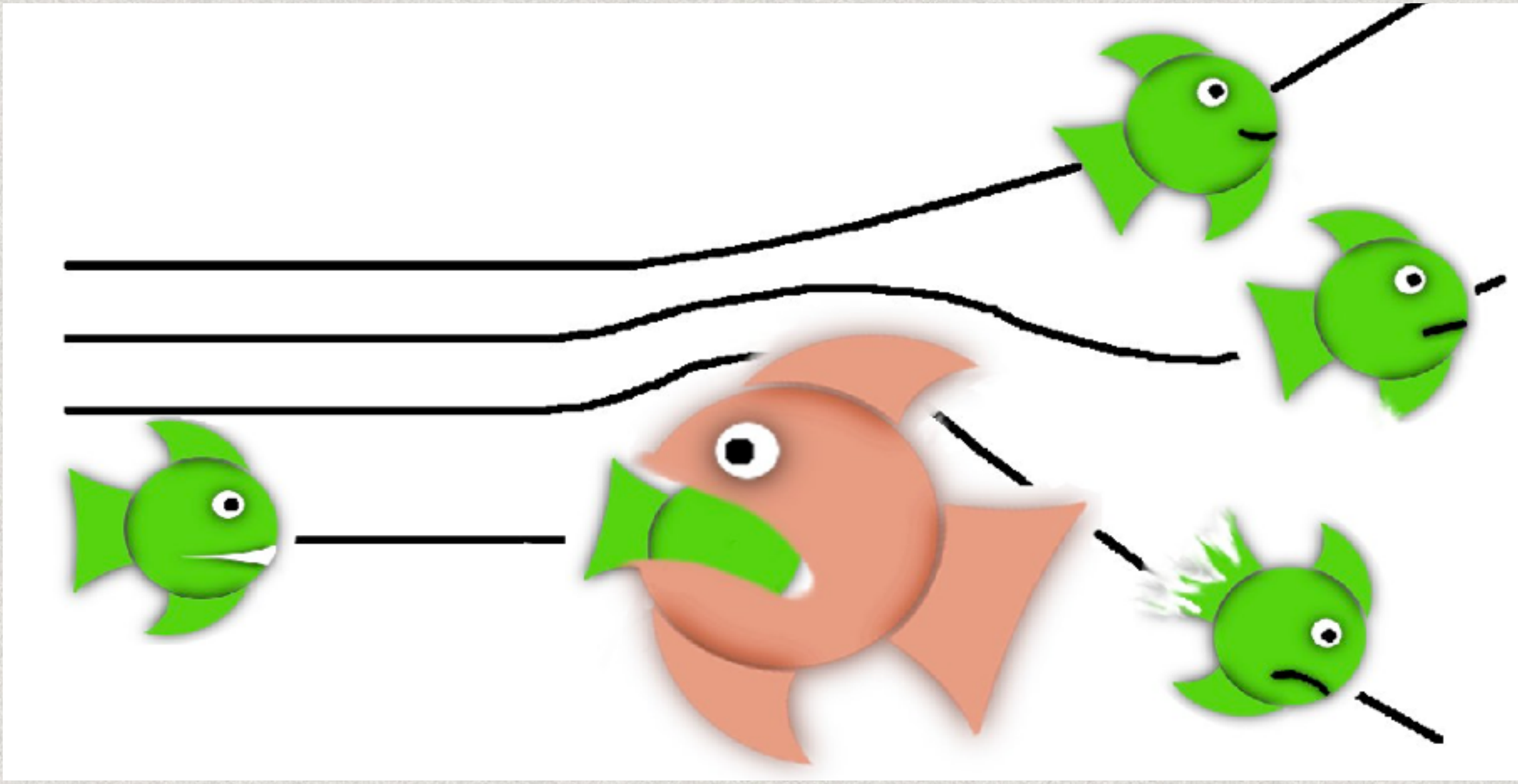

Identyfikacja jąder po energii stanów wzbudzonych

Wiązka
^{20}Ne (140, 150 MeV)
Tarcza
^{122}Sn
Jądro złożone (CN)
^{142}Nd

J.MIERZEJEWSKI, EGAN 2011

Identyfikacja jąder po energii stanów wzbudzonych

Wiązka
^{20}Ne (140, 150 MeV)
Tarcza
^{122}Sn
Jądro złożone (CN)
^{142}Nd

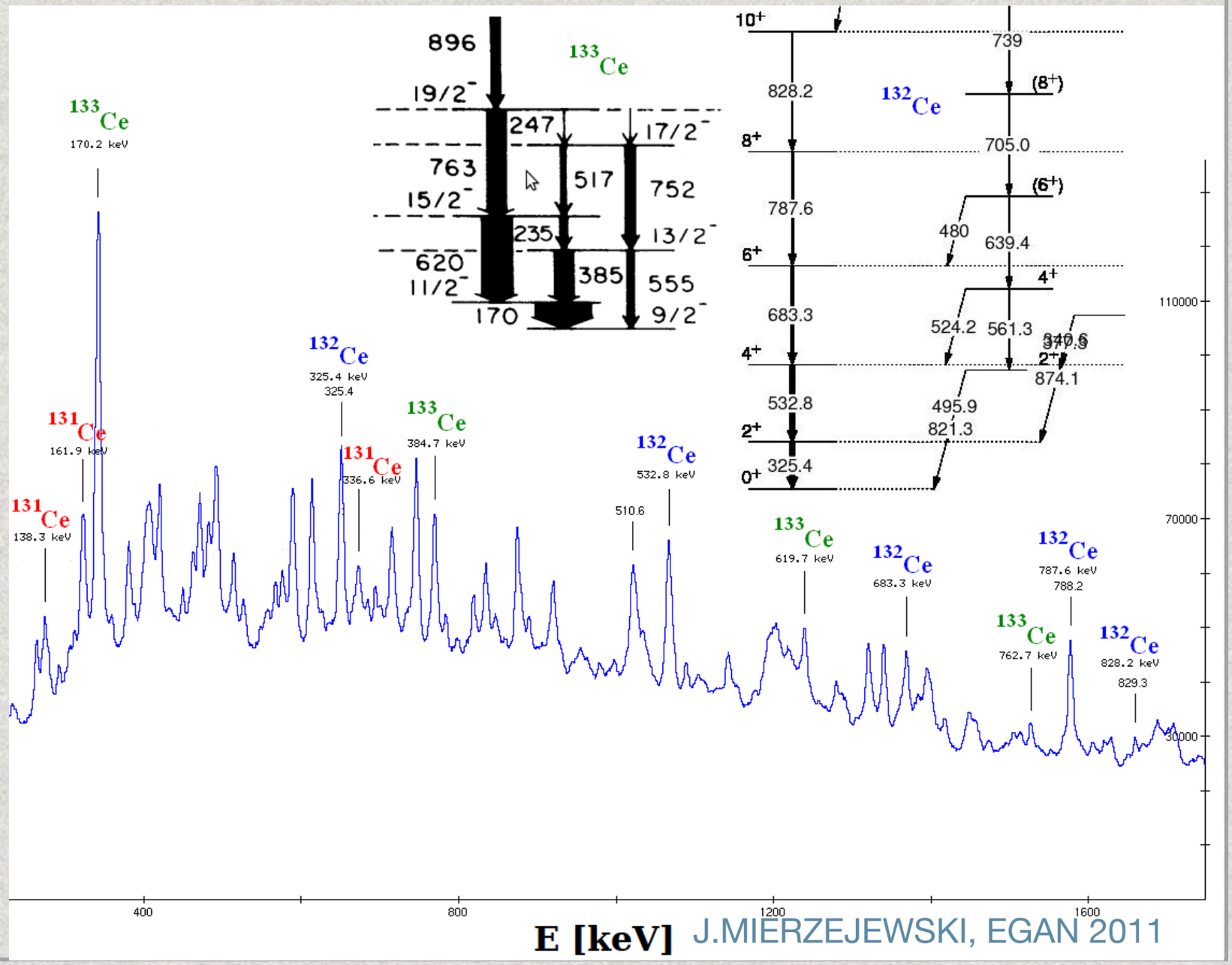

J.MIERZEJEWSKI, EGAN 2011

Identyfikacja jąder po energii stanów wzbudzonych

Wiązka
^{20}Ne (140, 150 MeV)
Tarcza
^{122}Sn
Jądro złożone (CN)
^{142}Nd

Reakcje:

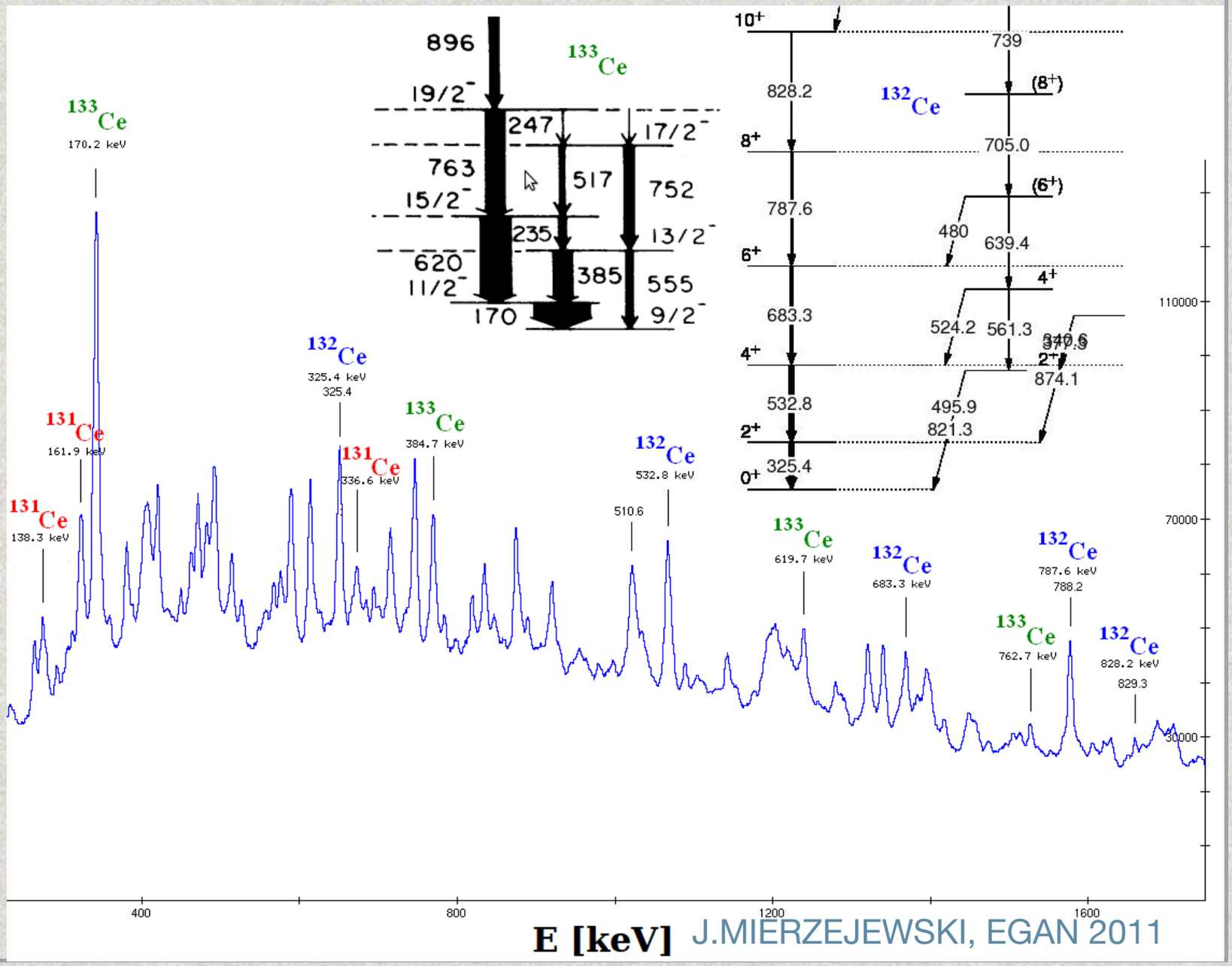

J.MIERZEJEWSKI, EGAN 2011

Identyfikacja jąder po energii stanów wzbudzonych

Wiązka
^{20}Ne (140, 150 MeV)
Tarcza
^{122}Sn
Jądro złożone (CN)
^{142}Nd

Reakcje:
Z: 50+10=2(α)+58(Ce)

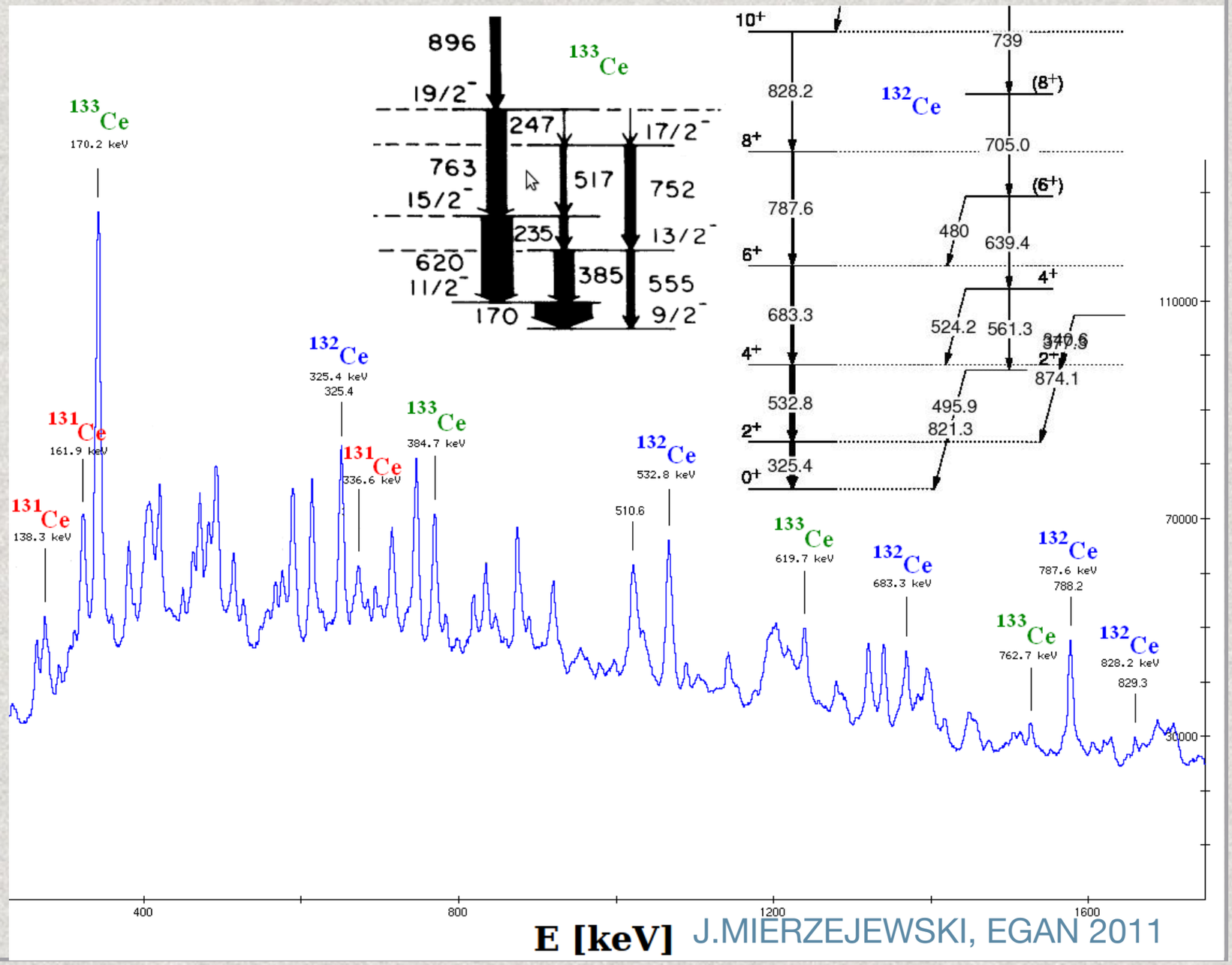

J.MIERZEJEWSKI, EGAN 2011

Identyfikacja jąder po energii stanów wzbudzonych

Wiązka
^{20}Ne (140, 150 MeV)
Tarcza
^{122}Sn
Jądro złożone (CN)
^{142}Nd

Reakcje:
Z: 50+10=2(α)+58(Ce)
A: 122+20=9+133

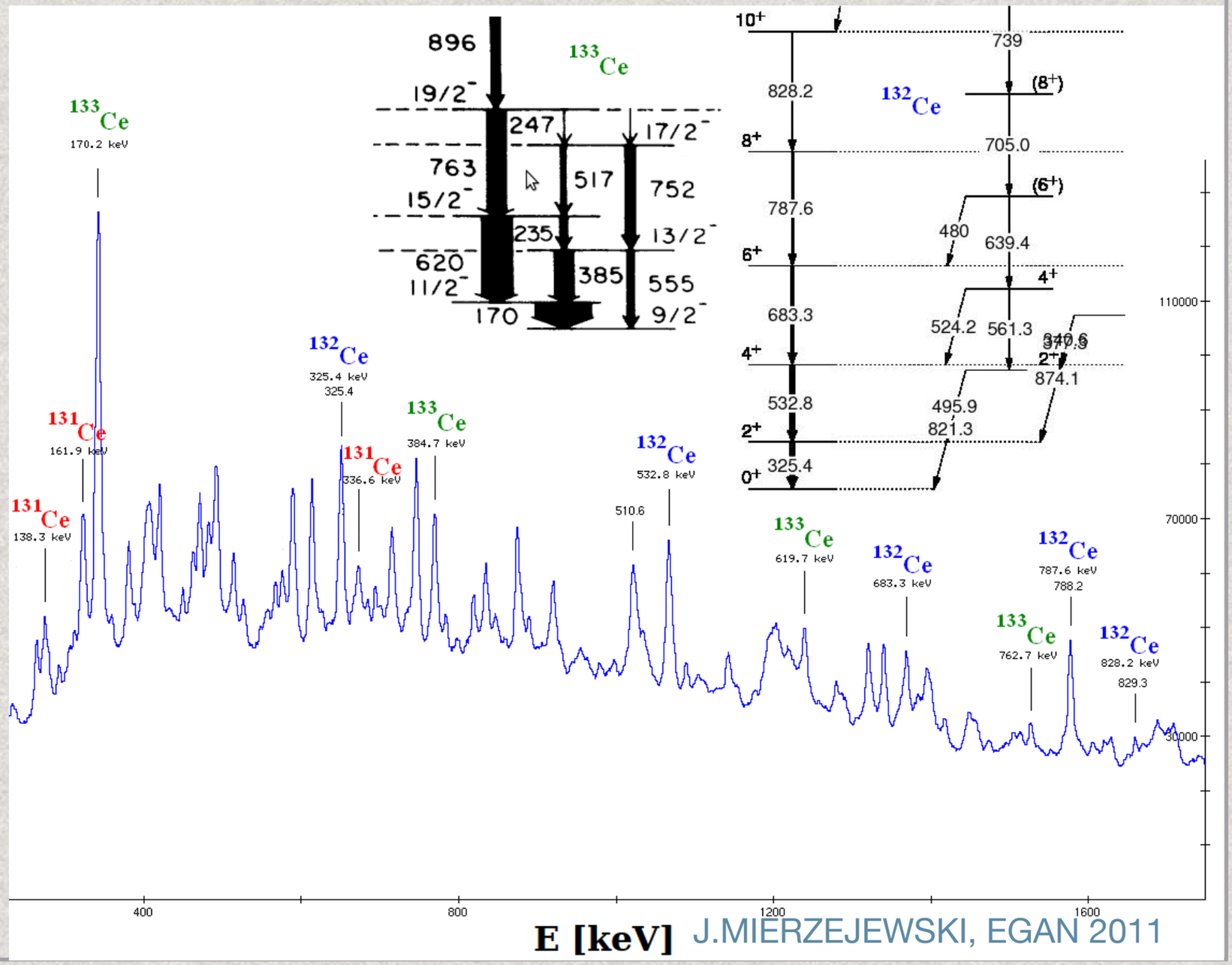

J.MIERZEJEWSKI, EGAN 2011

Identyfikacja jąder po energii stanów wzbudzonych

Wiązka
^{20}Ne (140, 150 MeV)
Tarcza
^{122}Sn
Jądro złożone (CN)
^{142}Nd

Reakcje:
Z: 50+10=2(α)+58(Ce)
A: 122+20=9+133

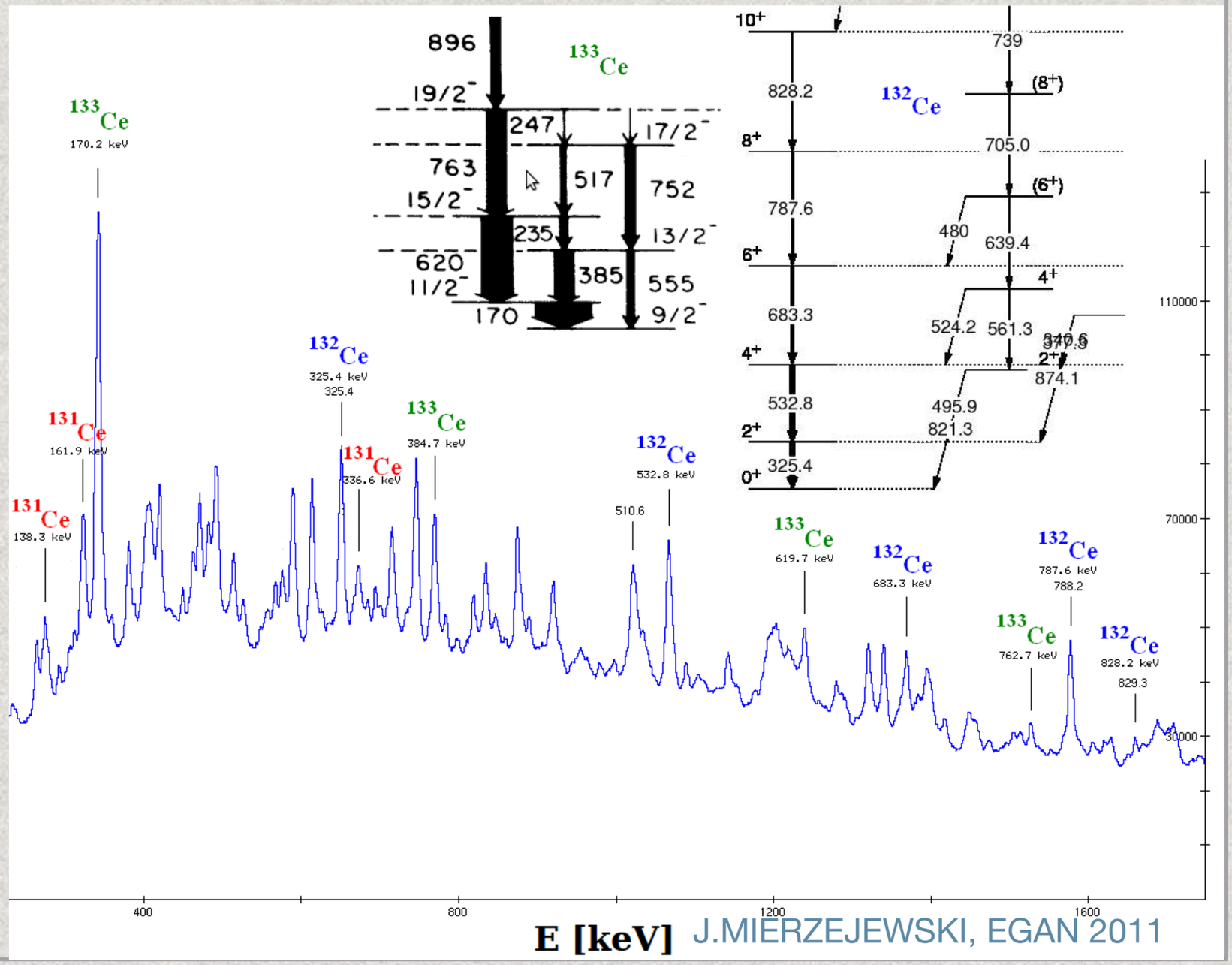

J.MIERZEJEWSKI, EGAN 2011

Identyfikacja jąder po energii stanów wzbudzonych

Wiązka
^{20}Ne (140, 150 MeV)
Tarcza
^{122}Sn
Jądro złożone (CN)
^{142}Nd

Reakcje:
Z: 50+10=2(α)+58(Ce)
A: 122+20=9+133

^{122}Sn(^{20}Ne,α5n) ^{133}Ce

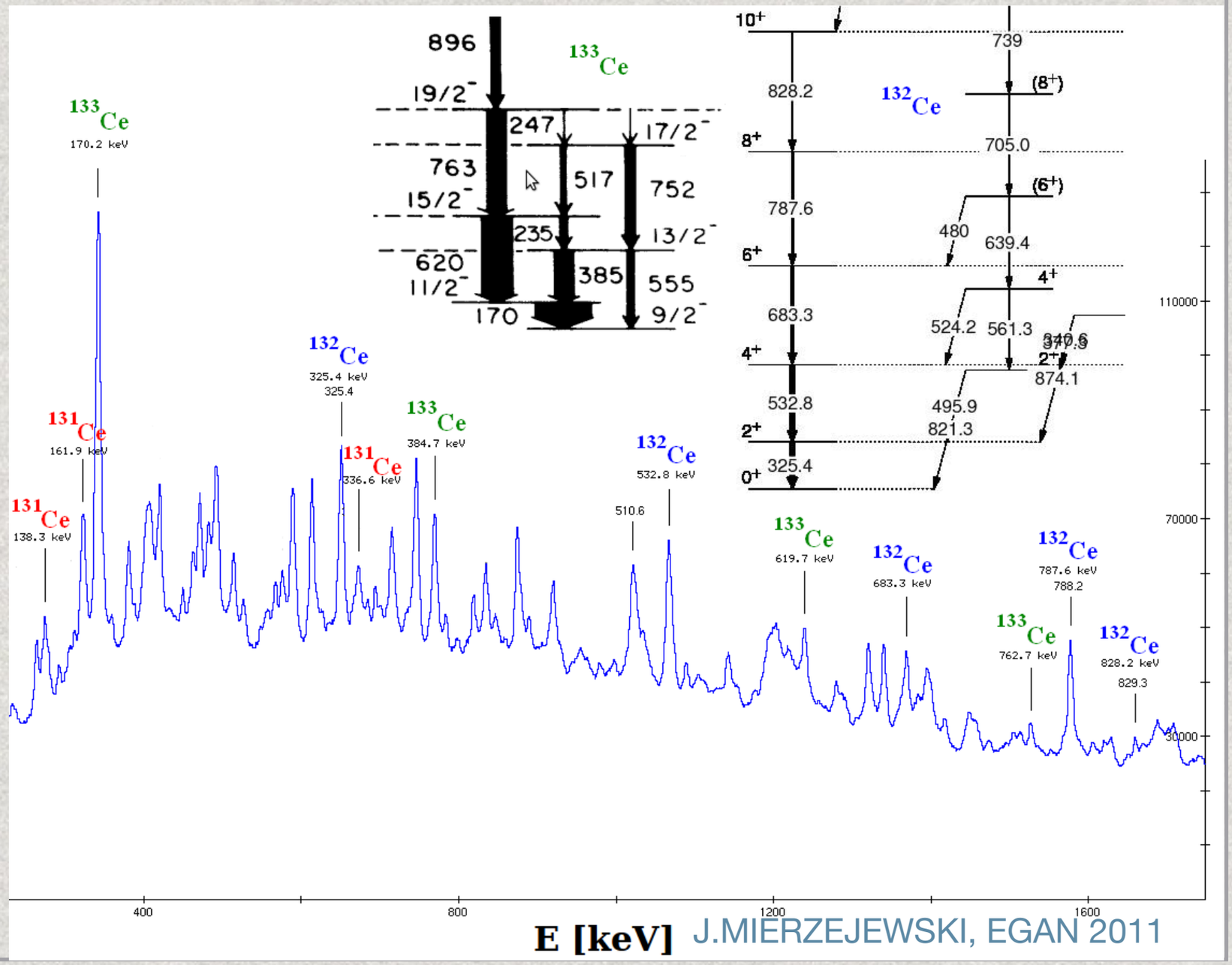

J.MIERZEJEWSKI, EGAN 2011

Identyfikacja jąder po energii stanów wzbudzonych

Wiązka
^{20}Ne (140, 150 MeV)
Tarcza
^{122}Sn
Jądro złożone (CN)
^{142}Nd

Reakcje:
Z: 50+10=2(α)+58(Ce)
A: 122+20=9+133

^{122}Sn(^{20}Ne,α5n) ^{133}Ce
^{122}Sn(^{20}Ne,α6n) ^{132}Ce

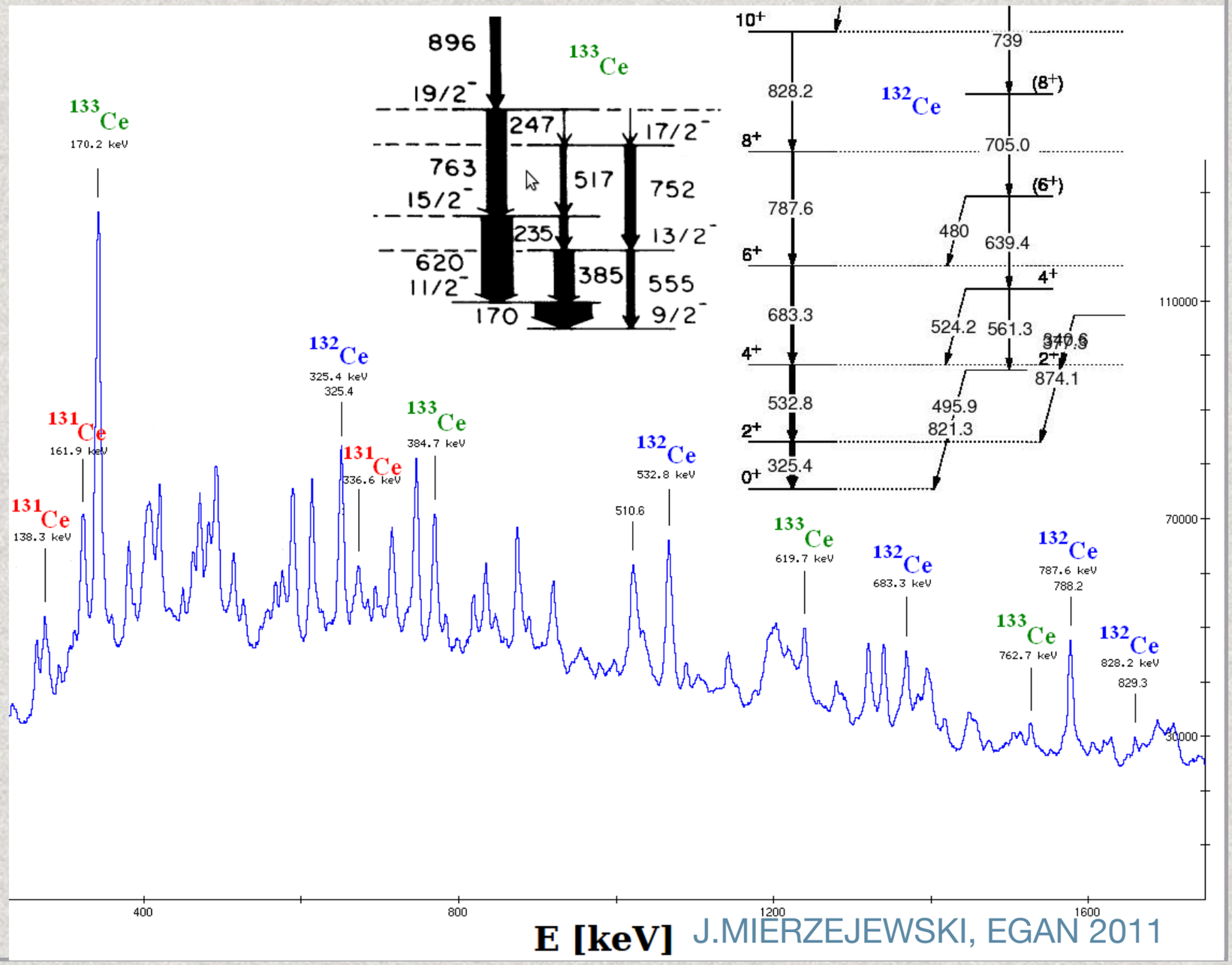

J.MIERZEJEWSKI, EGAN 2011

Stany wzbudzone jąder atomowych

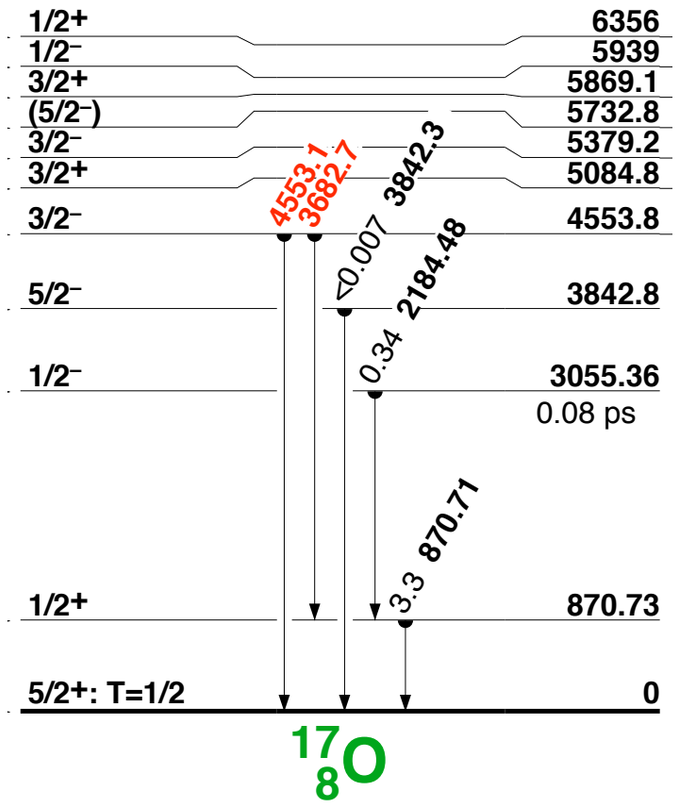

Stany wzbudzone jąder atomowych

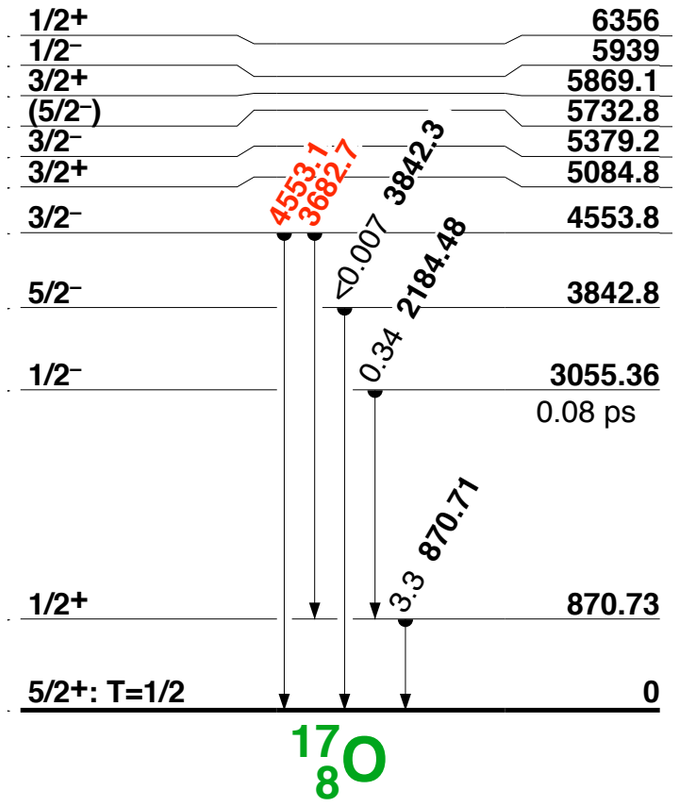

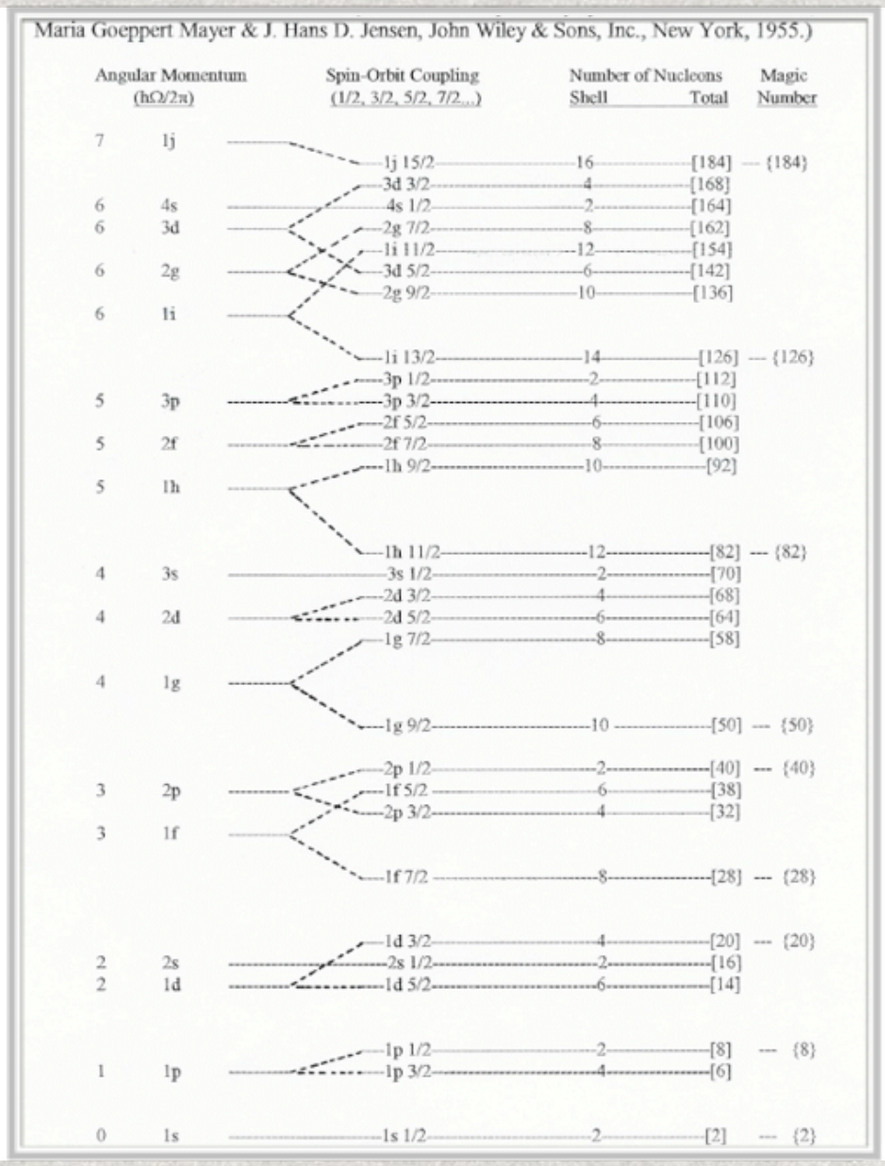

Stany wzbudzone jąder atomowych

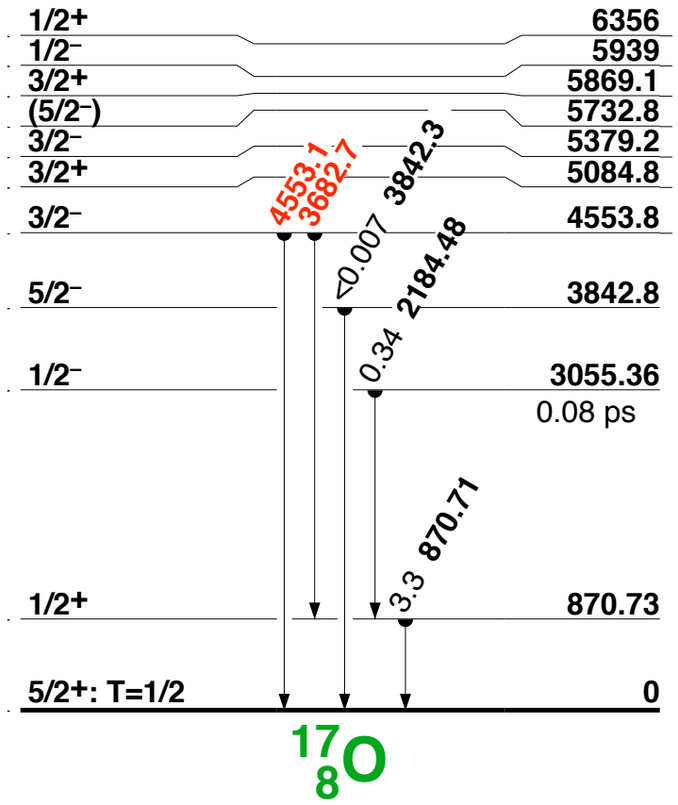

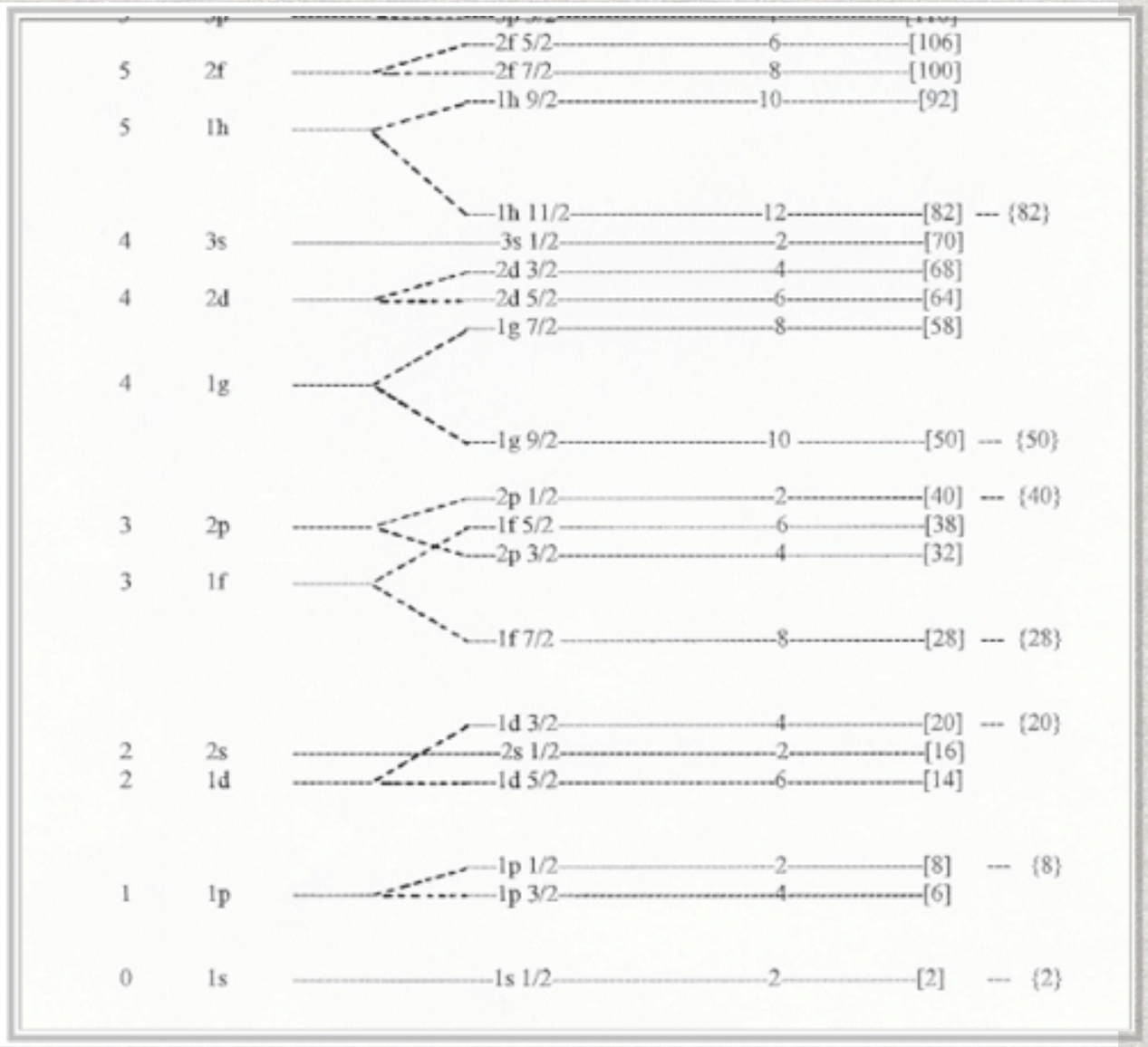

Stany wzbudzone jąder atomowych

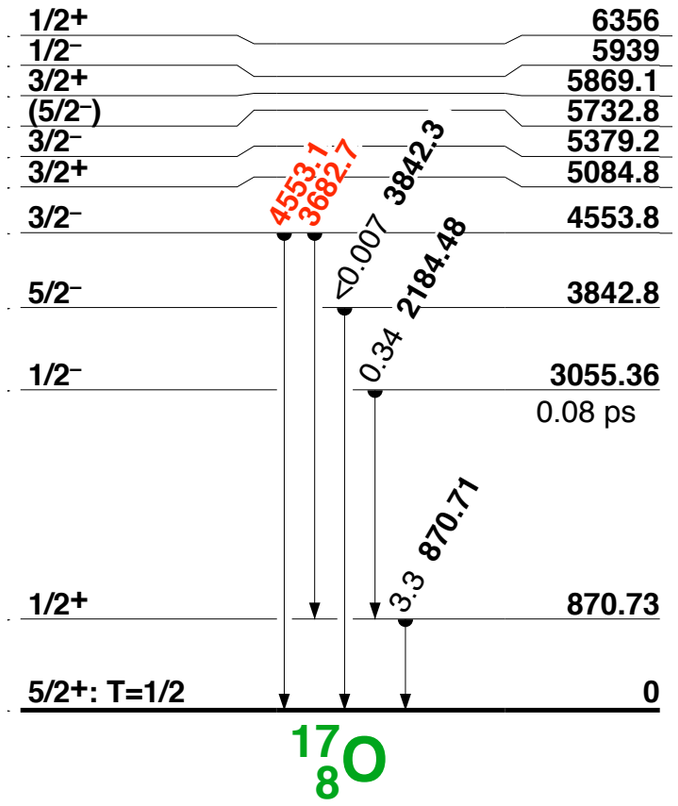

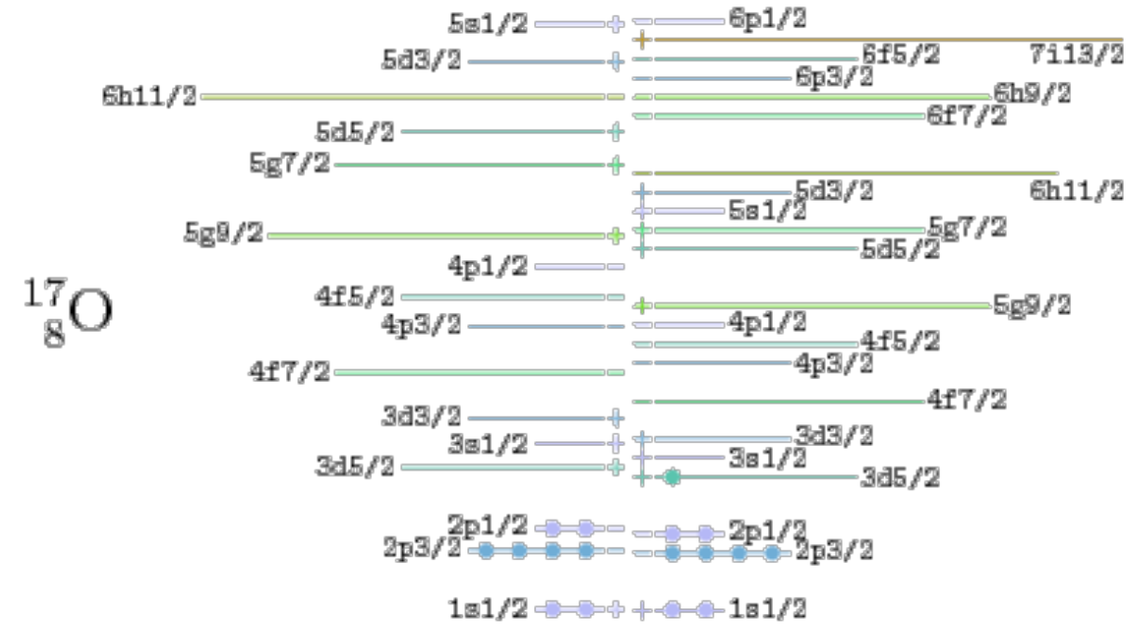

Stany wzbudzone jednocząstkowe

stany „jednocząstkowe” – związane z ruchem jednego nukleonu;
widoczne zwłaszcza w obszarach, gdzie liczby neutronów i protonów są bliskie liczbom magicznym
dają się opisać modelem powłokowym

Widmo i schemat poziomów ^{178}Hf

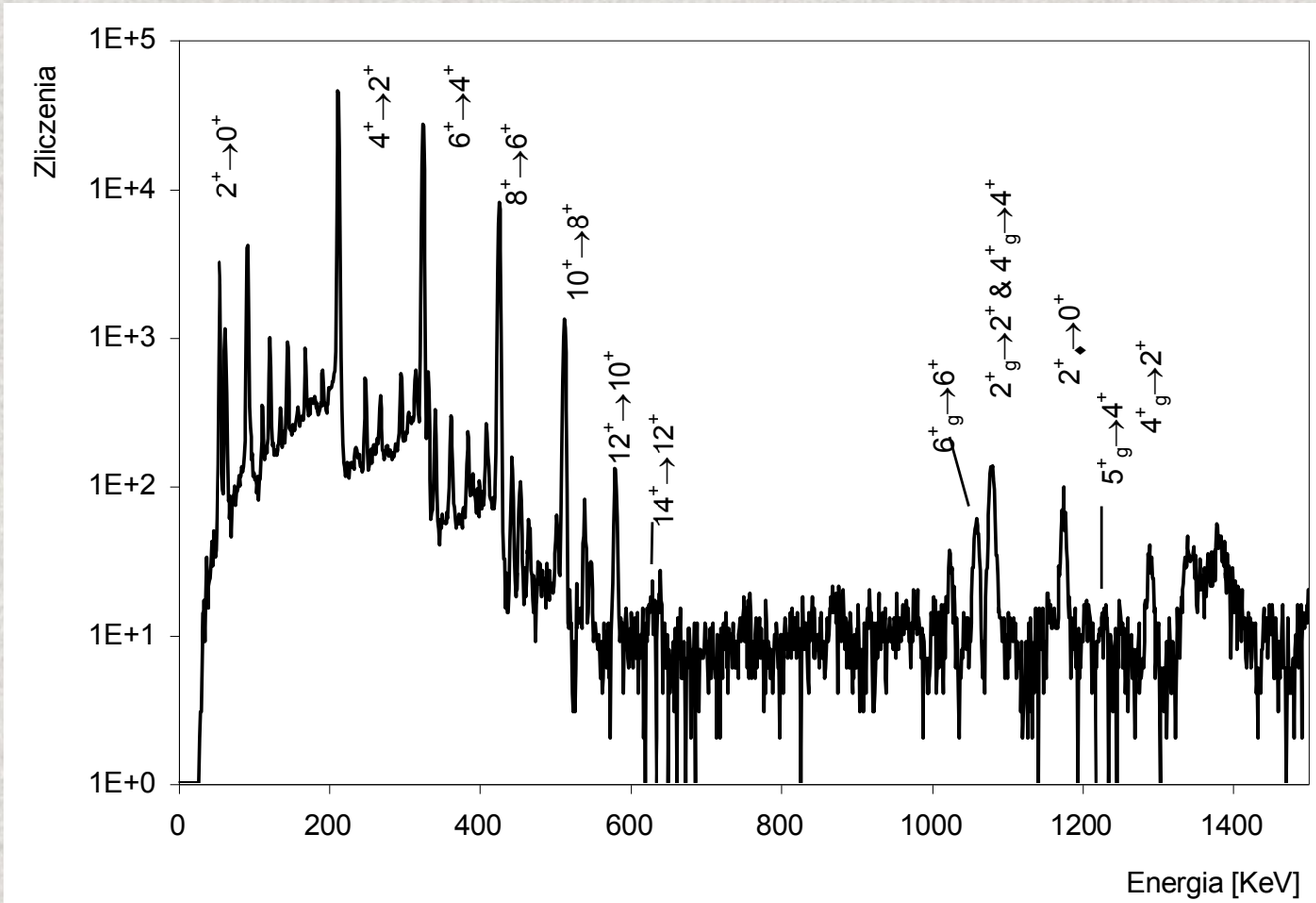

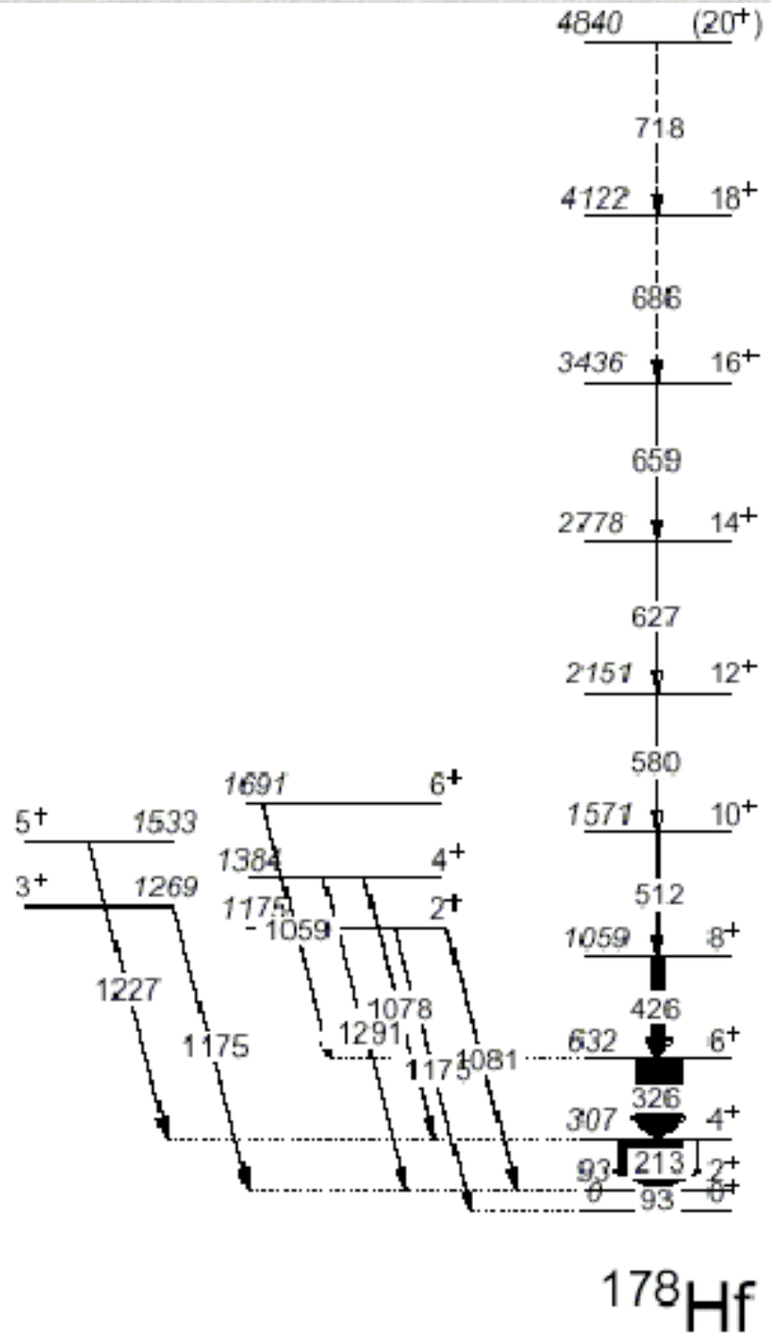

Widmo i schemat poziomów ^{178}Hf

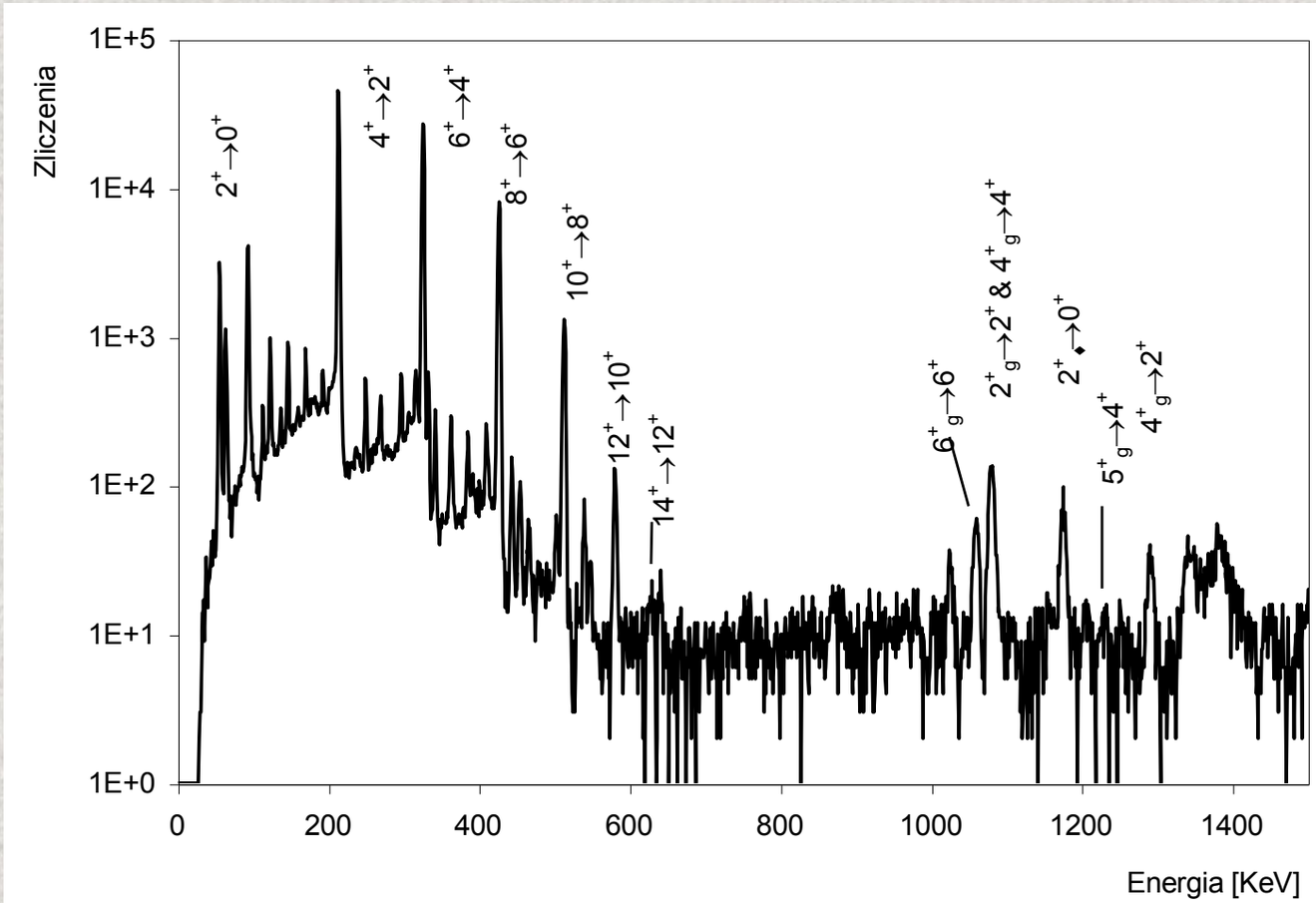

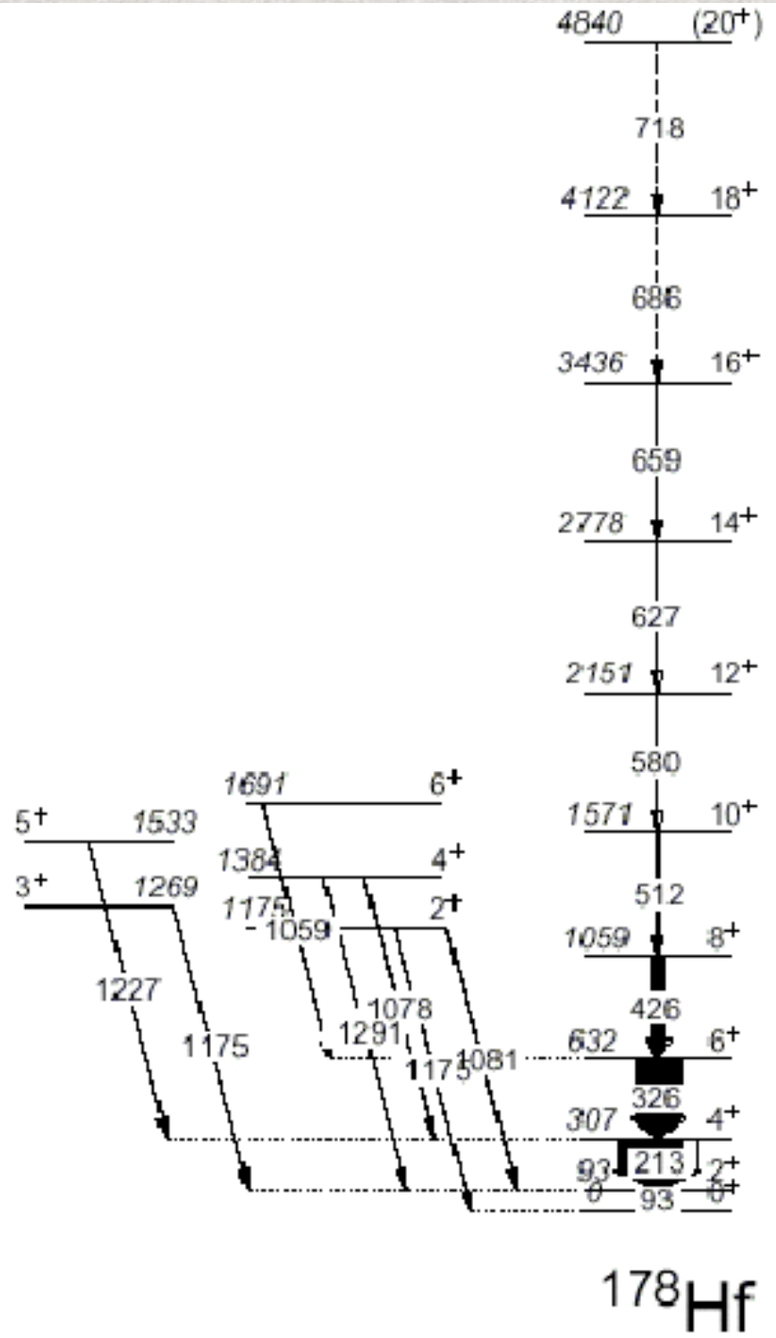

RUCH KOLEKTYWNY
ROTACJA JĄDRA ATOMOWEGO

Stany kolektywne

- stany kolektywne – związane z ruchem całego jądra powszechne w obszarach, gdzie liczba protonów i/lub neutronów jest daleka od liczb magicznych, a jądra atomowe mają kształt zdeformowany.

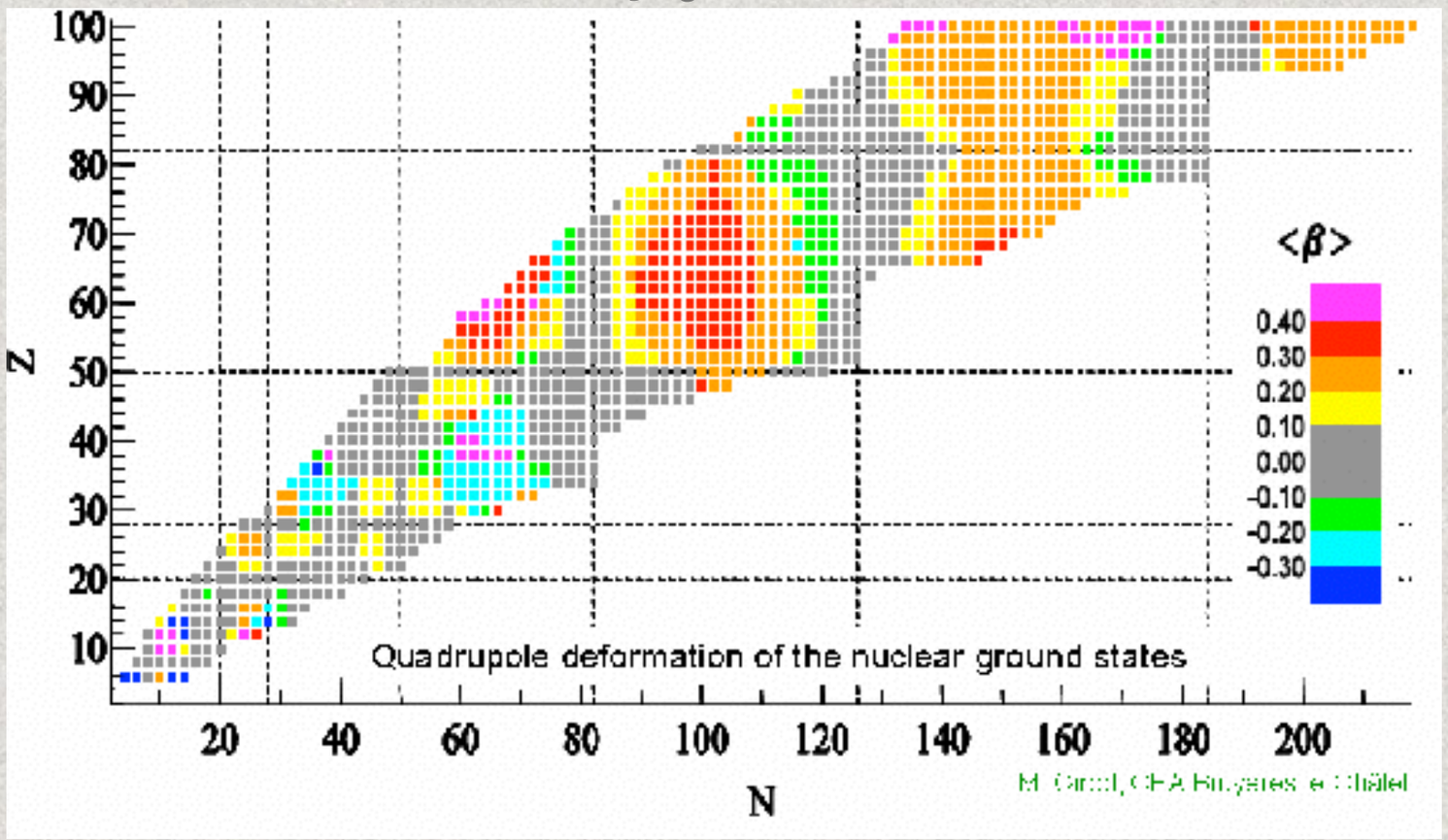

Kształty jąder atomowych

- opis kształtu $R(\theta,\phi)=R_0(1+\sum \beta_{\lambda\mu} Y_{\lambda\mu}(\theta,\phi))$
- istotne kształty:
  - β_2 deformacja kwadrupolowa (≈ elipsoida trójosiowa)
  - β_3 deformacja oktupolowa (≈ gruszka)
- najczęściej występuje deformacja kwadrupolowa

$$R(\theta,\phi)=R_0(1+\sum \alpha_{2\mu} Y_{2\mu}(\theta,\phi))$$

jeśli układ współrzędnych obrócimy zgodnie z kierunkami osi głównych,

to $\alpha_{21} = \alpha_{2-1} = 0$ i $\alpha_{22} = \alpha_{2-2}$

→ dwa parametry do opisu kształtu!

–

$$\alpha_{20}=\beta\cos(3\gamma)$$
$$\alpha_{22}=\frac{1}{\sqrt{2}}\beta\sin(3\gamma)$$

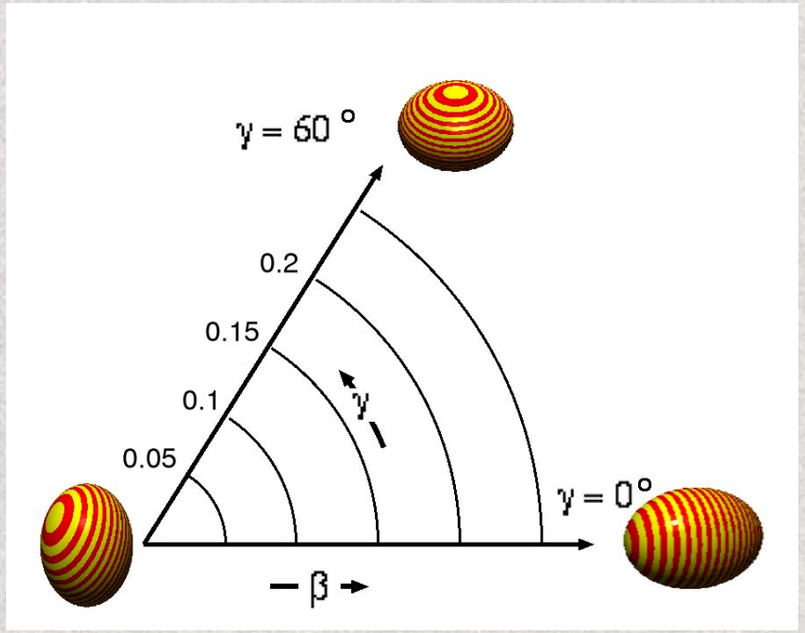

Rotacje jąder atomowych

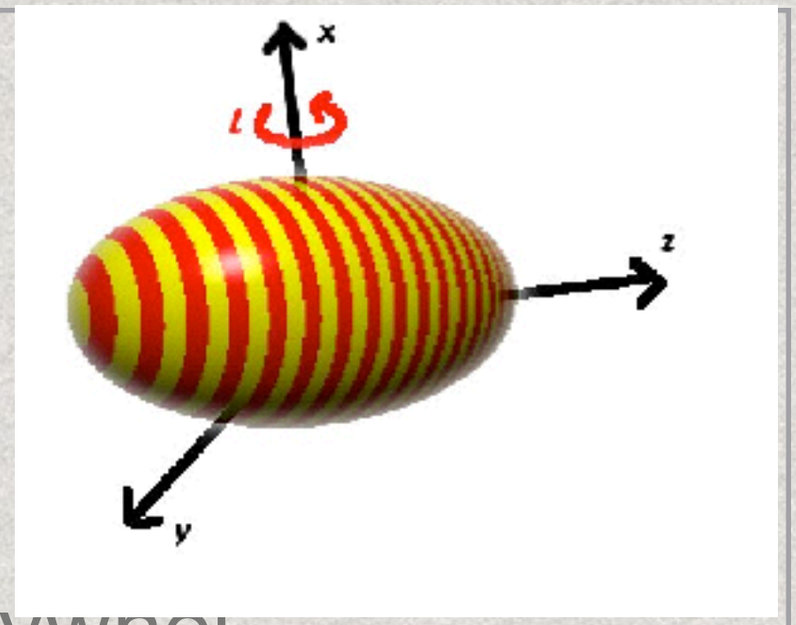

- Klasycznie: energia obrotu bryły sztywnej $E_{rot}=L^2/2J$
- Kwantowo: $L^2 \sim I(I+1)$
  $E_{rot} \sim I(I+1)/2J$
- Charakterystyczny układ poziomów:
  symetria dopuszcza tylko spiny parzyste dla jąder parzysto- parzystych.

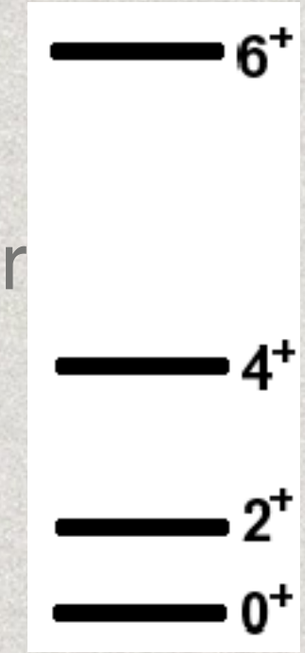

Widmo i schemat poziomów ^{178}Hf

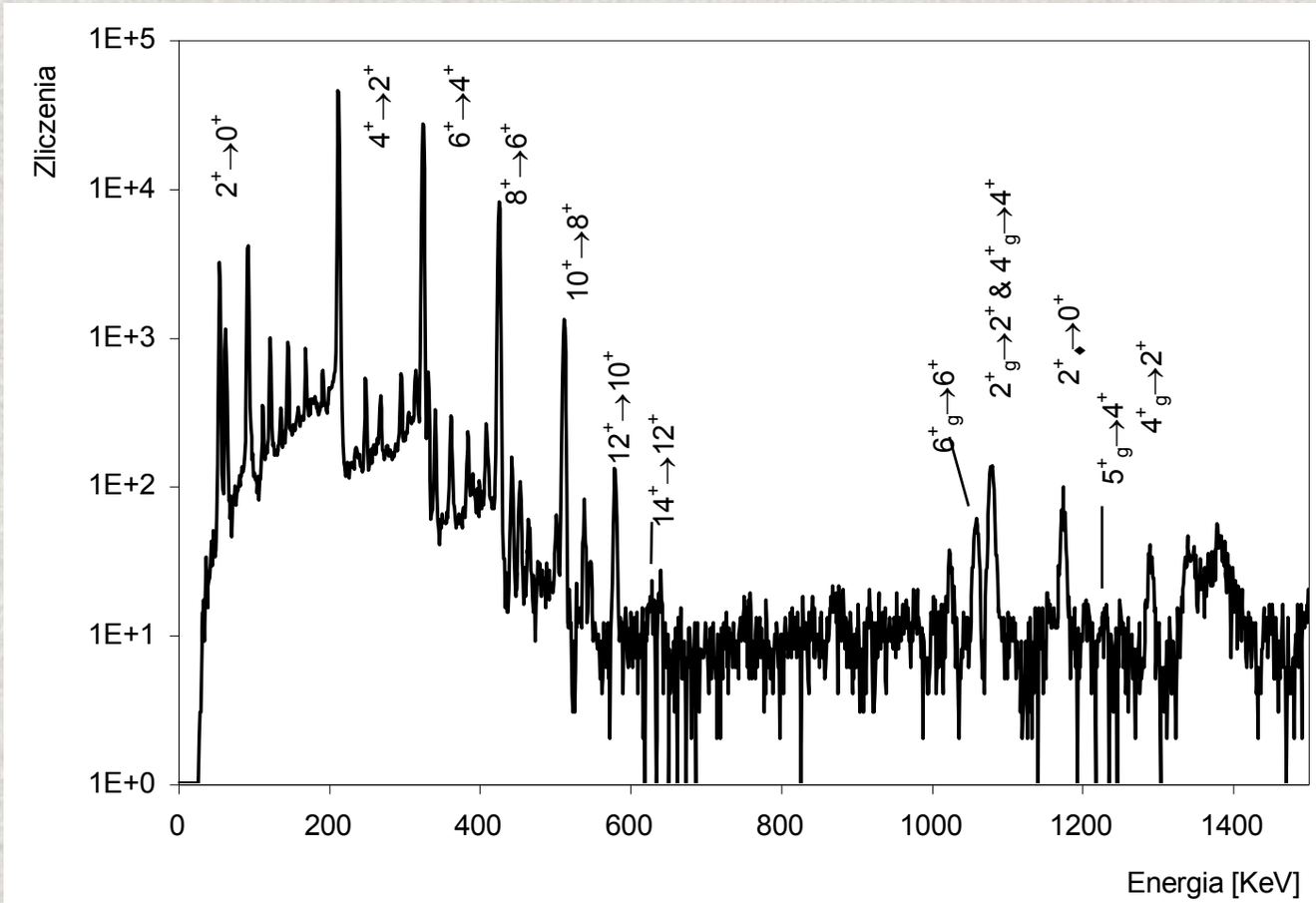

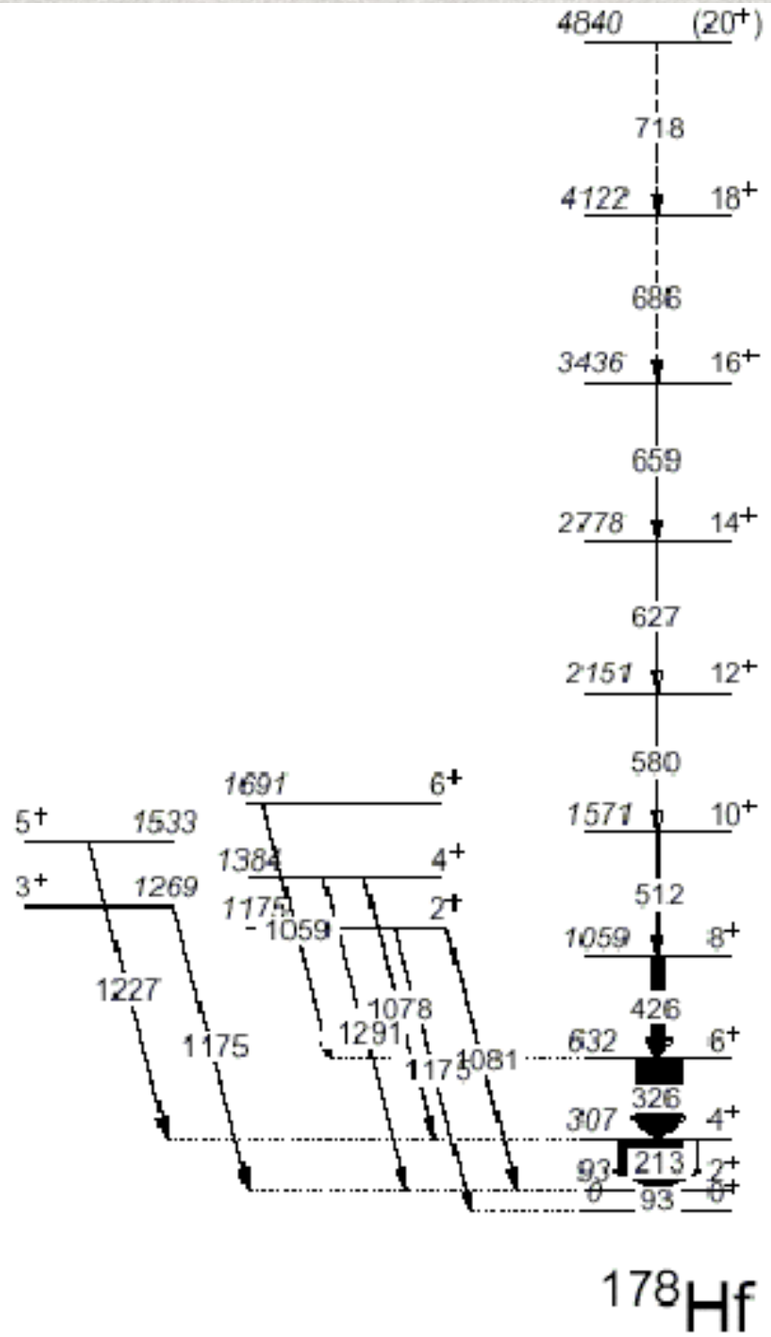

Stany wibracyjne

$$R(\theta,\phi)=R_0(1+\sum \alpha_{2\mu} Y_{2\mu}(\theta,\phi))$$

- parametry $\alpha_{\mu\lambda}$ określają kształt jądra atomowego
- rozważając oscylacje jądra jako drgania kropli cieczy dostajemy równanie oscylatora:

$$H_{osc}=\frac{1}{2}B_\lambda\left|\dot{\alpha_{\lambda\mu}}\right|^2+\frac{1}{2}C_\lambda\left|\alpha_{\lambda\mu}\right|^2$$

którego rozwiązaniem jest szereg stanów odległych o ħω, scharakteryzowanych liczbą fononów N_λ:

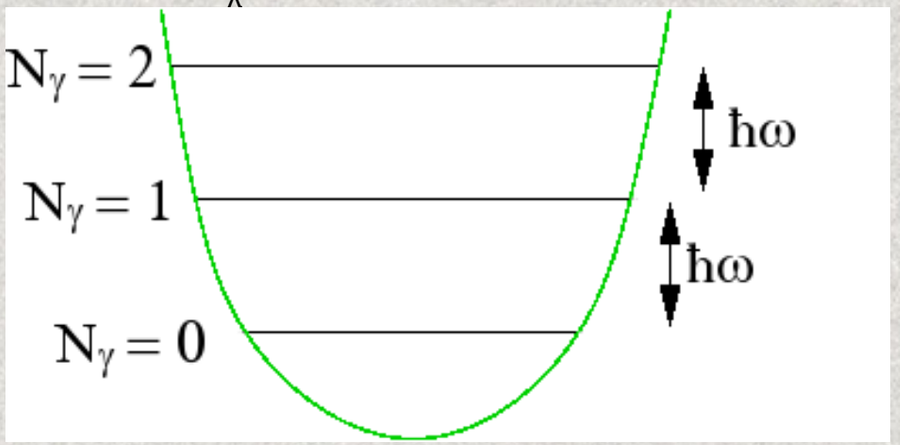

$$\omega=\sqrt{C_\lambda/B_\lambda}$$

energia fononu: ħω, moment pędu: λ
parzystość $(-1)^\lambda$

dla najpopularniejszych drgań kwadrupolowych λ = 2

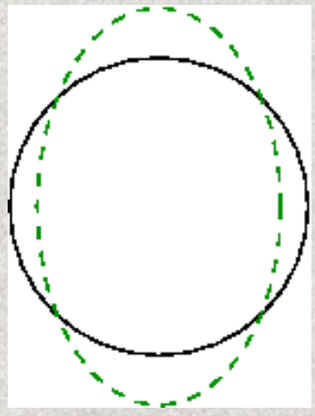

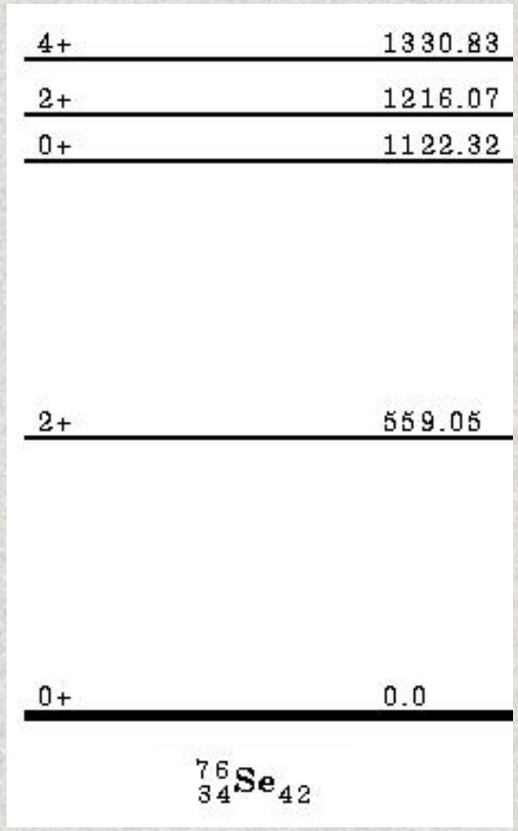

Jednostka Weisskopfa

- Zredukowane prawdopodobieństwo przejścia elektormagneytcznego.

$$B(T\lambda,\ j_1 \rightarrow j_2) \sim 1/\tau$$

- Dla stanów jednocząstkowych

a zredukowane prawdopodobieństwo przejścia dane jest przez

$$B_{sp}(E\lambda; j_1 \rightarrow j_2) = \frac{e^2}{4\pi}(2\lambda+1)\langle j_1\, \tfrac{1}{2}\, \lambda 0 | j_2\, \tfrac{1}{2}\rangle^2 \langle j_2 | r^\lambda | j_1\rangle^2.$$

$< \lambda+½,½,\lambda,0|½,½>^2 = 1/(2\lambda+1)$ $(3/(\lambda+3)\, R^\lambda)^2;\ R = 1.2\, A^{1/3}$

otrzymujemy

$$B_w(E\lambda) = \frac{(1,2)^{2\lambda}}{4\pi}\left(\frac{3}{\lambda+3}\right)^2 A^{2\lambda/3} e^2 (\mathrm{fm})^{2\lambda},$$

$$B_w(M\lambda) = \frac{10}{\pi}(1,2)^{2\lambda-2}\left(\frac{3}{\lambda+3}\right)^2 A^{(2\lambda-2)/3}\left(\frac{e\hbar}{2Mc}\right)^2 (\mathrm{fm})^{2\lambda-2}.$$

- Jednostka Weisskopfa miarą kolektywizmu.
- Typowe wartości B(E2)
  - 1 W.u. - przejście między stanmi jednocząstkowymi
  - 10-50 W.u. - przejścia kolektywne (np. związane z rotacją jądra)

A.Bohr, B.Mottelson, *Struktura jądra atomowego*, tom 1, Warszawa 1975

Pomiary czasów życia stanów jądrowych

- Fast Timing
  bezpośredni pomiar zaniku aktywności (T>100ps) - przy wykorzystaniu szybkich detektorów scyntylacyjnych np. LaBr3

- metody wykorzystujące efekt Dopplera (T>10 fs)
  - Recoil Distance Method (RDM)
    metoda odległości przelotu jąder odrzutu
  - Doppler Shift Attenuation Method (DSAM) – metoda osłabienia przesunięcia Dopplera dla hamujących jąder odrzutu

Fast Timing
Warsztaty międzynarodowe
ŚLCJ 2011

experimental setup

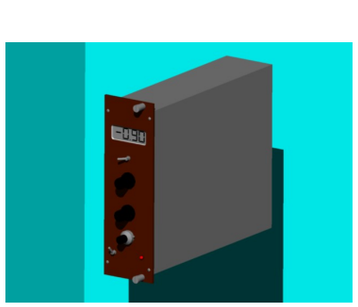

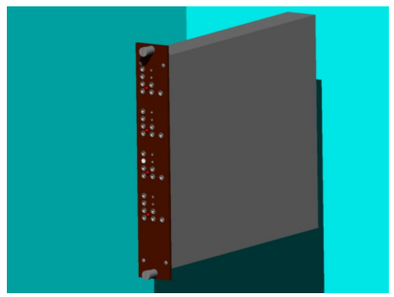

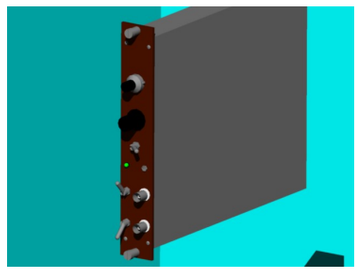

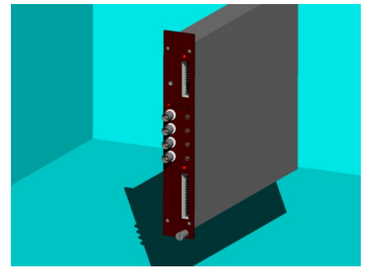

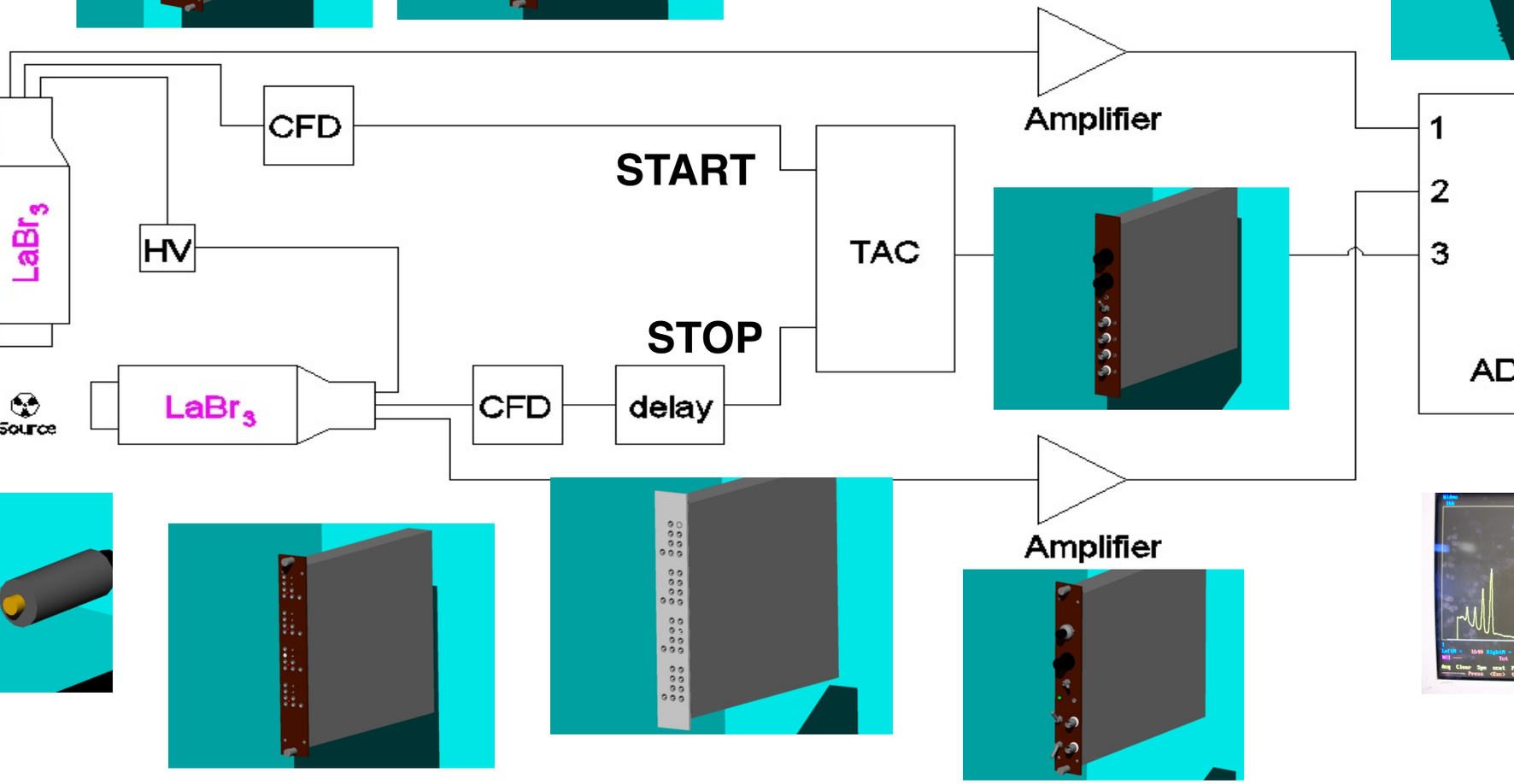

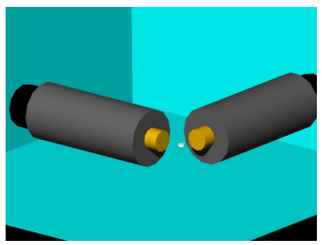

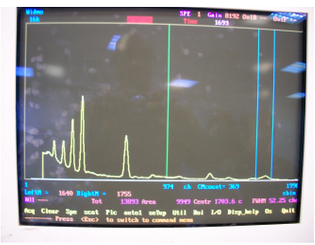

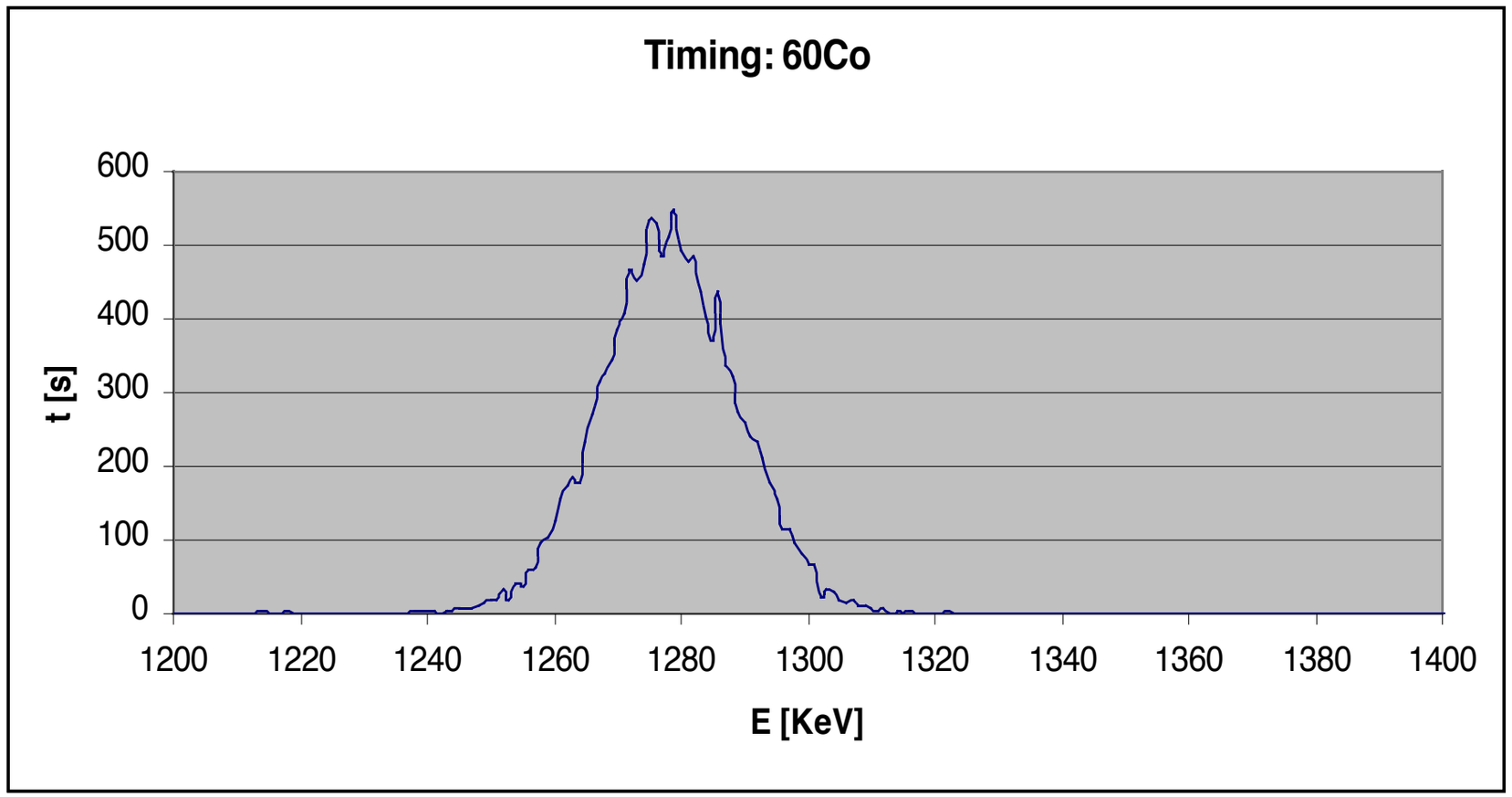
Timing: 60Co
600
500
400
300
200
100
0
t [s]
1200
1220
1240
1260
1280
1300
1320
1340
1360
1380
1400
E [KeV]

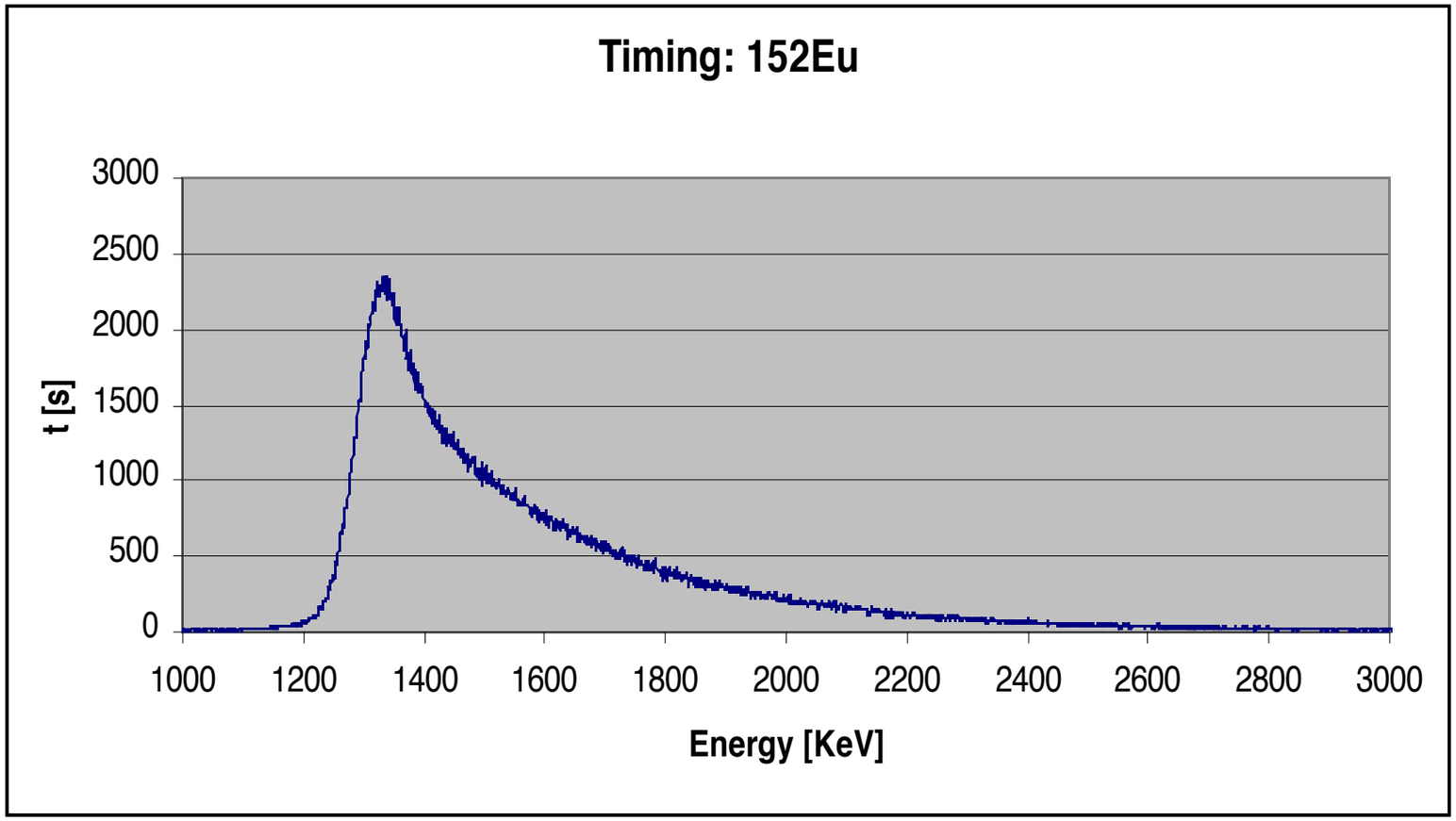
Timing: 152Eu
3000
2500
2000
1500
1000
500
0
t [s]
1000
1200
1400
1600
1800
2000
2200
2400
2600
2800
3000
Energy [KeV]

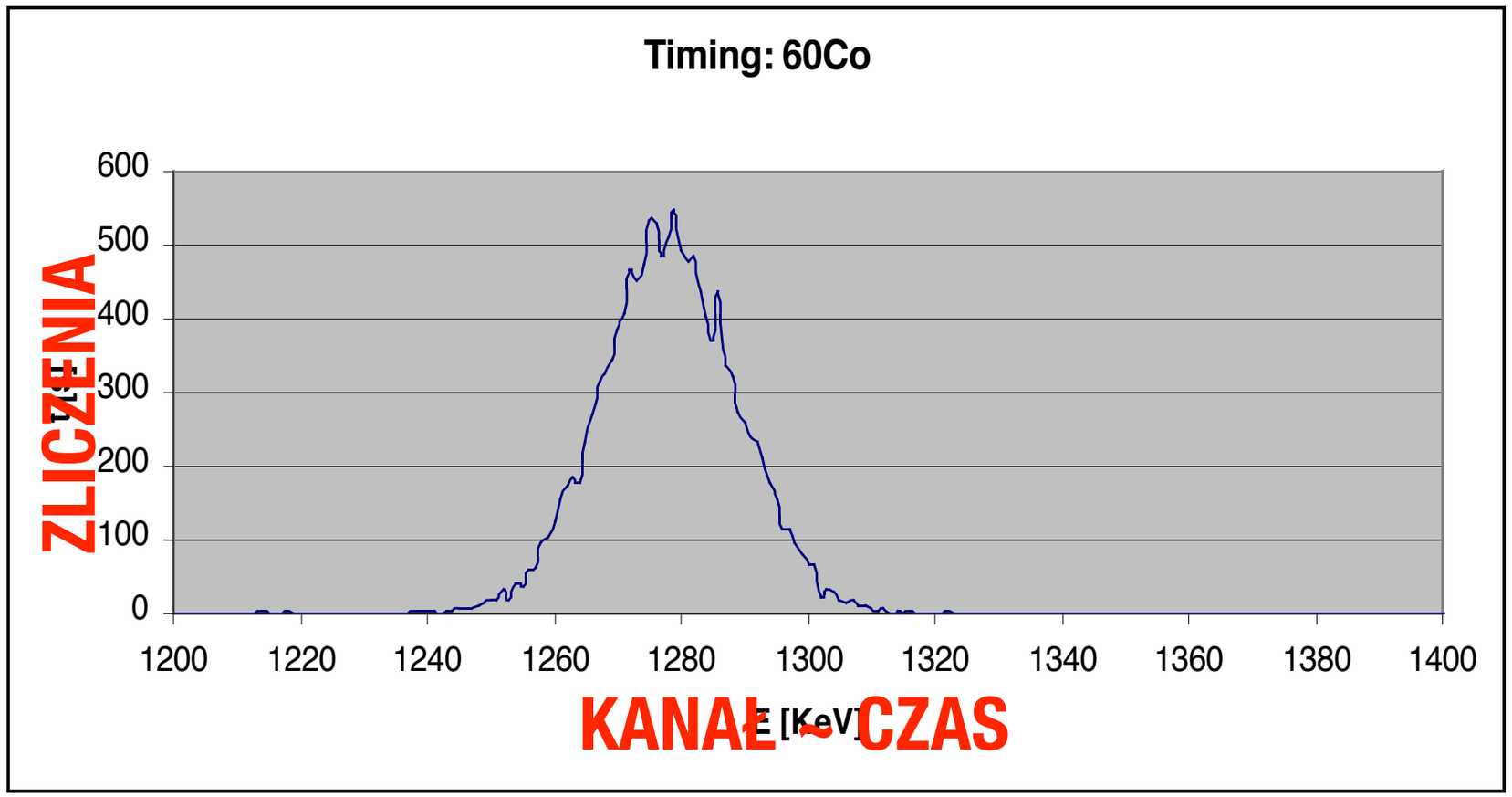
Timing: 60Co
600
500
400
300
200
100
0
1200
1220
1240
1260
1280
1300
1320
1340
1360
1380
1400
ZLICZENIA
KANAŁ ~ CZAS

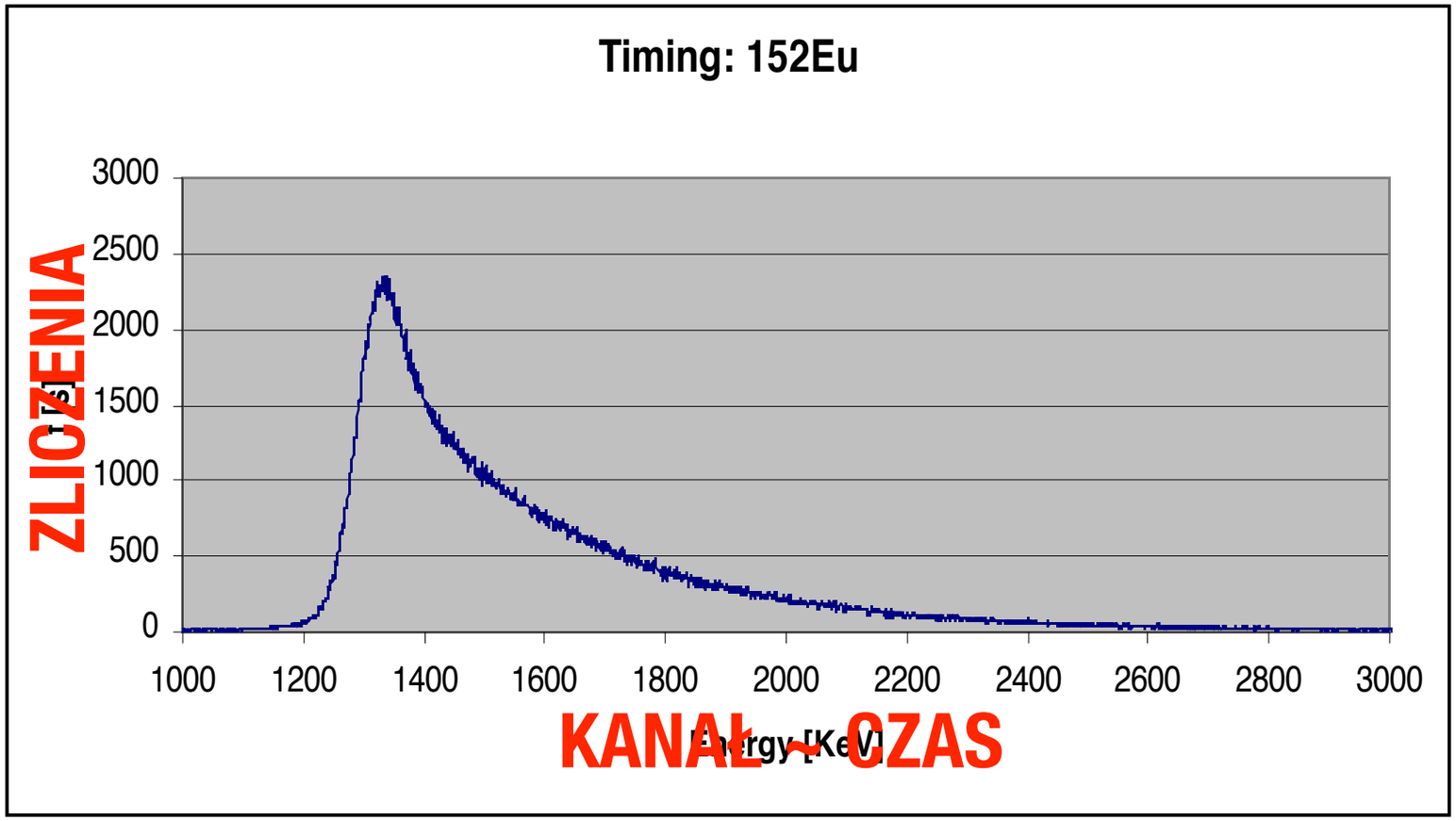
Timing: 152Eu
3000
2500
2000
1500
1000
500
0
1000
1200
1400
1600
1800
2000
2200
2400
2600
2800
3000
ZLICZENIA
KANAŁ ~ CZAS

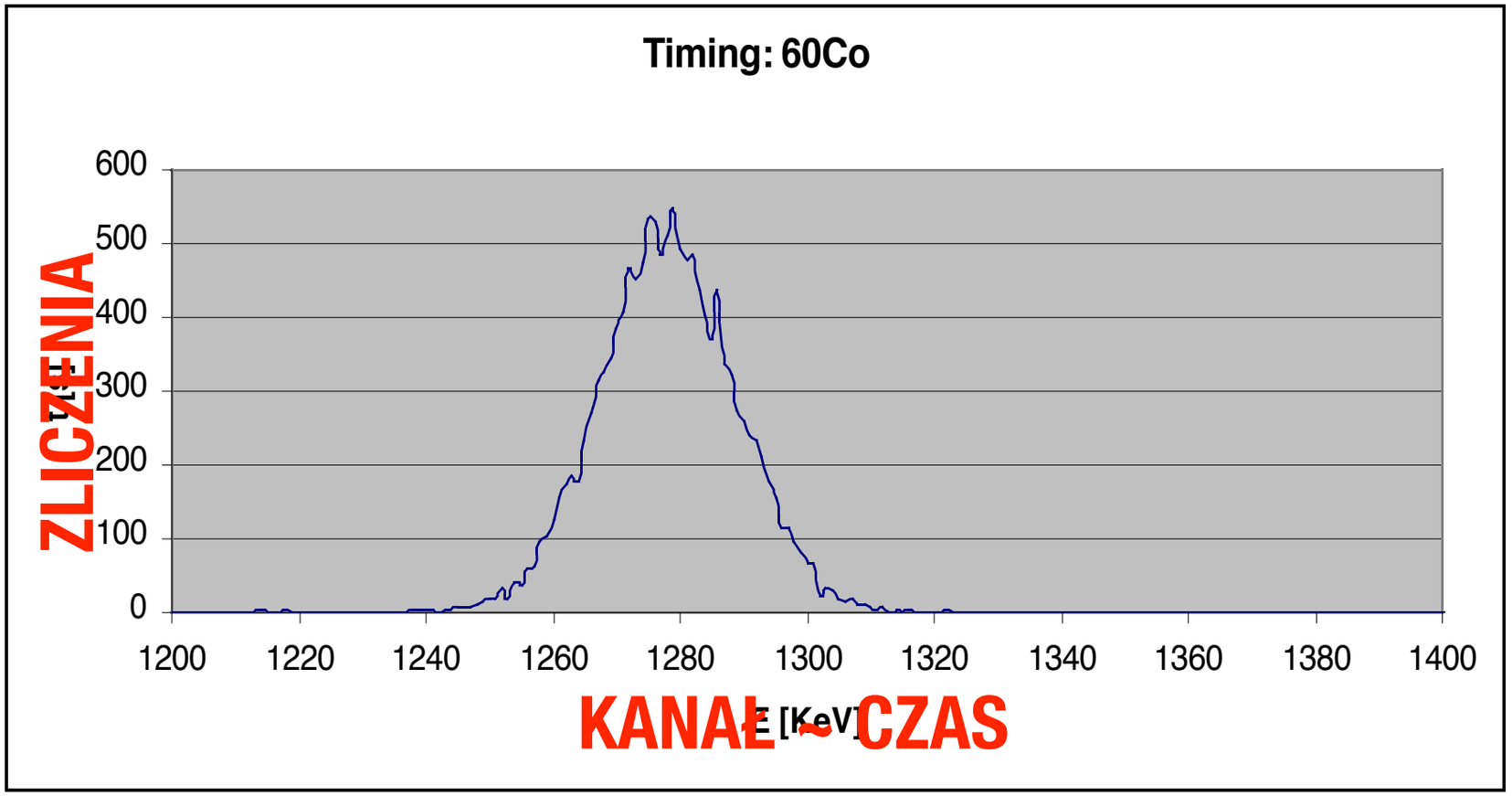
Timing: 60Co
ZLICZENIA
KANAŁ ~ CZAS
Energy [KeV]
600
500
400
300
200
100
0
1200
1220
1240
1260
1280
1300
1320
1340
1360
1380
1400

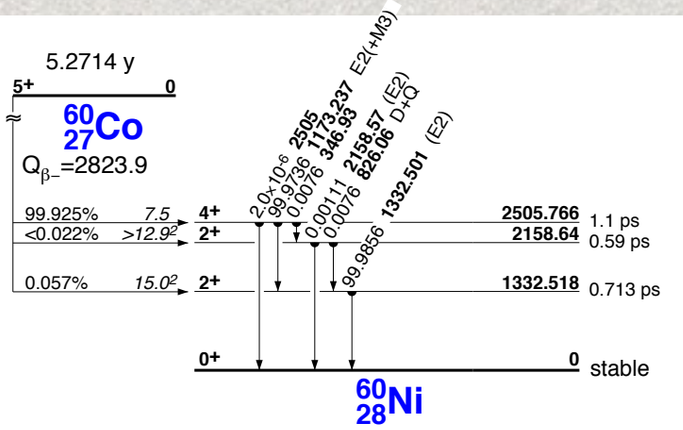
5.2714 y
5+
0
60 27Co
Qβ−=2823.9
99.925% 7.5
<0.022% >12.9²
0.057% 15.0²
4+
2+
2+
0+
0
2505.766
2158.64
1332.518
1.1 ps
0.59 ps
0.713 ps
stable
60 28Ni
2.0×10⁻⁶ 2505
99.9736 1173.237
0.0076 346.93
0.00111 2158.57 (E2)
0.0076 826.06 D+Q
99.9856 1332.501 (E2)
E2(+M3)

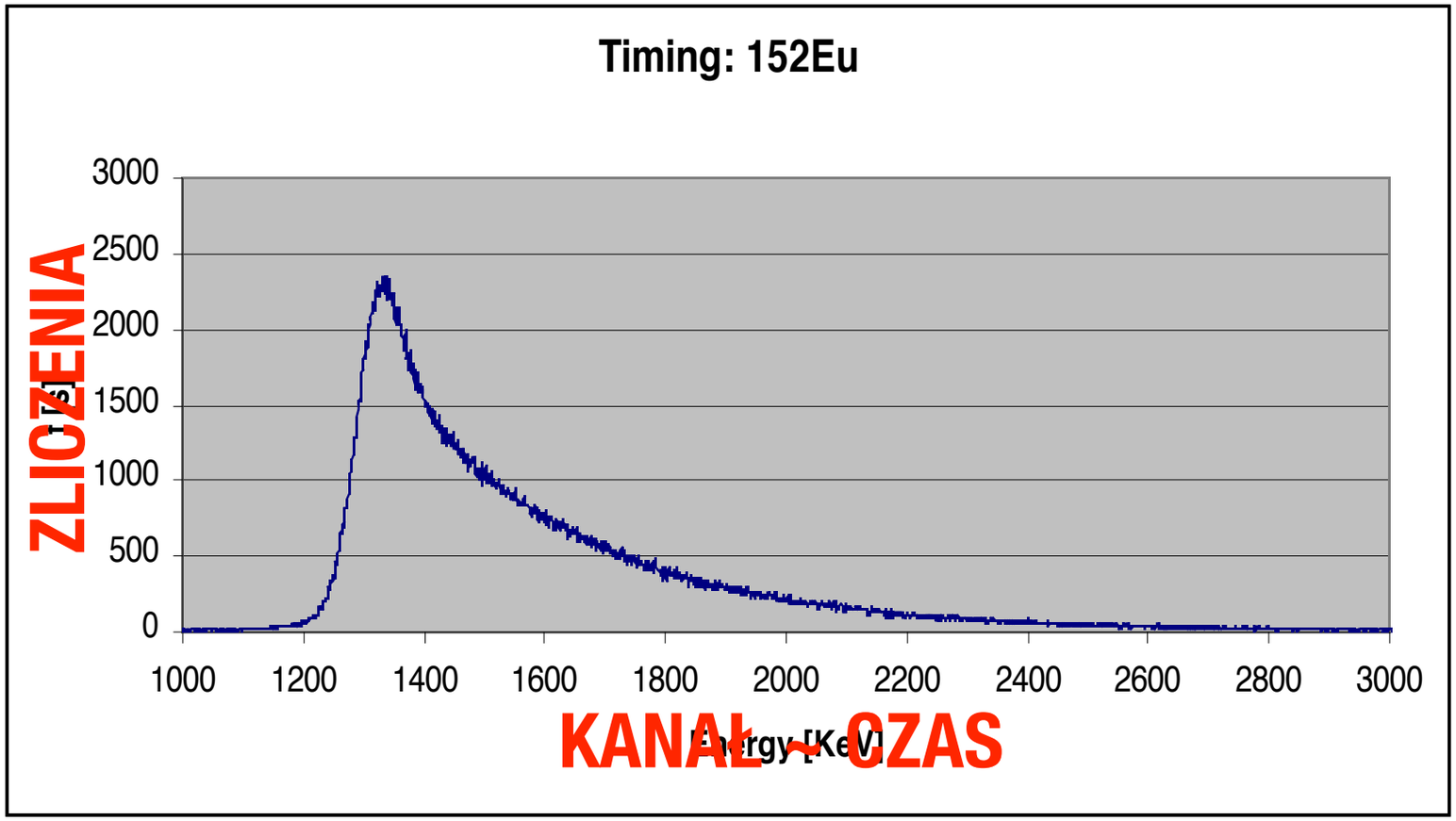
Timing: 152Eu
ZLICZENIA
KANAŁ ~ CZAS
Energy [KeV]
3000
2500
2000
1500
1000
500
0
1000
1200
1400
1600
1800
2000
2200
2400
2600
2800
3000

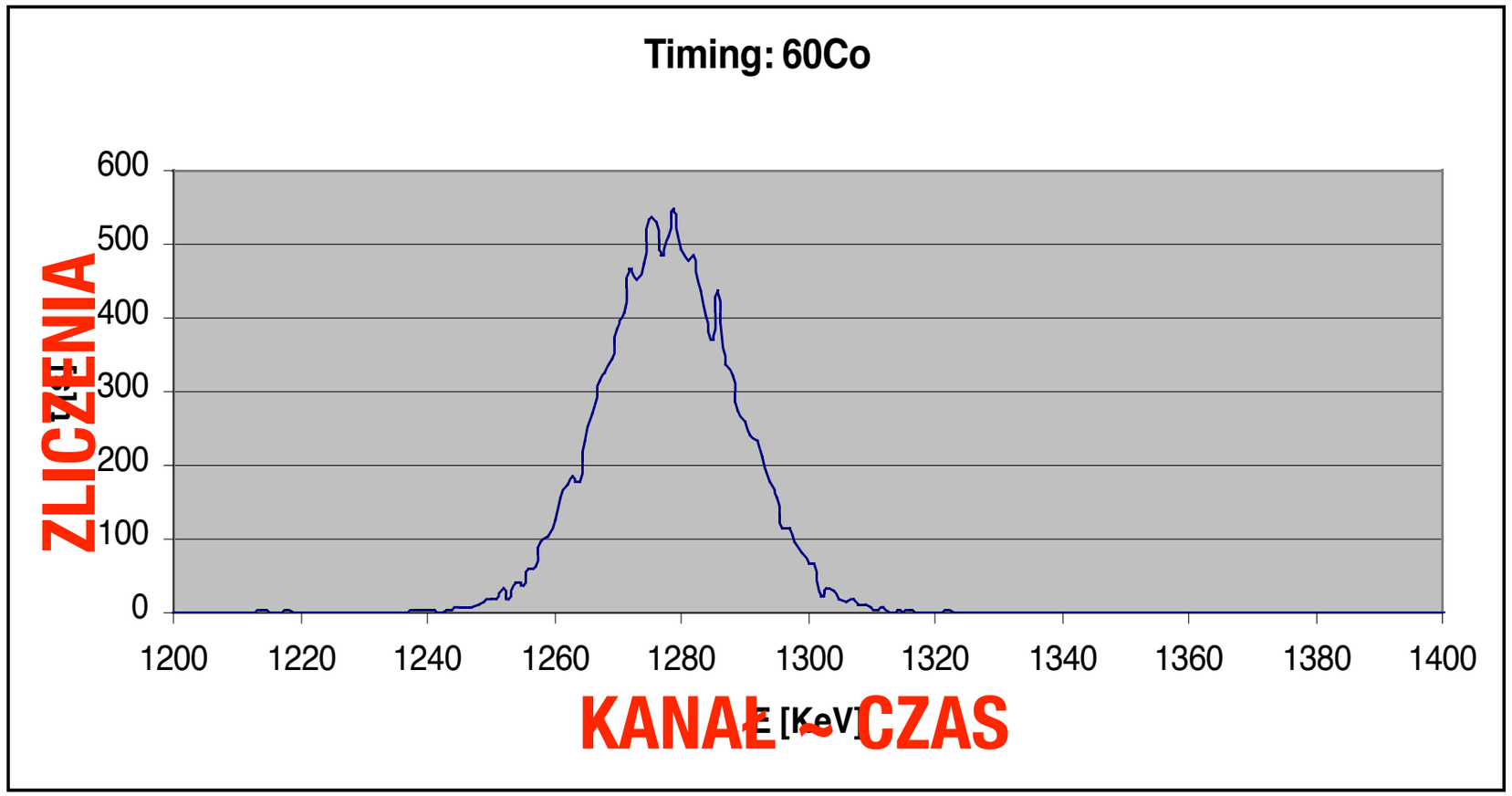
Timing: 60Co
ZLICZENIA
KANAŁ ~ CZAS
E [KeV]
600
500
400
300
200
100
0
1200
1220
1240
1260
1280
1300
1320
1340
1360
1380
1400

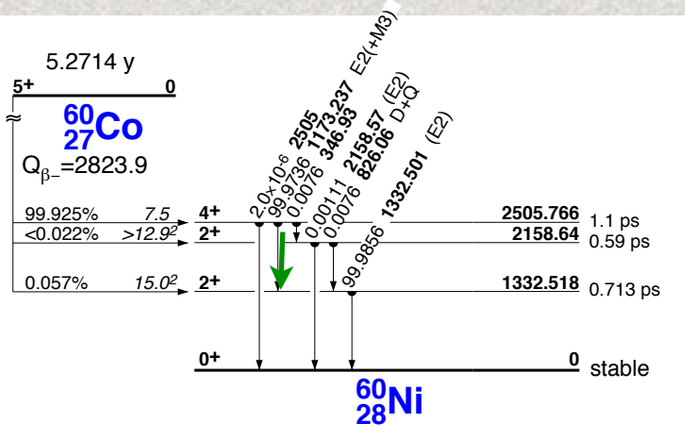
5.2714 y
5+
0
60 27 Co
Q β− =2823.9
99.925% 7.5
<0.022% >12.9²
0.057% 15.0²
4+
2+
2+
0+
2505.766
2158.64
1332.518
0
1.1 ps
0.59 ps
0.713 ps
stable
2.0×10⁻⁶ 2505 E2(+M3)
99.9936 1173.237
0.0076 346.93
0.00111 2158.57 (E2)
0.0076 826.06 D+Q
99.9856 1332.501 (E2)
60 28 Ni

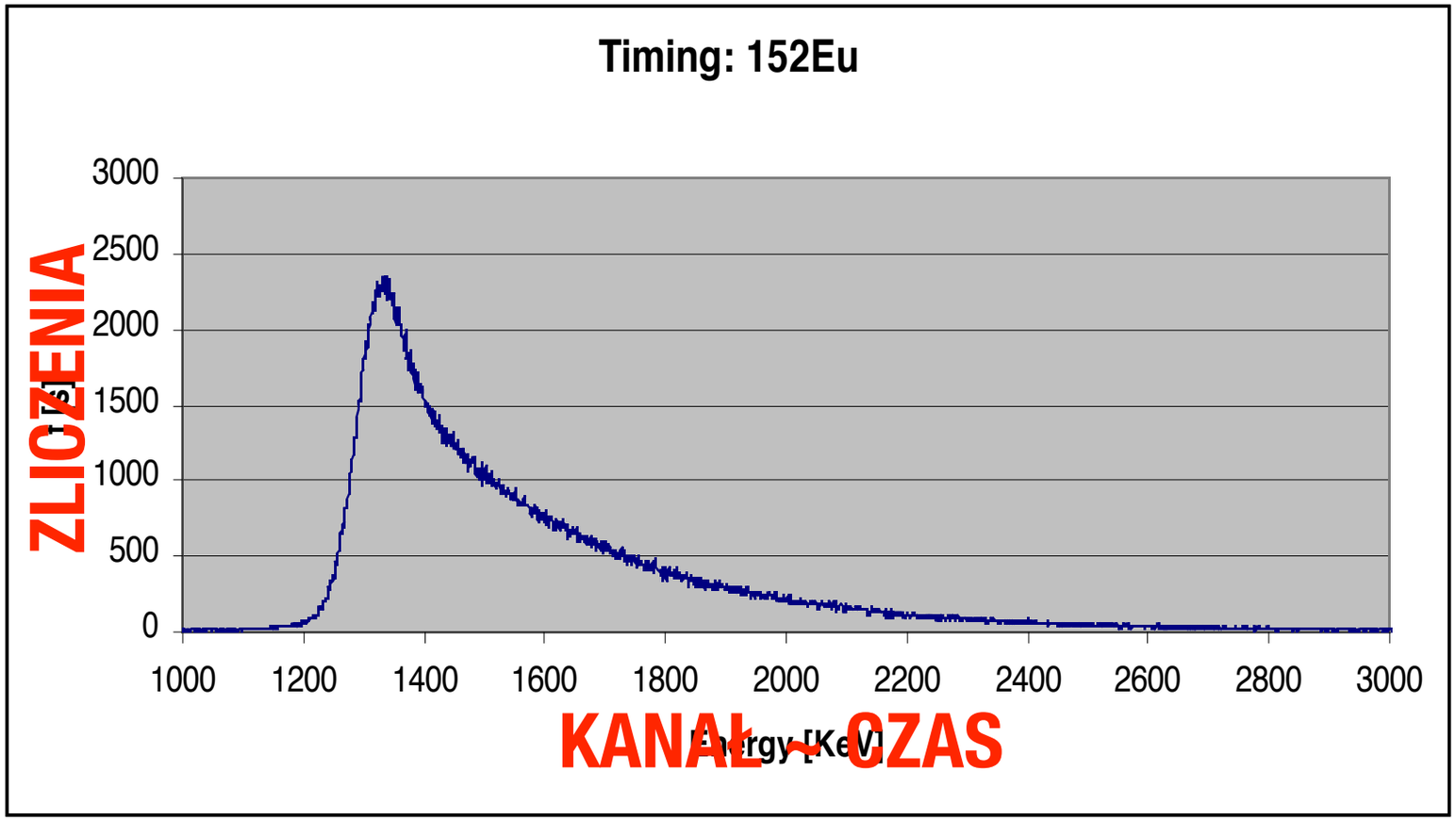
Timing: 152Eu
ZLICZENIA
KANAŁ ~ CZAS
Energy [KeV]
3000
2500
2000
1500
1000
500
0
1000
1200
1400
1600
1800
2000
2200
2400
2600
2800
3000

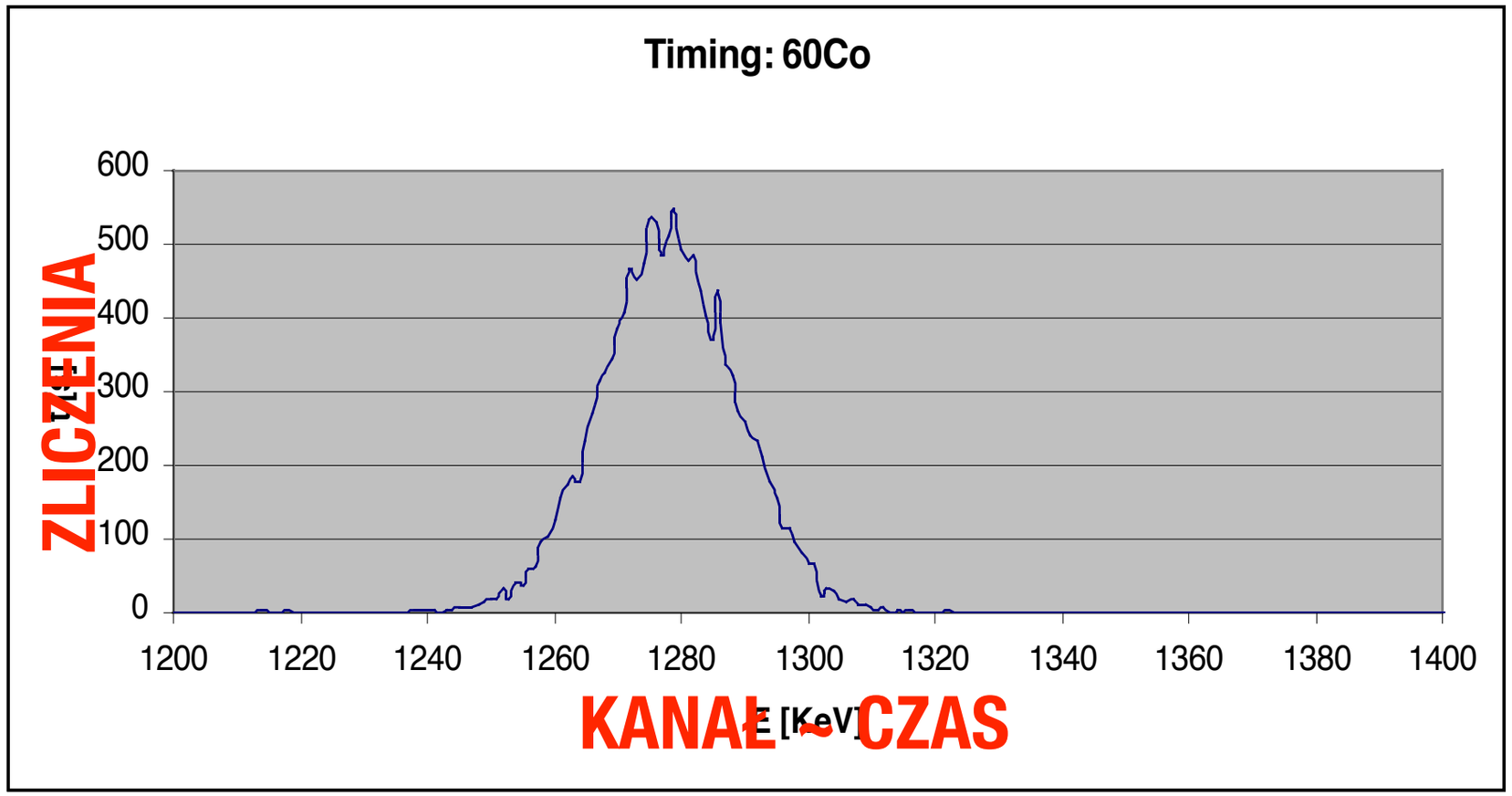
Timing: 60Co
ZLICZENIA
600
500
400
300
200
100
0
1200
1220
1240
1260
1280
1300
1320
1340
1360
1380
1400
KANAŁ ~ CZAS

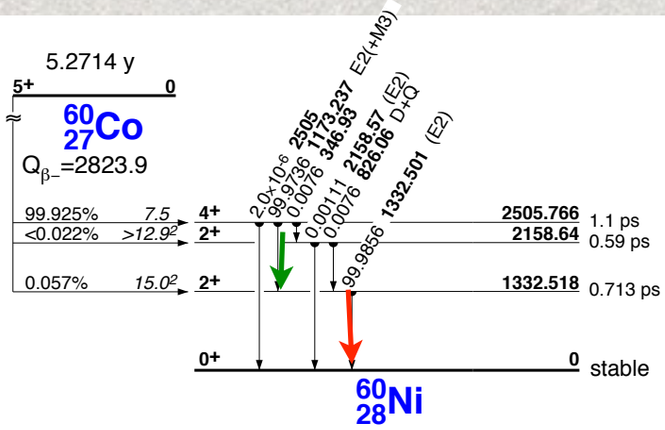
5.2714 y
5+
0
60 27 Co
Q β− =2823.9
99.925% 7.5
<0.022% >12.9²
0.057% 15.0²
4+
2+
2+
0+
2505.766
2158.64
1332.518
0
1.1 ps
0.59 ps
0.713 ps
stable
2.0×10⁻⁶ 2505 E2(+M3)
99.9936 1173.237
0.0076 346.93
0.00111 2158.57 (E2)
0.0076 826.06 D+Q
1332.501 (E2)
99.9856
60 28 Ni

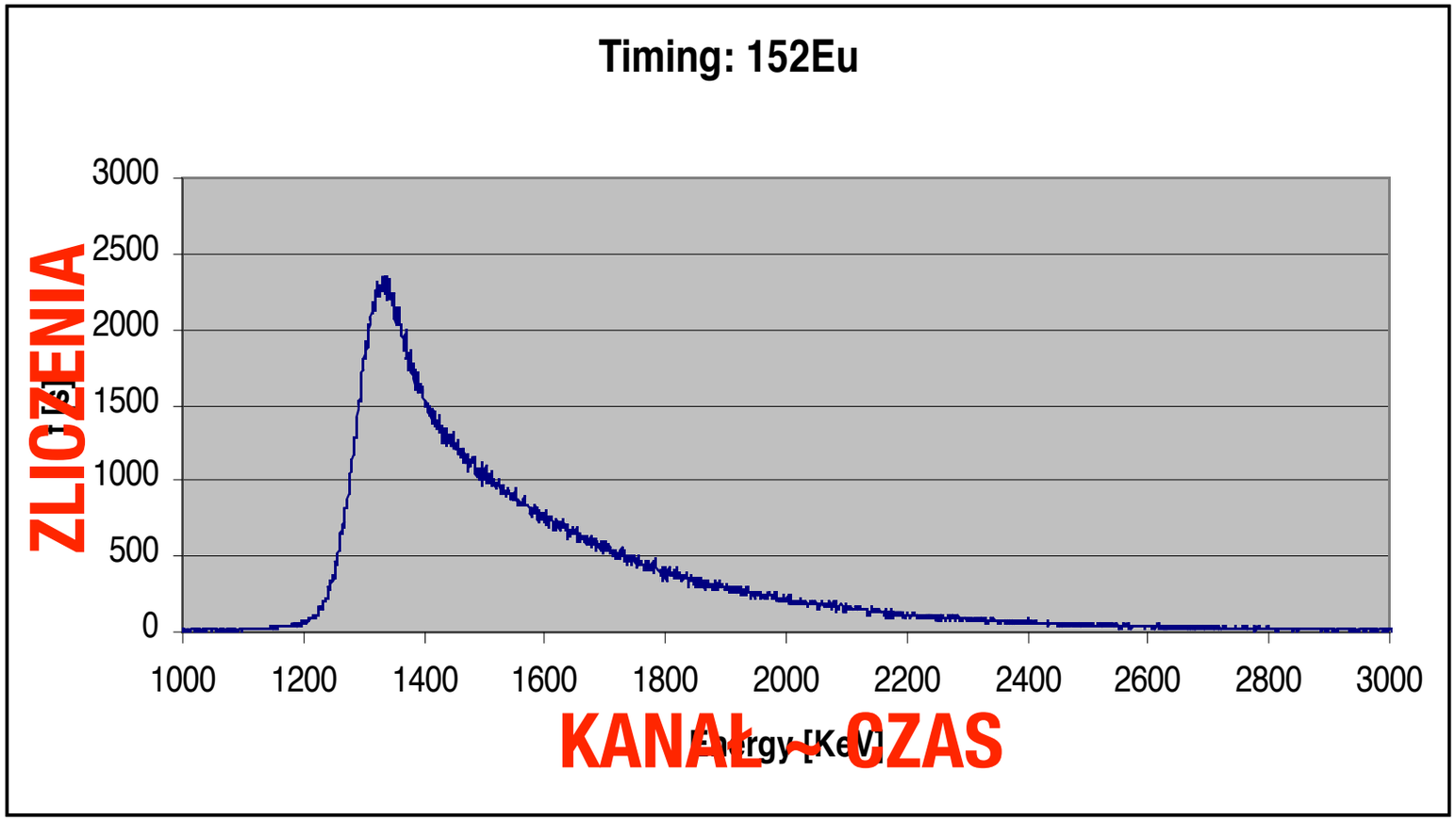
Timing: 152Eu
ZLICZENIA
3000
2500
2000
1500
1000
500
0
1000
1200
1400
1600
1800
2000
2200
2400
2600
2800
3000
KANAŁ ~ CZAS

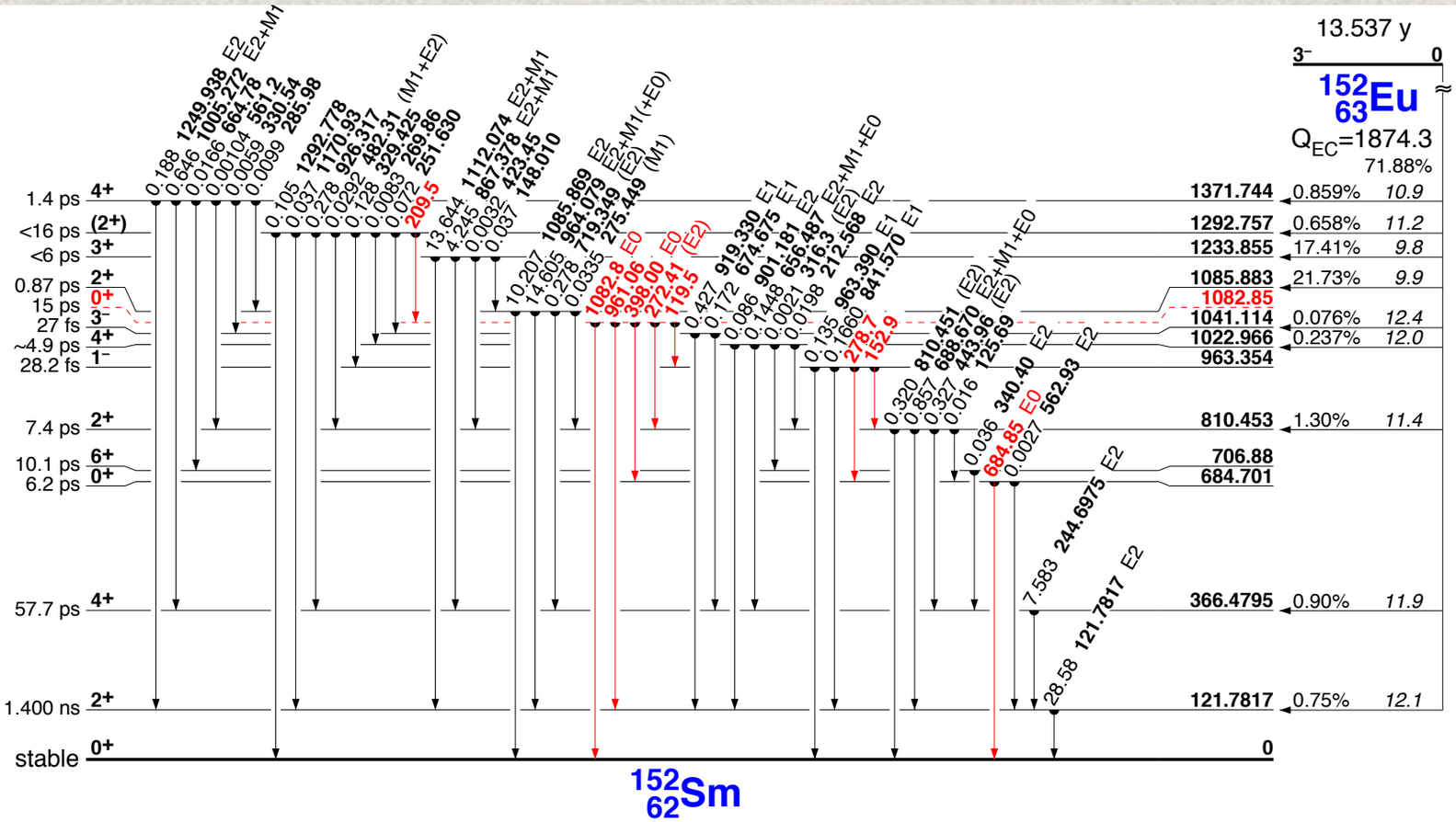
13.537 y
3⁻ 0
152 63Eu
Q_EC=1874.3
71.88%
1.4 ps 4+
<16 ps (2+)
<6 ps 3+
0.87 ps 2+
15 ps 0+
27 fs 3⁻
~4.9 ps 4+
28.2 fs 1⁻
7.4 ps 2+
10.1 ps 6+
6.2 ps 0+
57.7 ps 4+
1.400 ns 2+
stable 0+
1371.744 0.859% 10.9
1292.757 0.658% 11.2
1233.855 17.41% 9.8
1085.883 21.73% 9.9
1082.85
1041.114 0.076% 12.4
1022.966 0.237% 12.0
963.354
810.453 1.30% 11.4
706.88
684.701
366.4795 0.90% 11.9
121.7817 0.75% 12.1
0
152 62Sm

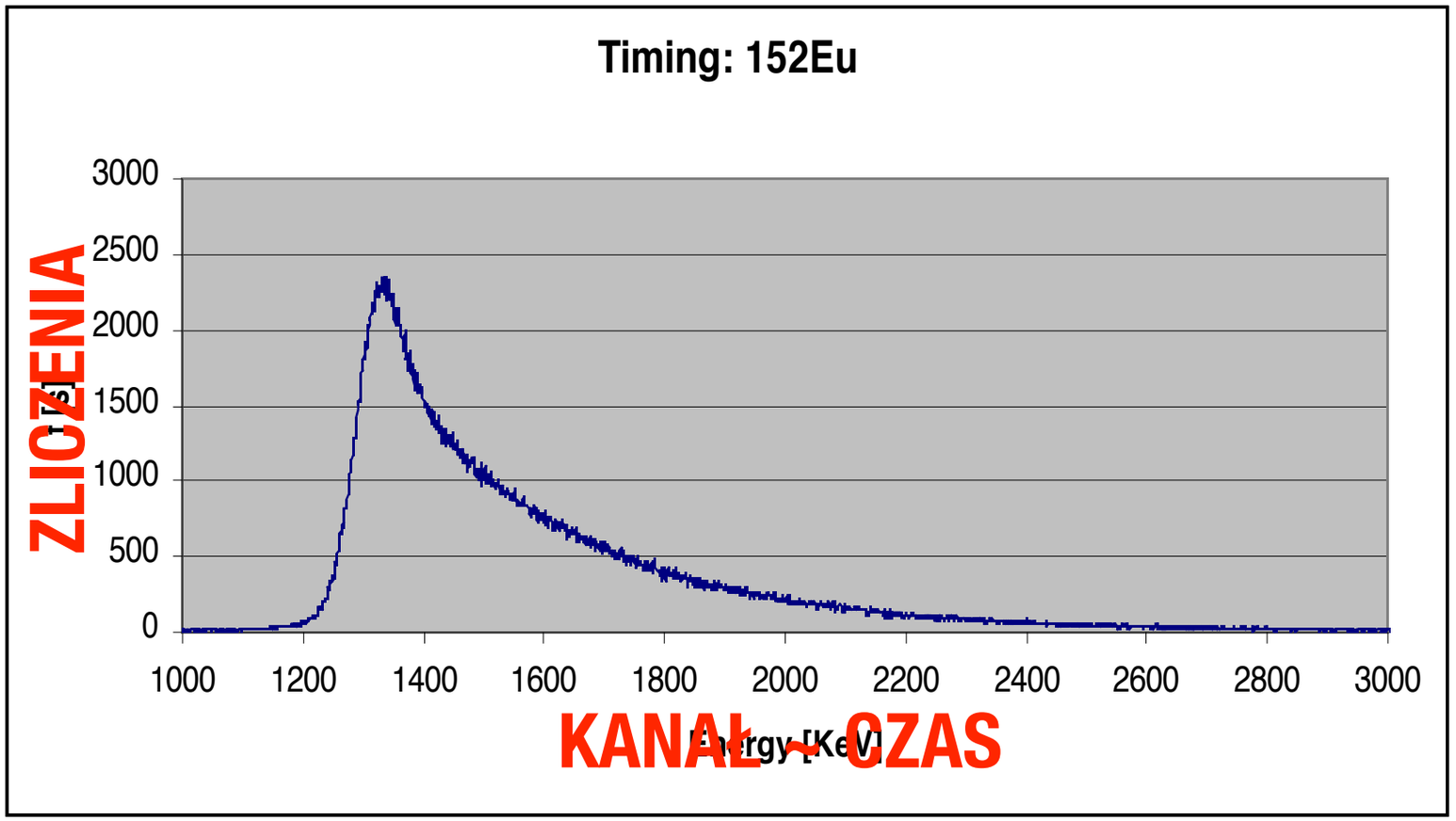
Timing: 152Eu
ZLICZENIA
3000
2500
2000
1500
1000
500
0
1000 1200 1400 1600 1800 2000 2200 2400 2600 2800 3000
KANAŁ ~ CZAS

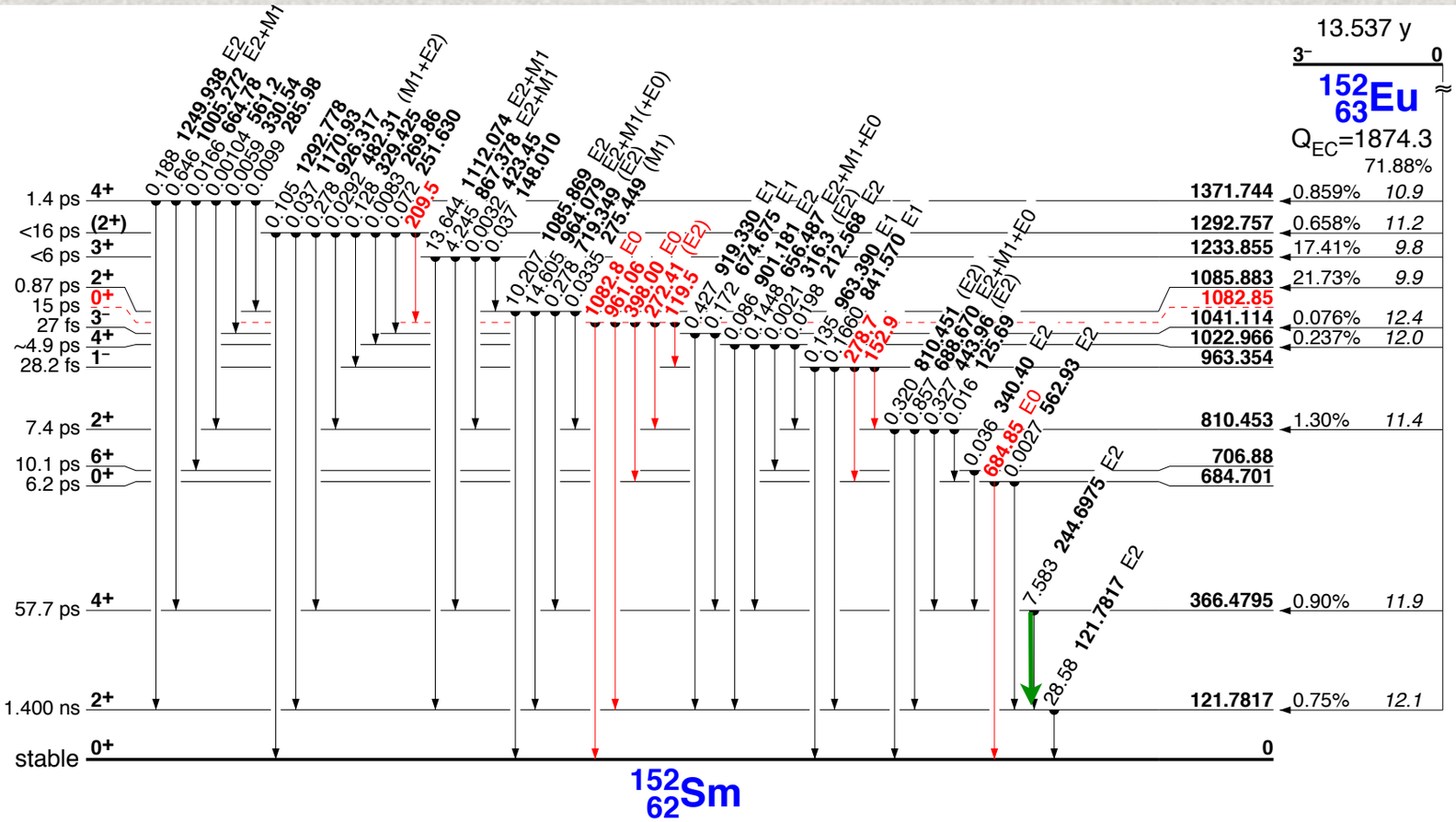
13.537 y
3⁻ 0
152 63Eu
Q_EC=1874.3
71.88%
1.4 ps 4+ 1371.744 0.859% 10.9
<16 ps (2+) 1292.757 0.658% 11.2
<6 ps 3+ 1233.855 17.41% 9.8
0.87 ps 2+ 1085.883 21.73% 9.9
15 ps 0+ 1082.85
27 fs 3⁻ 1041.114 0.076% 12.4
~4.9 ps 4+ 1022.966 0.237% 12.0
28.2 fs 1⁻ 963.354
7.4 ps 2+ 810.453 1.30% 11.4
10.1 ps 6+ 706.88
6.2 ps 0+ 684.701
57.7 ps 4+ 366.4795 0.90% 11.9
1.400 ns 2+ 121.7817 0.75% 12.1
stable 0+ 0
152 62Sm

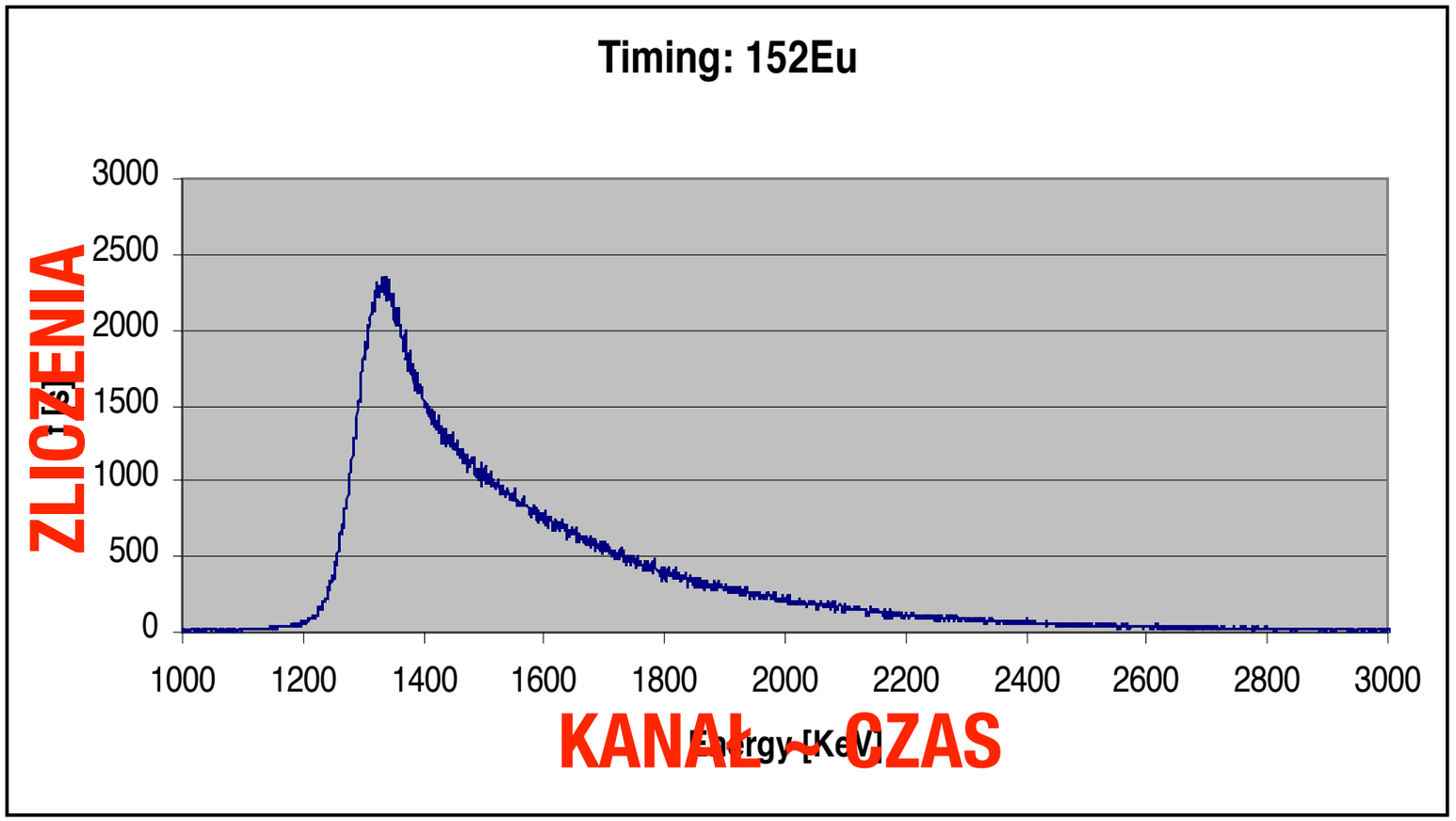
Timing: 152Eu
ZLICZENIA
3000
2500
2000
1500
1000
500
0
1000 1200 1400 1600 1800 2000 2200 2400 2600 2800 3000
KANAŁ ~ CZAS

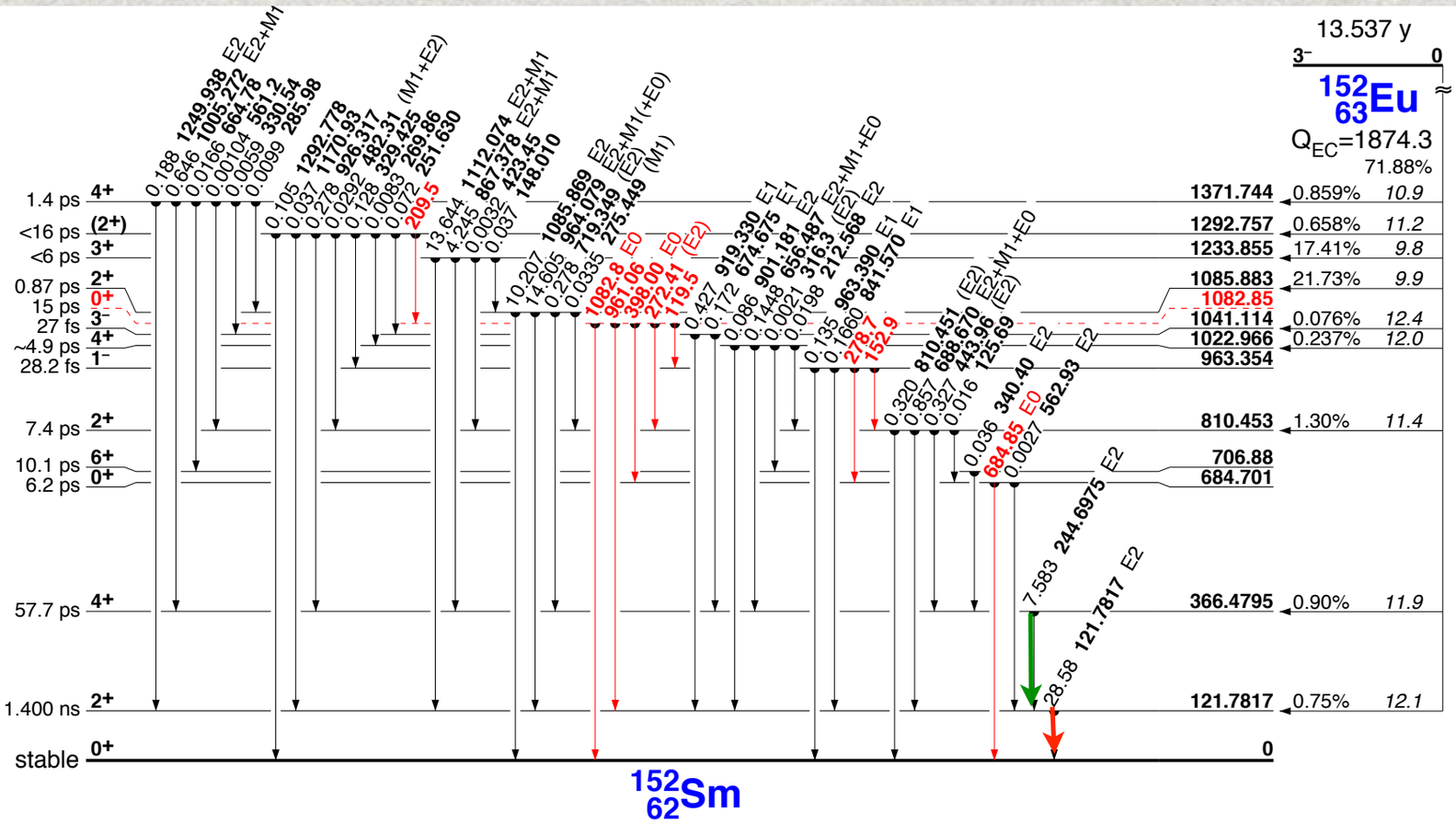
13.537 y
3⁻ 0
152 63Eu
Q_EC=1874.3
71.88%
1.4 ps 4+
<16 ps (2+)
<6 ps 3+
0.87 ps 2+
15 ps 0+
27 fs 3⁻
~4.9 ps 4+
28.2 fs 1⁻
7.4 ps 2+
10.1 ps 6+
6.2 ps 0+
57.7 ps 4+
1.400 ns 2+
stable 0+
1371.744 0.859% 10.9
1292.757 0.658% 11.2
1233.855 17.41% 9.8
1085.883 21.73% 9.9
1082.85
1041.114 0.076% 12.4
1022.966 0.237% 12.0
963.354
810.453 1.30% 11.4
706.88
684.701
366.4795 0.90% 11.9
121.7817 0.75% 12.1
0
152 62Sm

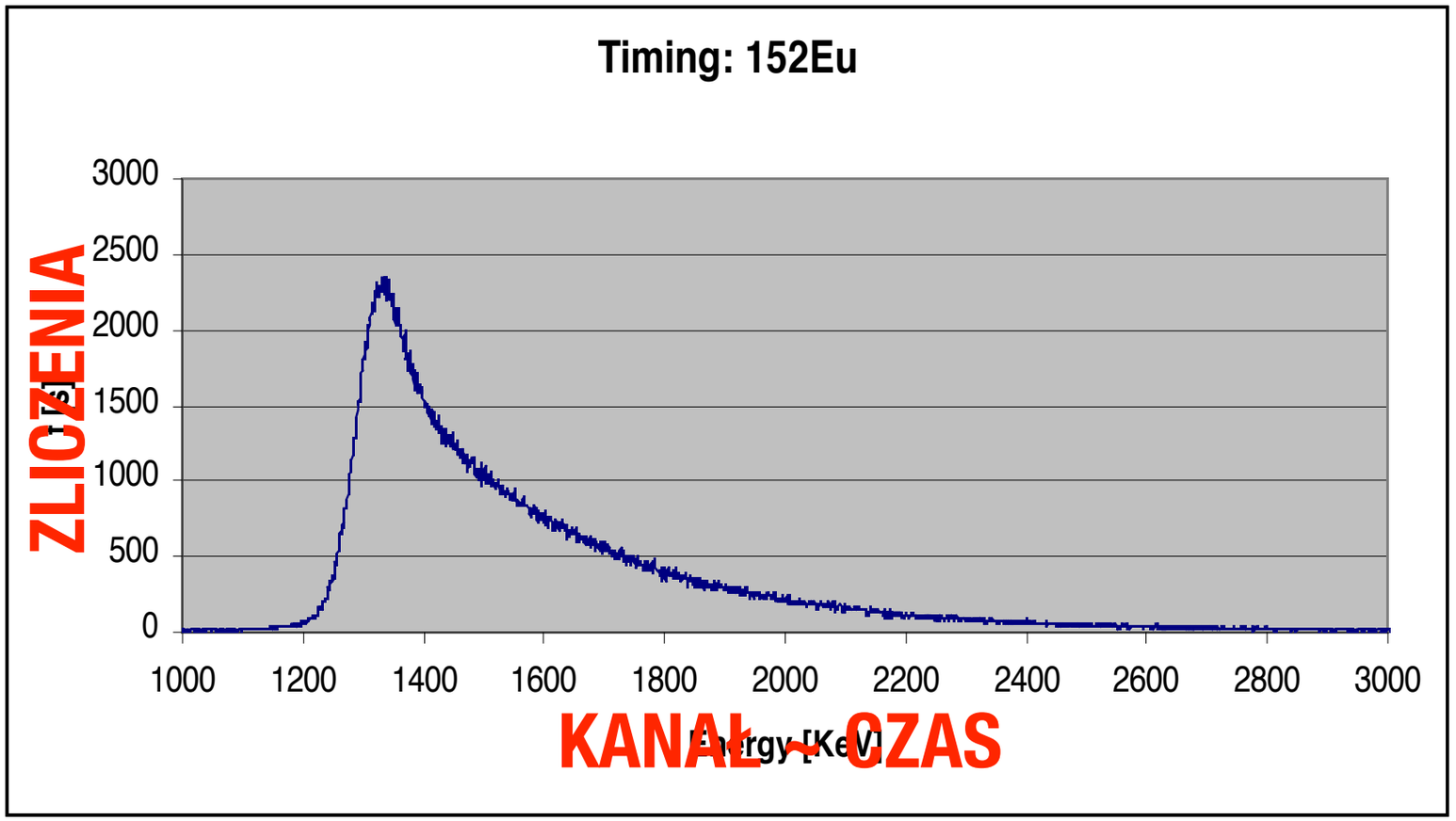
Timing: 152Eu
ZLICZENIA
3000
2500
2000
1500
1000
500
0
1000 1200 1400 1600 1800 2000 2200 2400 2600 2800 3000
KANAŁ ~ CZAS

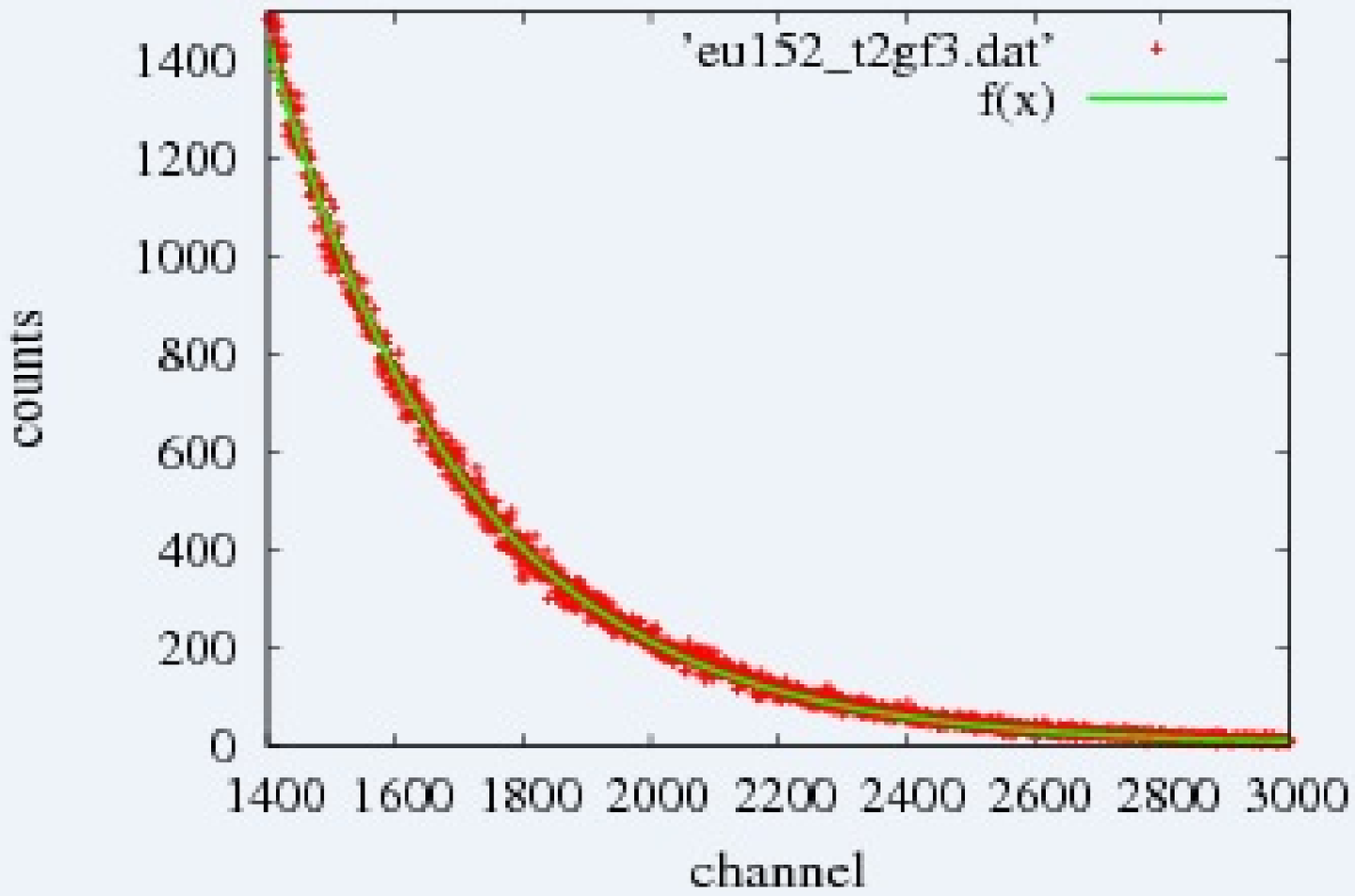

- **Our results:**
  1,43 ns

- **Literature result:**
  1,44 ns

Recoil Distance Method

odpowiednia dla czasów życia
ok. 10^{-9} – 10^{-12} s

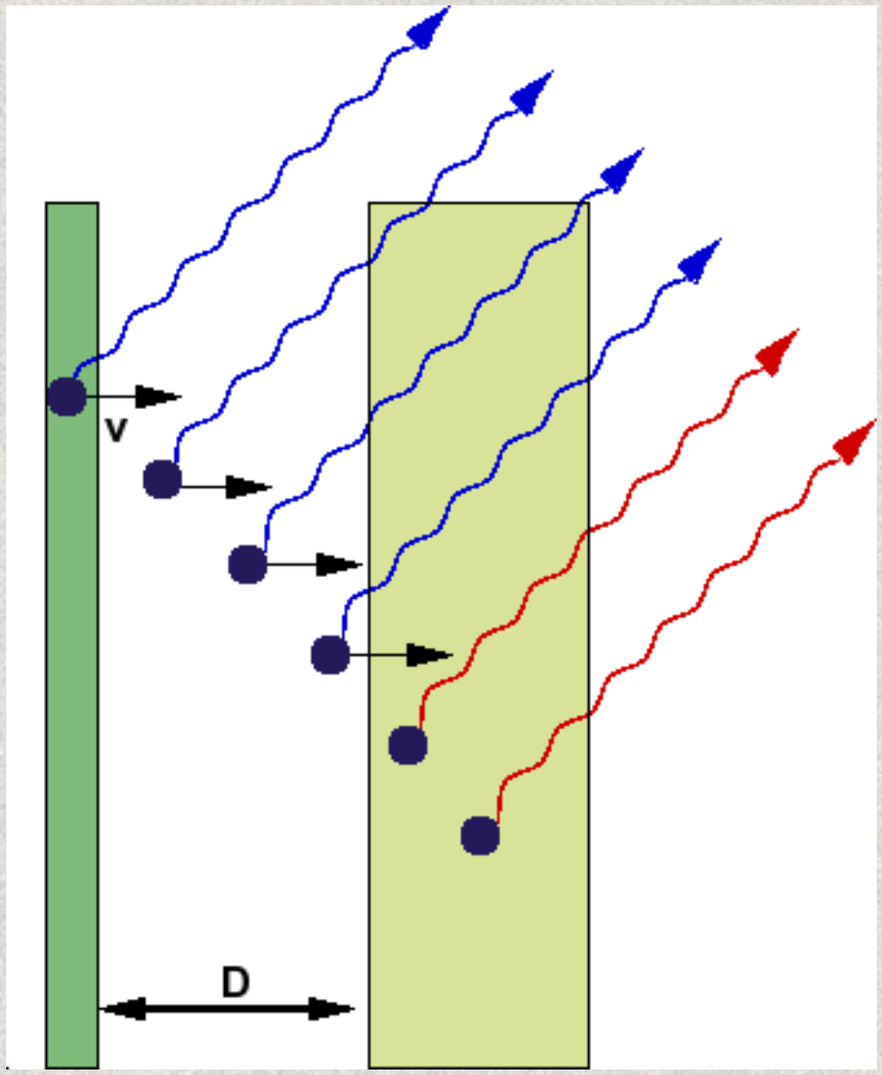

$$E_\gamma = E_0\left(1+\frac{v}{c}\cos\theta\right)$$

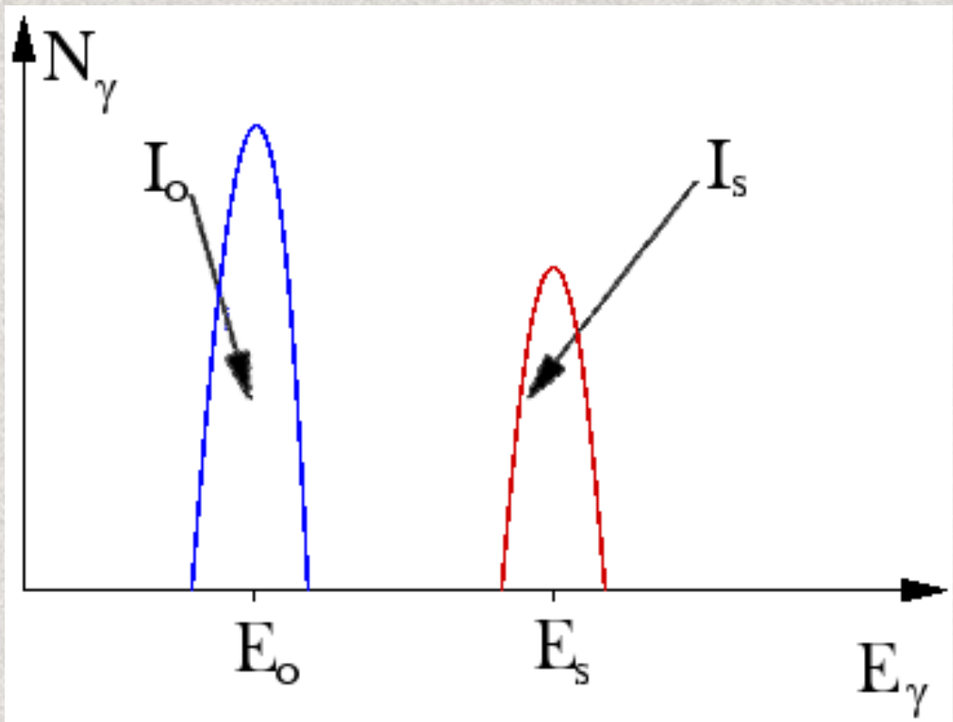

czas przelotu pomiędzy foliami odległymi o D

$$t_D = \frac{D}{v}$$

liczba kwantów wyemitowanych po zatrzymaniu

$$I_s = N_0\exp\left(-\frac{t_D}{\tau}\right) = N_0\exp\left(-\frac{D}{v\,\tau}\right)$$

Recoil Distance Method

zmniejszamy odległość D:

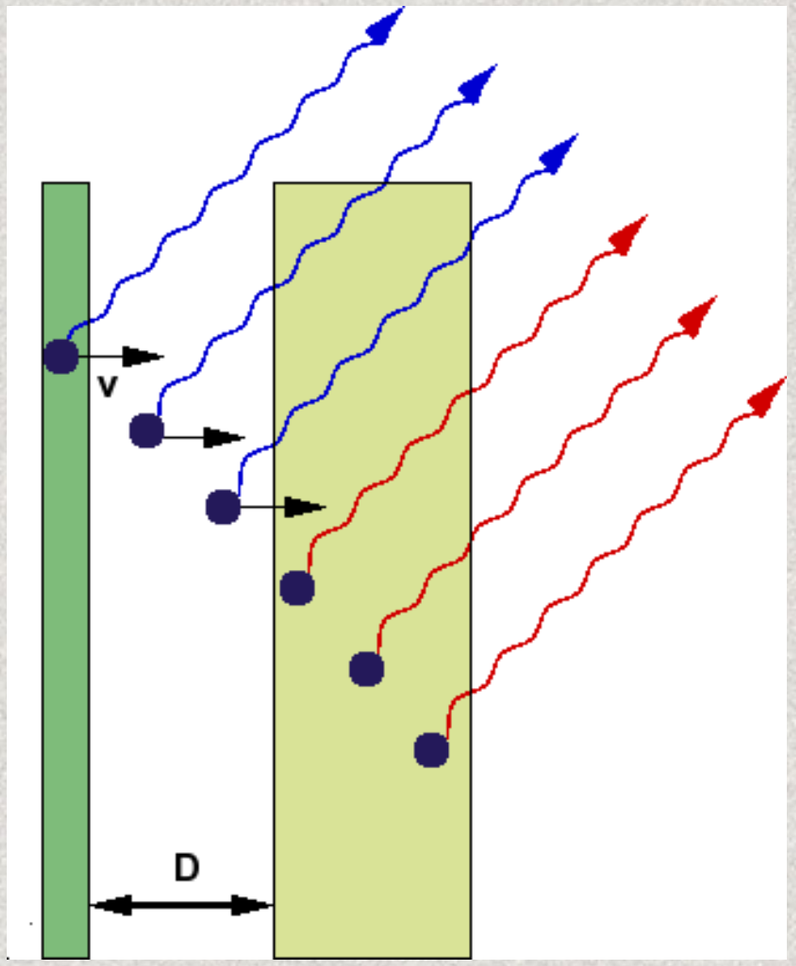

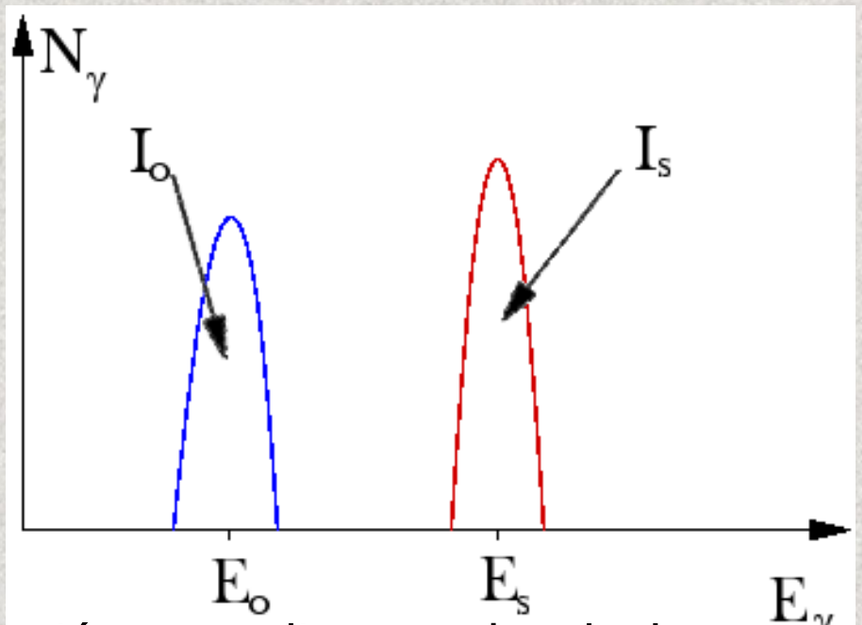

liczba kwantów wyemitowanych w locie:

$$I_o = N_o - I_s = N_0\left(1-\exp\left(-\frac{D}{v\tau}\right)\right)$$

zwykle analizujemy wielkość

$$R(D) = \frac{I_o}{I_o + I_s} = \exp\left(-\frac{D}{v\tau}\right)$$

Przykład ^{74}Kr (M.Zielińska)

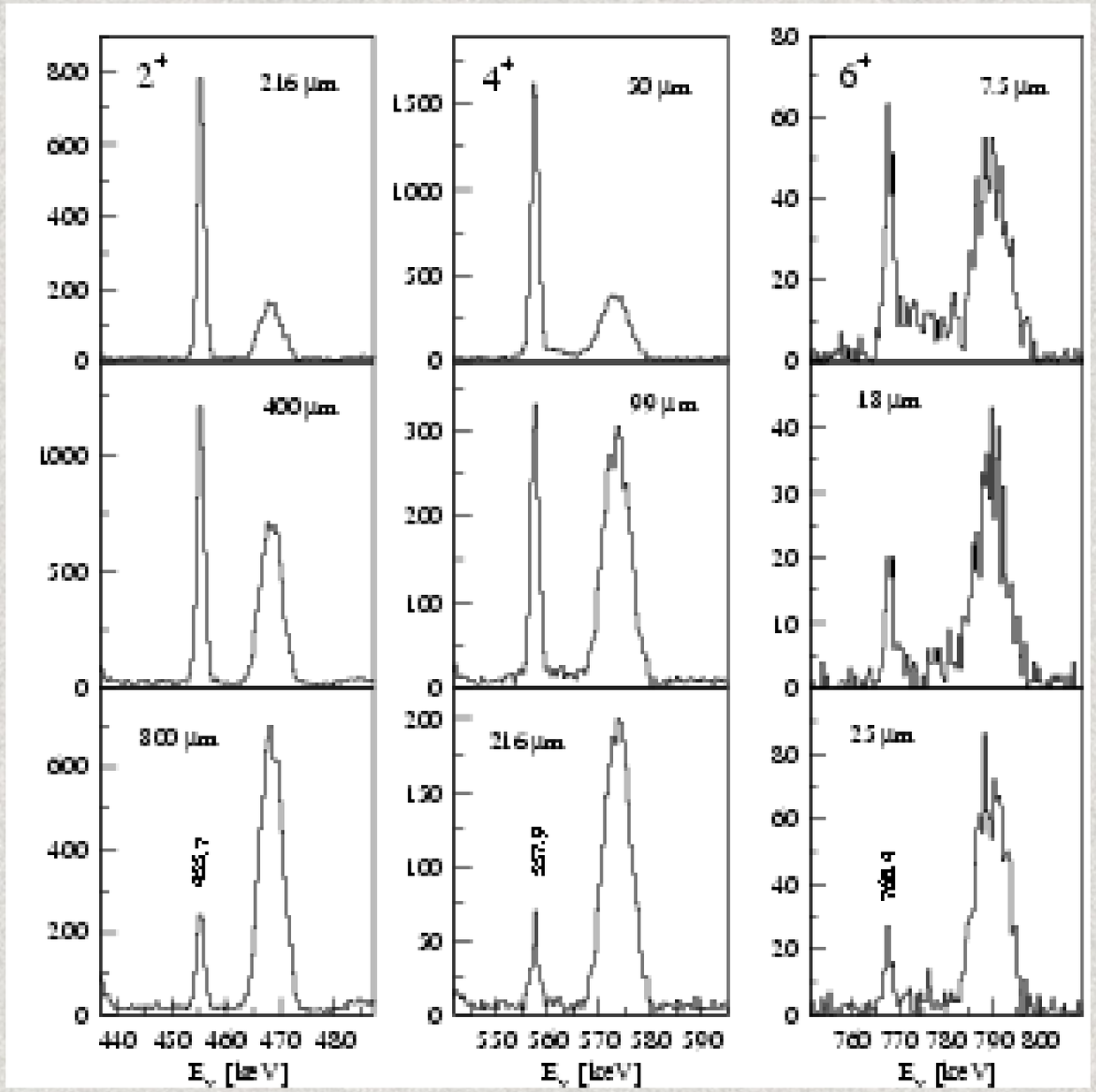

Example: ^{74}Kr , 4^+, 36˚

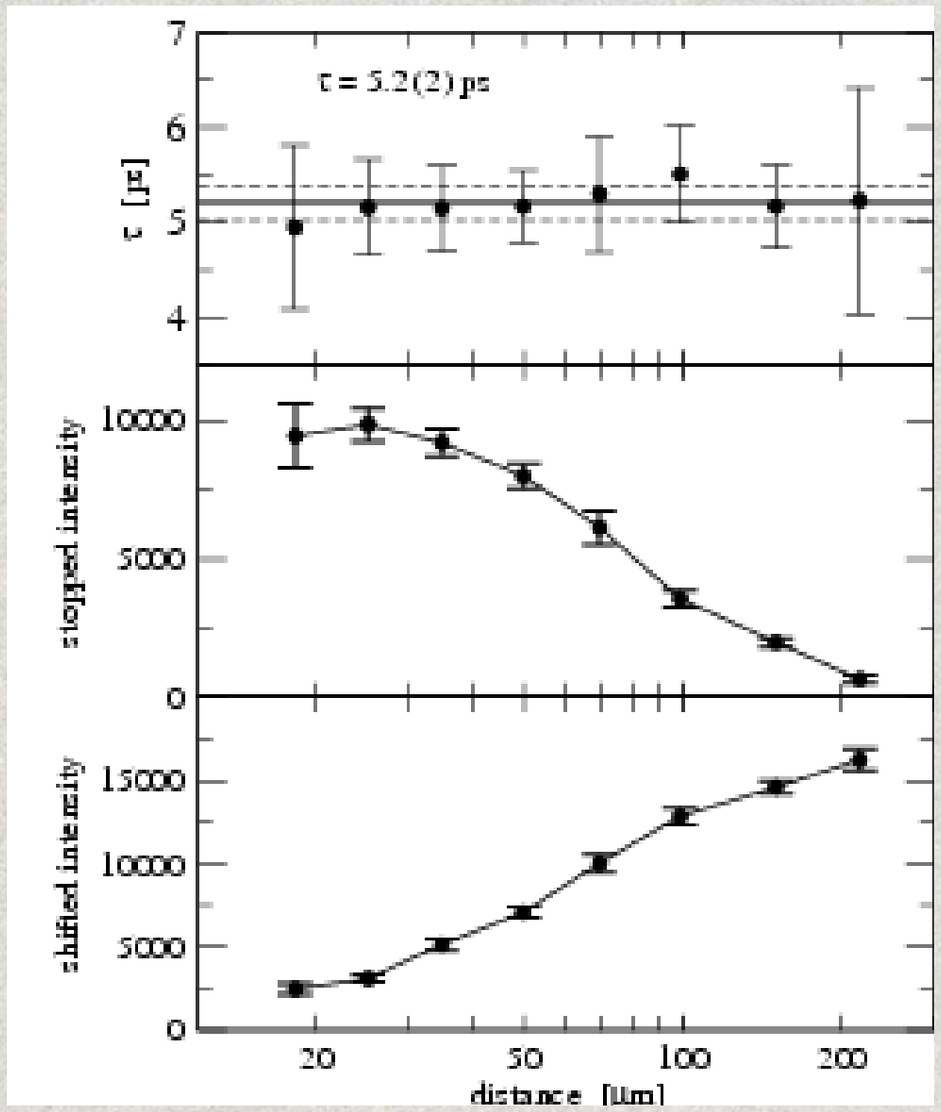

Plunger by A. Devald

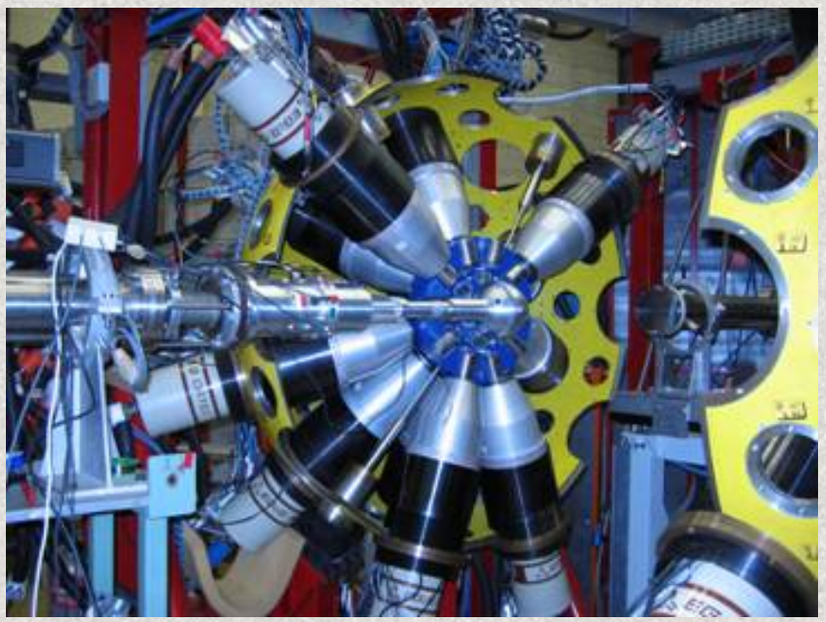

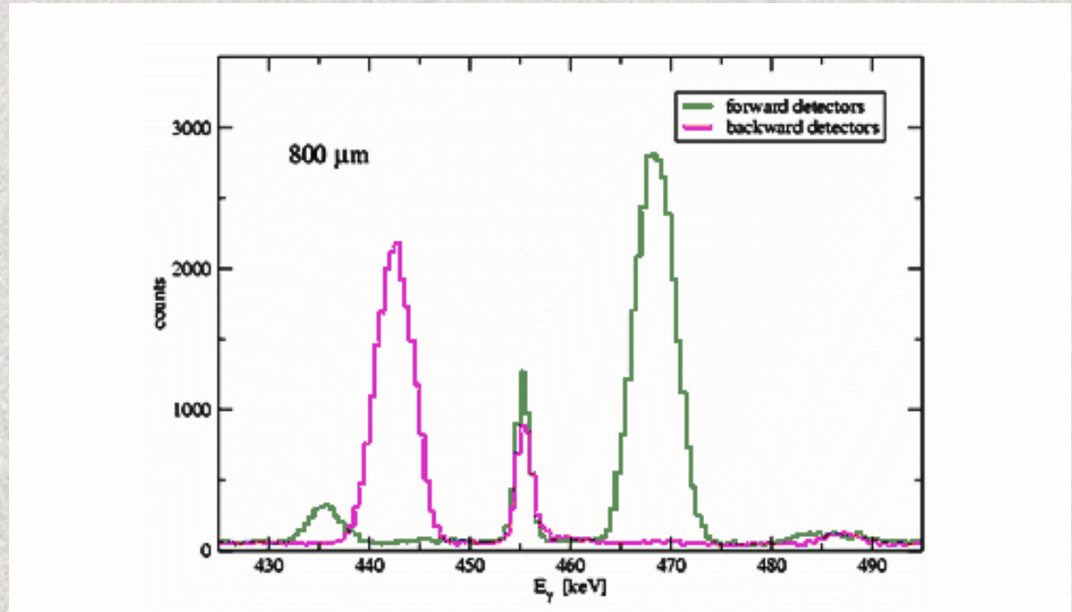

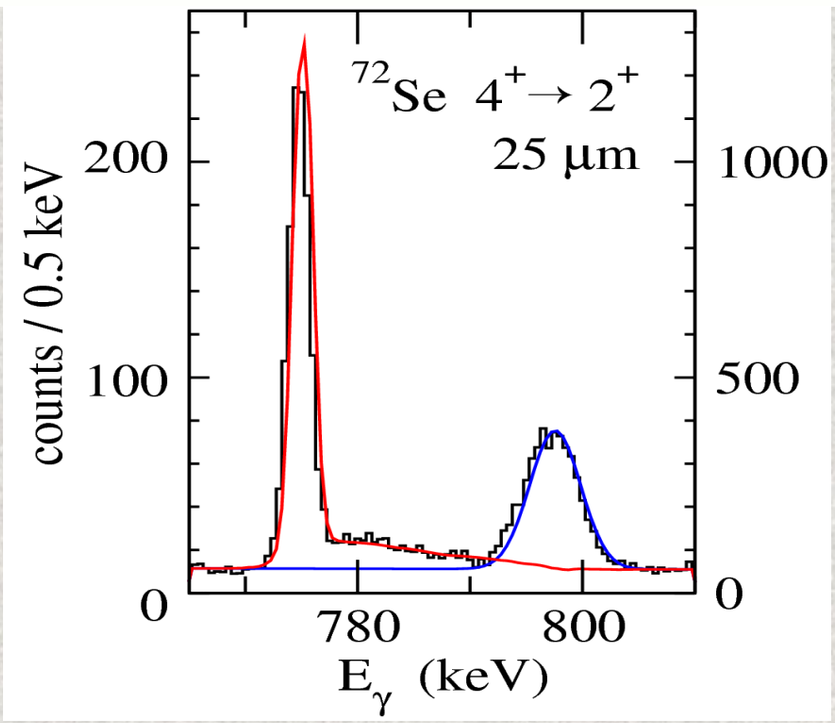

Doppler Shift Attenuation Method

odpowiednia dla czasów życia
ok. 10^{-11}– 10^{-14} s

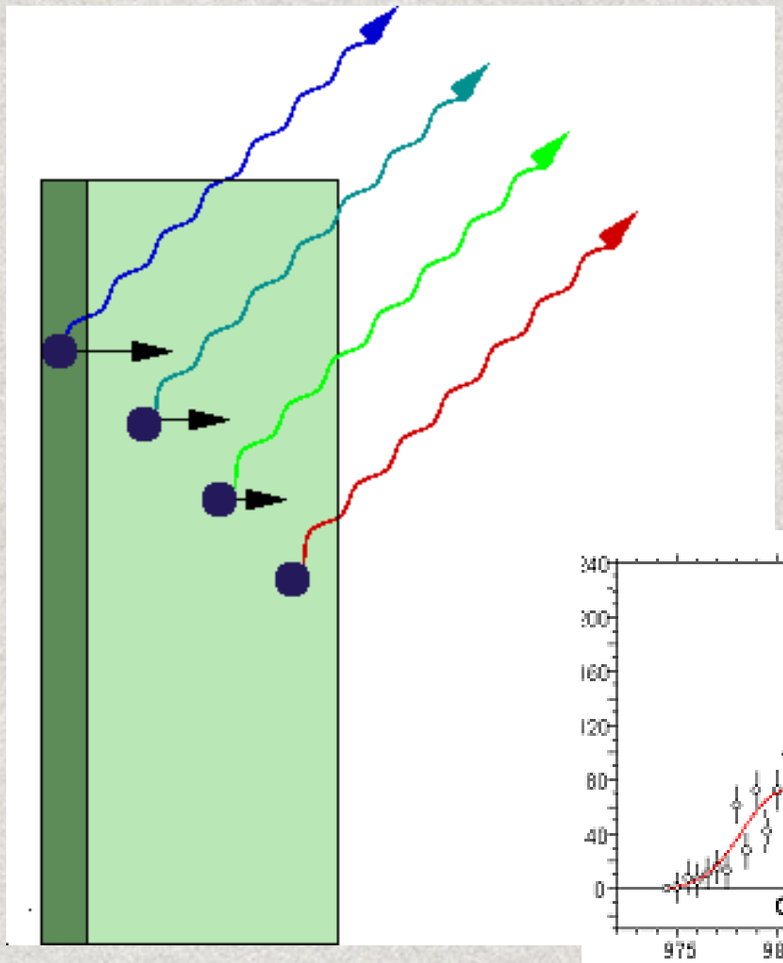

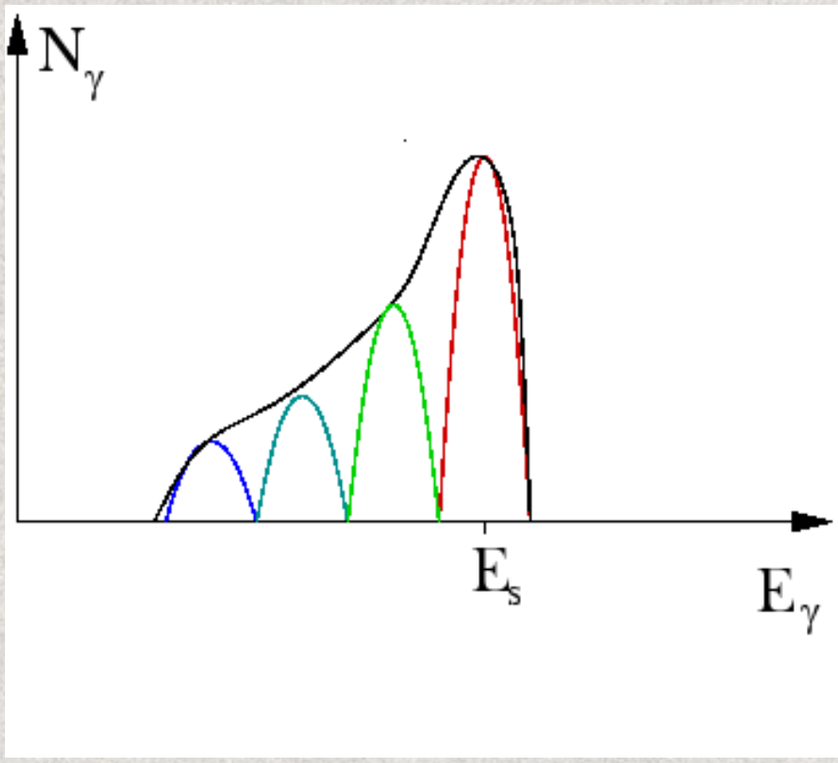

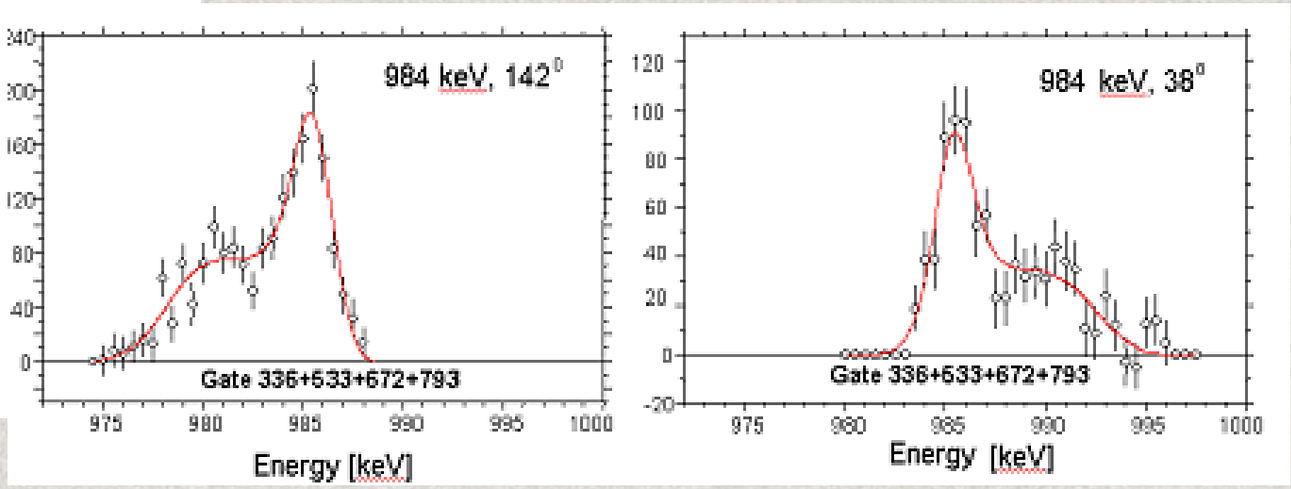

Wzbudzenia kulombowskie

- Wyznaczenie rozkładu ładunku we wzbudzonych stanach jądra atomowego
  mikroskop jądrowy

- Przy ograniczonej energii cząstki padającej (odległość 5 fm między powierzchniami jądrowym) można zaniedbać siły jądrowe opisując proces formalizmem oddziaływania kulombowskiego

$$E_{\max}(MeV) = 1.44\frac{A_1 + A_2}{A_2} \cdot \frac{Z_1 Z_2}{1.25(A_1^{1/3} + A_2^{1/3}) + 5} \qquad (2.2)$$

- obserwowane wzbudzenie zależy silnie od kąta rozproszenia, liczb Z partnerów reakcji, deformacji rozkładu ładunku jąder (a więc struktury jąder atomowych)

Schemat układu eksperymentalnego

Detektory cząstek

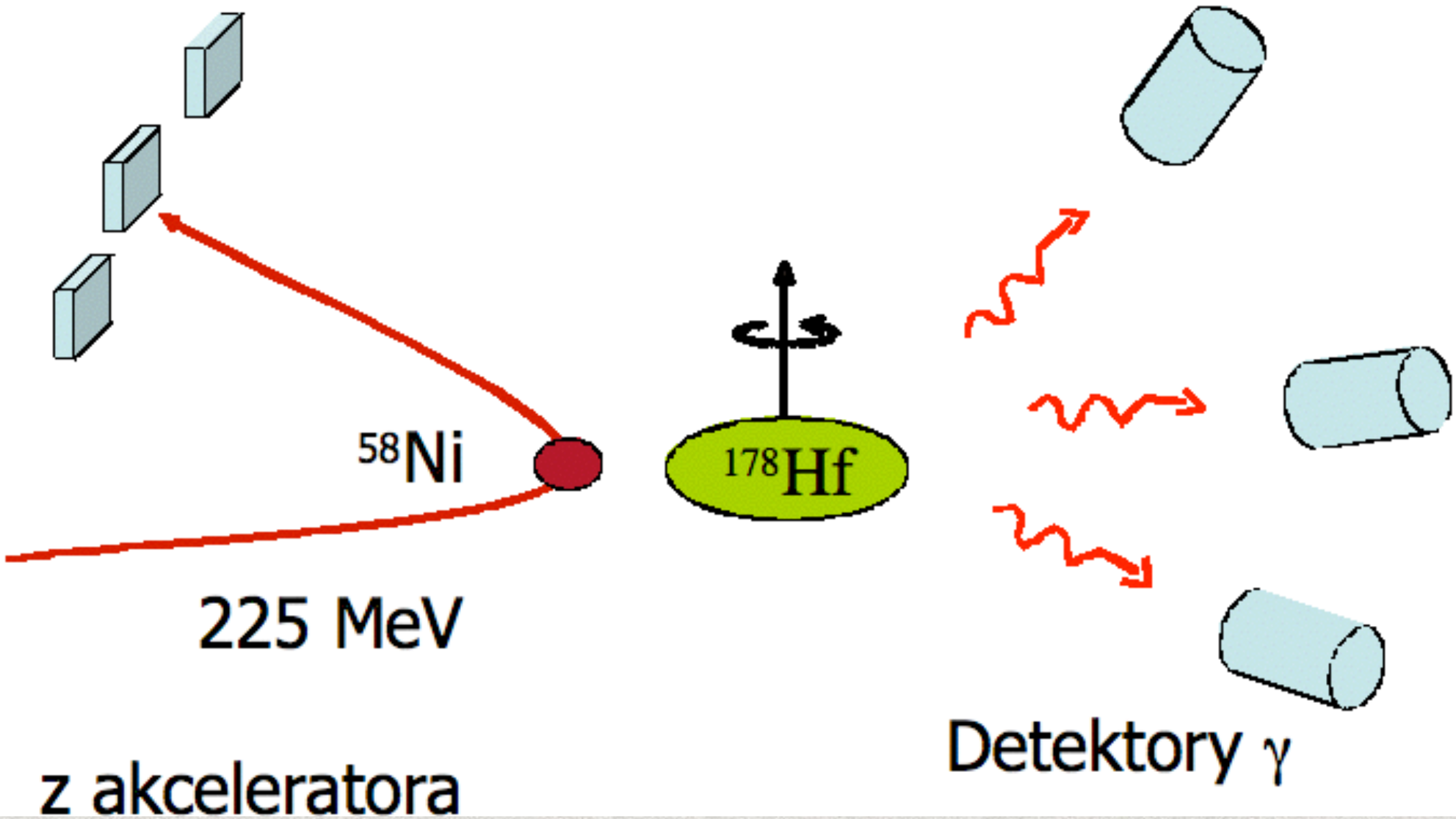

Schemat układu eksperymentalnego

Detektory cząstek

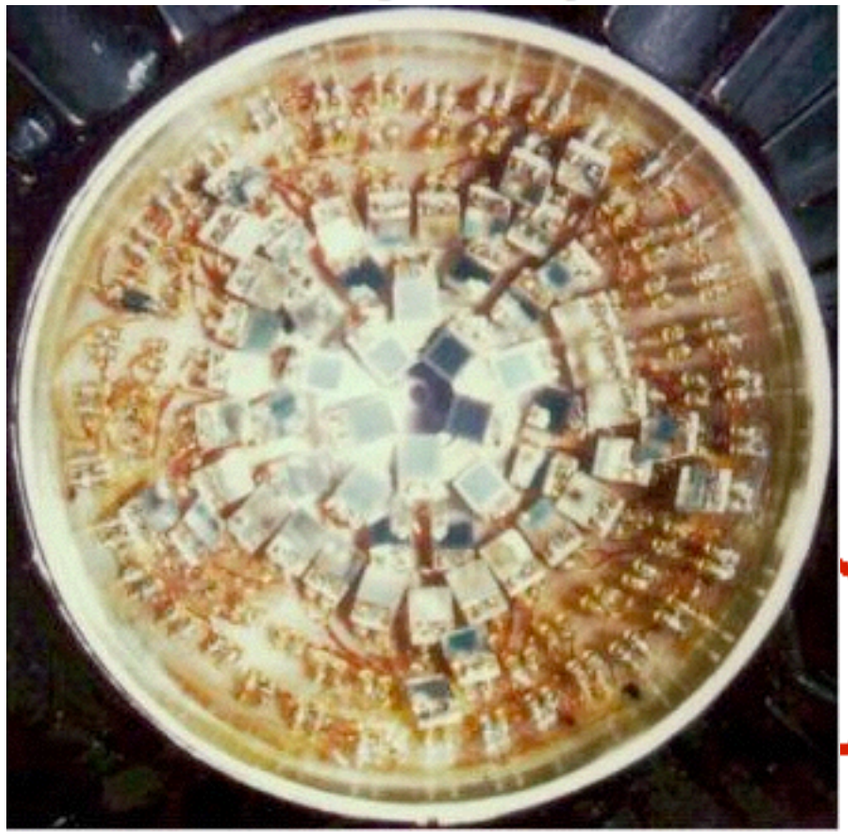

225 MeV

z akceleratora

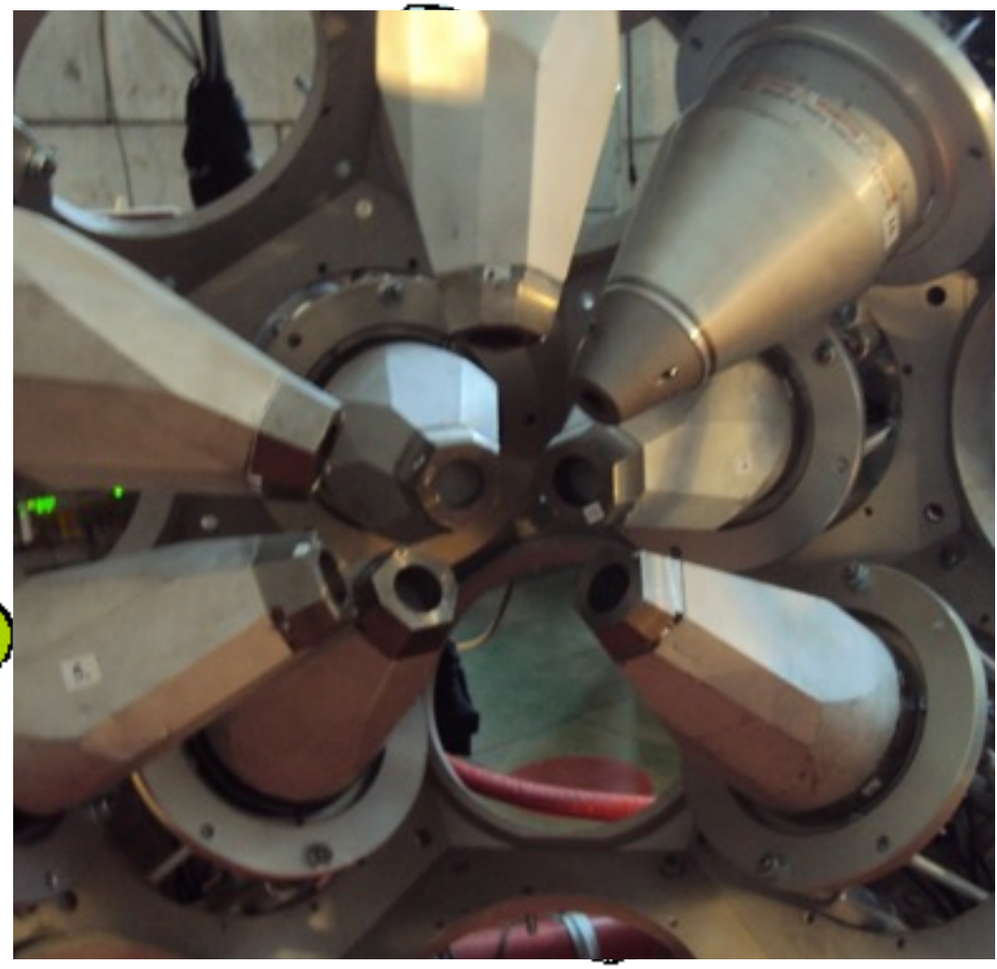

Detektory γ

ROZPRASZANIE ^{58}NI NA ^{178}HF

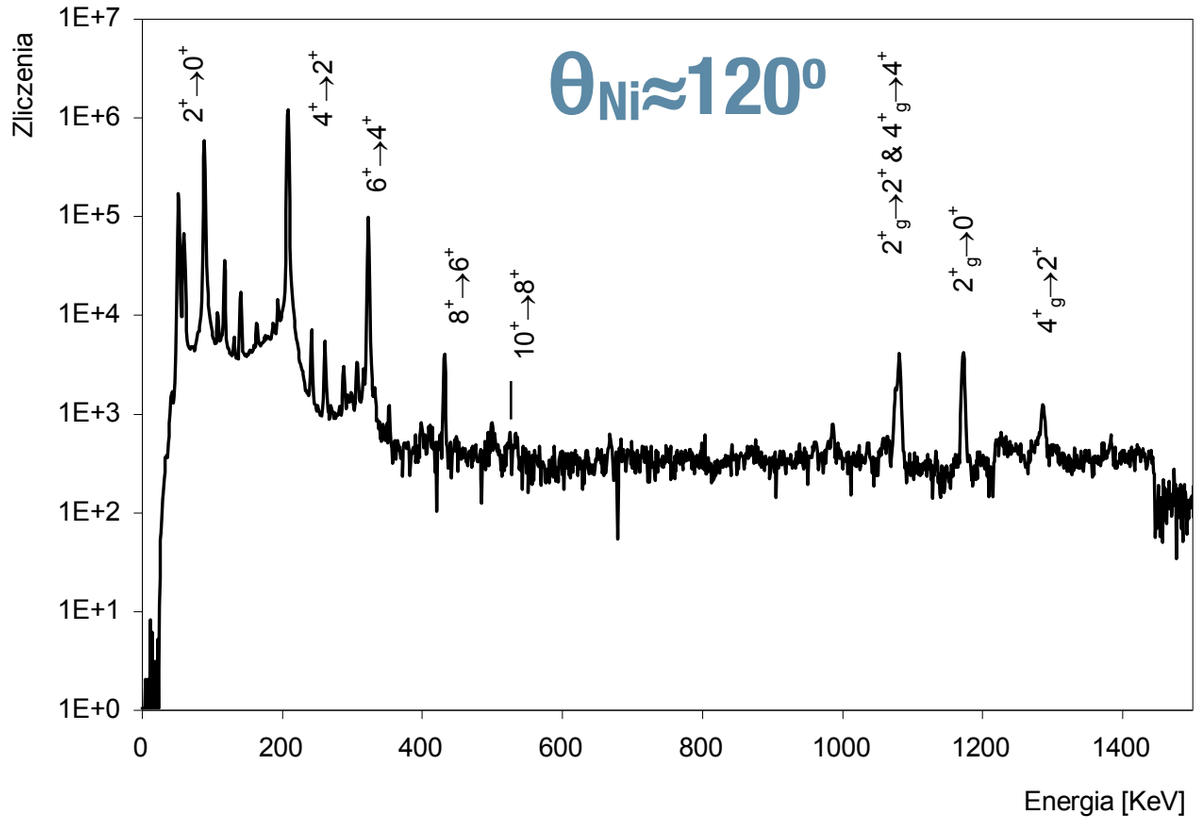

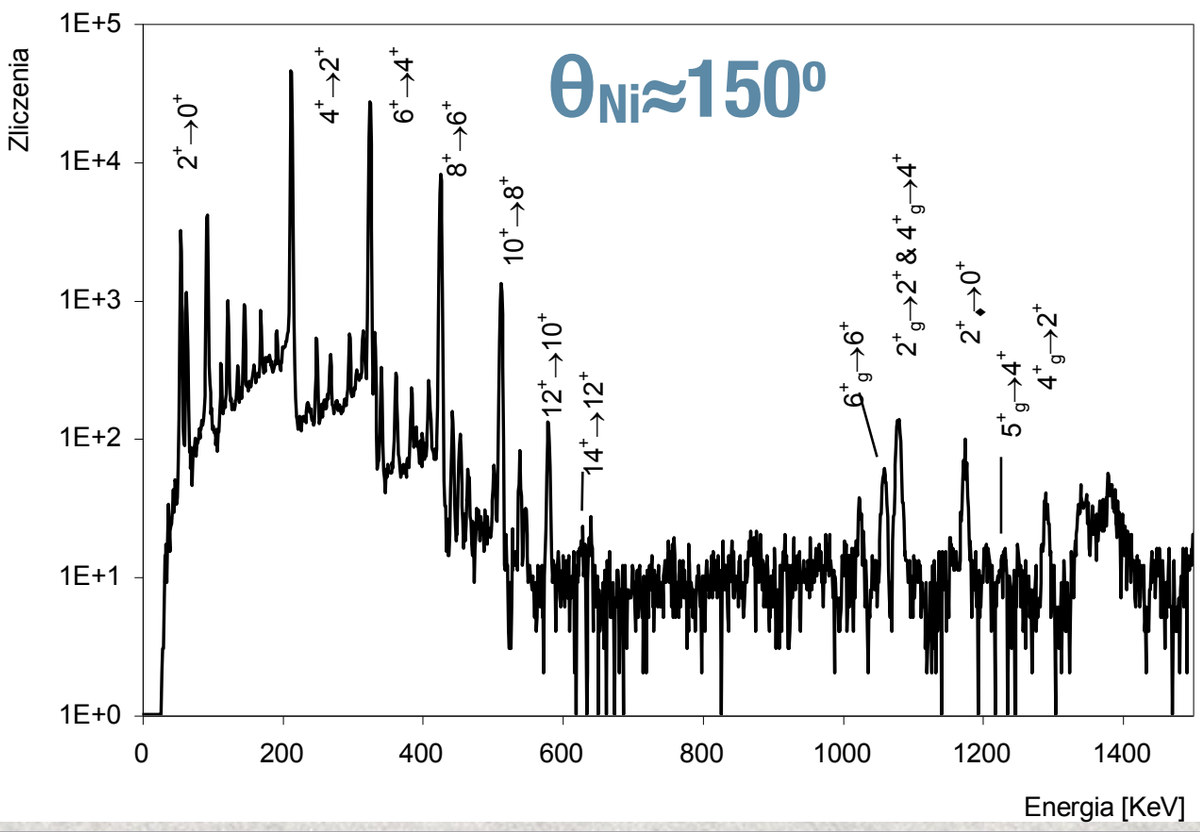

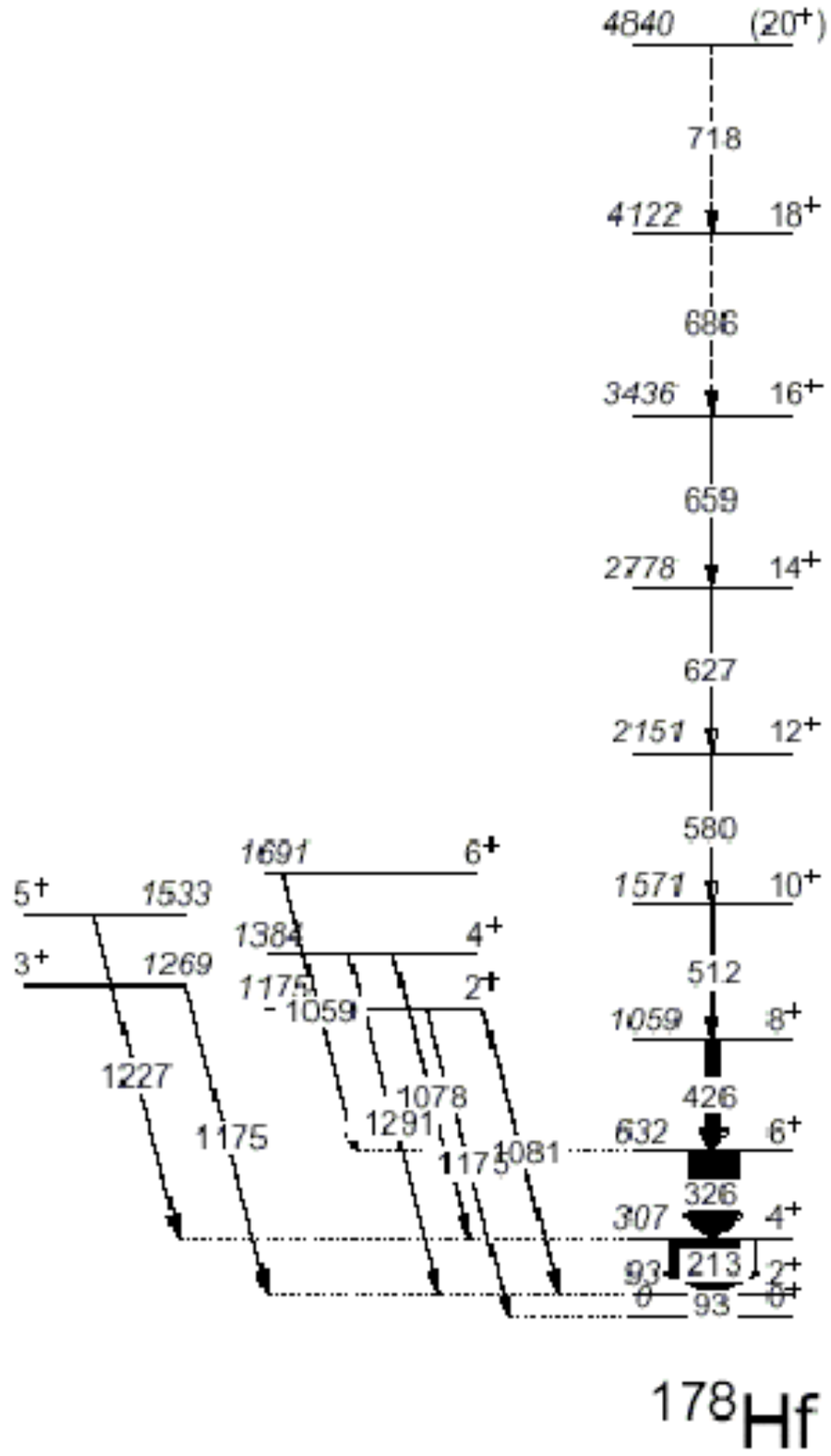

Deformacja

Quadrupole deformation (Left) oblate, $\beta < 0$ (Right) prolate, $\beta > 0$

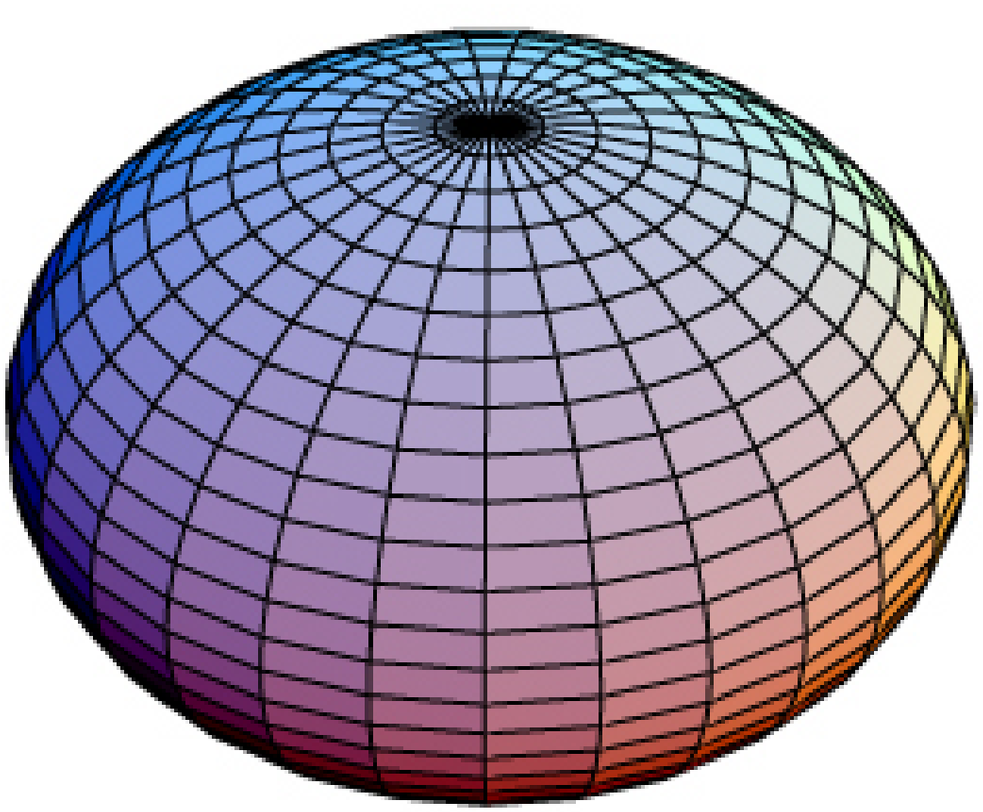

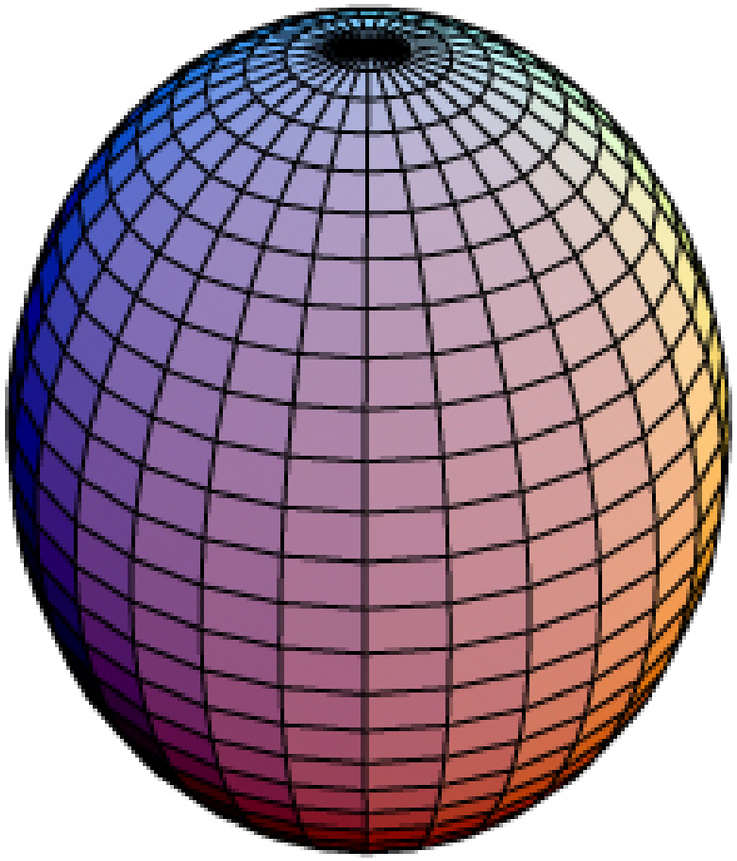

NEWS & VIEWS

FORUM Nuclear physics

Exotic pear-shaped nuclei

The elusive pear shapes of certain nuclei, which are challenging to predict theoretically, have at last been measured precisely. Two experts offer their views on what the results mean for nuclear physics and particle physics. SEE ARTICLE P.199

THE PAPER IN BRIEF

- Atomic nuclei are not only spherical, but can be found in a variety of shapes — for example, squashed or stretched spheres.
- The existence of pear-shaped nuclei has long been predicted, but although some qualitative signatures of this nuclear shape have been found, only sparse quantitative information has been obtained.
- Using accelerated beams of heavy, radioactive ions, Gaffney *et al.*[1] have studied short-lived isotopes of radon and radium that are expected to be pear-shaped, and found a clear pear shape in the radium nucleus.
- The results have ramifications both for the understanding of nuclear structure and for testing the standard model of particle physics.

Novel nuclear antennas

C. J. (KIM) LISTER

At the centre of every atom lies a dense, highly charged nucleus containing 99.999% of the atom's mass. Although this has been known for 100 years — since Ernest Rutherford's discovery of the nucleus — there is still much that we do not understand about nuclei and nuclear matter. Gaffney *et al.* have improved our knowledge of nuclear structure by quantifying one specific and unusual nuclear shape.

In an atom, the static external electric field generated by the tiny central nuclear charge is spherical, so the cloud of electrons that defines its chemical and mechanical properties is always spherical. The nucleus, however, is very different. It generates its own binding field, driven by the strong force that exists between all of its constituent nucleons (neutrons and protons). As such, nuclei have a much less well-defined 'centre'. Nuclei are easily polarized away from spherical shapes (Fig. 1) — in fact, more than one-third of all nuclei are bound most tightly if they settle away from sphericity and into elongated, axially symmetrical 'rugby ball' shapes.

Quantum correlations between the nucleons are expected occasionally to favour more exotic shapes, such as pears, bananas or pyramids, although few of these shapes have been proven to exist in nature. These special nuclei represent specific tests of such correlations, so experimental verification of exotic shapes allows a direct comparison of theoretical models to data. Gaffney and colleagues' study was specifically aimed at testing the octupole correlations that are predicted to lead to asymmetrical pear-shaped nuclei. These particular correlations arise only when a certain combination of quantum states straddles the Fermi surface, the boundary between states that are occupied by particles and those that are empty. Excitation of coherent correlated pairs of nucleons between these states drives the whole nucleus into a pear shape. Of all known nuclei, the isotopes of radon, radium, thorium and uranium are predicted to have the strongest octupole correlations of this type, leading to static pear shapes as the most bound configuration.

Although the existence of pear-shaped nuclei has been predicted for a long time[2], many of those anticipated to be the best candidates do not occur as stable nuclei in nature, so they have to be synthesized in a nuclear reaction before study. Practically, the nuclear charge distribution is a small rotating aerial, or antenna, so it radiates a special pattern of electromagnetic radiation. A pear-shaped antenna should emit enhanced electric-dipole and electric-octupole radiation patterns. In their study, Gaffney *et al.* report a direct measurement of these radiation patterns and their enhancement.

Their experiment is special: instead of using nuclei from the world around us, the authors tailor-made specific isotopes of radon and radium in a preparatory nuclear reaction. These special short-lived isotopes were harvested, prepared for acceleration by tearing off many of their electrons and then accelerated to about 10% of the speed of light as a beam of particles. The beams of heavy radioactive nuclei can then be scattered off thin metal foils to excite the antennas and make them radiate. This is the technique of Coulomb excitation — a purely electromagnetic technique for probing nuclear shapes

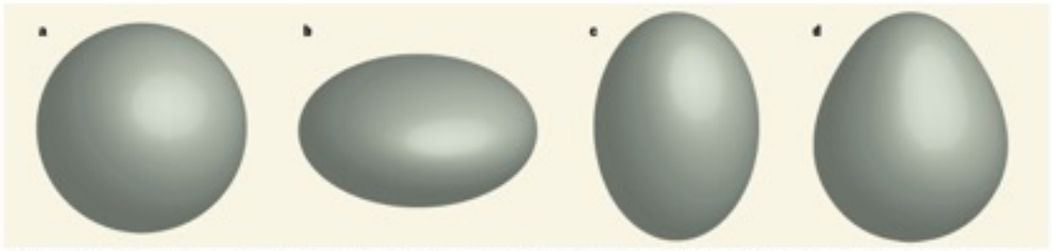

Figure 1 | Nuclear shapes. Nuclei can take several shapes, including a sphere (**a**), an oblate spheroid (**b**) and a prolate spheroid (**c**). Gaffney *et al.*[1] have observed the more exotic pear shape (**d**).

doi:10.1038/nature12073

Studies of pear-shaped nuclei using accelerated radioactive beams

L. P. Gaffney[1], P. A. Butler[1], M. Scheck[1,2], A. B. Hayes[3], F. Wenander[4], M. Albers[5], B. Bastin[6], C. Bauer[2], A. Blazhev[5], S. Bönig[2], N. Bree[7], J. Cederkäll[8], T. Chupp[9], D. Cline[3], T. E. Cocolios[4], T. Davinson[10], H. De Witte[7], J. Diriken[7,11], T. Grahn[12], A. Herzan[12], M. Huyse[7], D. G. Jenkins[13], D. T. Joss[1], N. Kesteloot[7,11], J. Konki[12], M. Kowalczyk[14], Th. Kröll[2], E. Kwan[15], R. Lutter[16], K. Moschner[5], P. Napiorkowski[14], J. Pakarinen[4,12], M. Pfeiffer[5], D. Radeck[5], P. Reiter[5], K. Reynders[7], S. V. Rigby[1], L. M. Robledo[17], M. Rudigier[5], S. Sambi[7], M. Seidlitz[5], B. Siebeck[5], T. Stora[4], P. Thoele[5], P. Van Duppen[7], M. J. Vermeulen[13], M. von Schmid[2], D. Voulot[4], N. Warr[5], K. Wimmer[18], K. Wrzosek-Lipska[7,14], C. Y. Wu[15] & M. Zielinska[14,19]

There is strong circumstantial evidence that certain heavy, unstable atomic nuclei are 'octupole deformed', that is, distorted into a pear shape. This contrasts with the more prevalent rugby-ball shape of nuclei with reflection-symmetric, quadrupole deformations. The elusive octupole deformed nuclei are of importance for nuclear structure theory, and also in searches for physics beyond the standard model; any measurable electric-dipole moment (a signature of the latter) is expected to be amplified in such nuclei. Here we determine electric octupole transition strengths (a direct measure of octupole correlations) for short-lived isotopes of radon and radium. Coulomb excitation experiments were performed using accelerated beams of heavy, radioactive ions. Our data on ^{220}Rn and ^{224}Ra show clear evidence for stronger octupole deformation in the latter. The results enable discrimination between differing theoretical approaches to octupole correlations, and help to constrain suitable candidates for experimental studies of atomic electric-dipole moments that might reveal extensions to the standard model.

The atomic nucleus is a many-body quantum system, and hence its shape is determined by the number of nucleons present in the nucleus and the interactions between them. For example, nuclei in their ground state in which the proton and neutron shells are completely filled ('doubly magic' nuclei) are spherical. If this configuration is excited, or if more nucleons are added, the long-range correlations between valence nucleons distort the shape from spherical symmetry and the nucleus becomes deformed. In most of these cases, it is well established that the shape assumed has quadrupole deformation with axial and reflection symmetry; that is, the nucleus is shaped like a rugby ball (prolate deformation) or as a discus (oblate deformation). For certain combinations of protons and neutrons, there is also the theoretical expectation that the shape of nuclei can assume octupole deformation, corresponding to reflection asymmetry or a 'pear-shape' in the intrinsic frame, either in a dynamic way (octupole vibrations) or having a static shape (permanent octupole deformation).

Octupole deformation and EDMs

Atoms with octupole-deformed nuclei are very important in the search for permanent atomic electric-dipole moments (EDMs). The observation of a non-zero EDM at the level of contemporary experimental sensitivity would indicate time-reversal (T) or equivalently charge–parity (CP) violation due to physics beyond the standard model. In fact, experimental limits on EDMs provide important constraints on many proposed extensions to the standard model[1,2]. For a neutral atom in its ground state, the Schiff moment (the electric-dipole distribution weighted by radius squared[3]) is the lowest-order observable nuclear moment. Octupole-deformed nuclei with odd nucleon number A ($= Z + N$, see below) will have enhanced nuclear Schiff moments owing to the presence of the large octupole collectivity (spatial correlation between particle states) and the occurrence of nearly degenerate parity doublets that naturally arise if the deformation is static[3–5]. Because a CP-violating Schiff moment induces a contribution to the atomic EDM, the sensitivity of the EDM measurement to CP violation over non-octupole-enhanced systems such as ^{199}Hg (ref. 2), currently providing the most stringent limit for atoms, can be improved by a factor of 100–1,000 (ref. 4). Essential in the interpretation of such limits in terms of new physics is a detailed understanding of the structure of these nuclei. Experimental programmes are in place to measure EDMs in atoms of odd-A Rn and Ra isotopes in the octupole region (see for example, ref. 6) but so far there is little direct information on octupole correlations in these nuclei.

Strong octupole correlations leading to pear shapes can arise when nucleons near the Fermi surface occupy states of opposite parity with orbital and total angular momentum differing by 3ħ. This condition is met for proton number $Z \approx 34$, 56 and 88 and neutron number $N \approx 34$, 56, 88 and 134. The largest array of evidence for reflection asymmetry is seen at the values of $Z \approx 88$ and $N \approx 134$, where phenomena such as interleaved positive- and negative-parity rotational bands in even–even nuclei[7], parity doublets in odd-mass nuclei[8], and enhanced electric-dipole (E1) transition moments[9] have been observed. Many theoretical approaches have been developed to describe the observed

[1]Oliver Lodge Laboratory, University of Liverpool, Liverpool L69 7ZE, UK. [2]Institut für Kernphysik, Technische Universität Darmstadt, Darmstadt D-64289, Germany. [3]Department of Physics and Astronomy, University of Rochester, Rochester, New York 14627-0171, USA. [4]ISOLDE, CERN (Organisation Européenne pour la Recherche Nucléaire), Geneva CH-1211, Switzerland. [5]Institut für Kernphysik, Universität zu Köln, Köln D-50937, Germany. [6]GANIL (Grand Accélérateur National d'Ions Lourds), Caen, BP 55027, F-14076, France. [7]Instituut voor Kern- en Stralingfysica, KU Leuven, Leuven B-3001, Belgium. [8]Department of Nuclear Physics, Lund University, Lund, PO Box 118, 221 00, Sweden. [9]Department of Physics, University of Michigan, Ann Arbor, Michigan 48104, USA. [10]School of Physics & Astronomy, University of Edinburgh, Edinburgh EH9 3JZ, UK. [11]SCK•CEN (Studiecentrum voor Kernenergie - Centre d'Etude de l'énergie Nucléaire), Mol B-2400, Belgium. [12]Department of Physics, University of Jyväskylä, Jyväskylä FI-40014, Finland, and Helsinki Institute of Physics, PO Box 64, FI-00014 Helsinki, Finland. [13]Department of Physics, University of York, York YO10 5DD, UK. [14]Heavy Ion Laboratory, University of Warsaw, Warsaw 02-093, Poland. [15]Physics Division, Lawrence Livermore National Laboratory, Livermore, California 94551, USA. [16]Maier-Leibnitz-Laboratorium, Ludwig-Maximilians-Universität and Technische Universität München, Garching D-85748, Germany. [17]Departamento de Física Teorica, Universidad Autónoma de Madrid, Madrid 28049, Spain. [18]Physik Department E12, Technische Universität München, Garching D-85748, Germany. [19]DSM/IRFU/SPhN, CEA Saclay, Gif-sur-Yvette F-91191, France.

Table 2 | The values of the E2 and E3 intrinsic moments, Q_λ

Q_λ	Nucleus						
	^{208}Pb	^{220}Rn	^{224}Ra	^{226}Ra	^{230}Th	^{232}Th	^{236}U
Q_2 (e fm^2)	179 ± 4 (ref. 44)	434 ± 14	632 ± 10	717 ± 3 (ref. 23)	900 ± 6 (ref. 45)	932 ± 5 (ref. 46)	1,047 ± 5 (ref. 45)
Q_3 (e fm^3)	2,100 ± 20 (ref. 44)	2,180 ± 130	2,520 ± 90	2,890 ± 80 (ref. 23)	2140 ± 100 (ref. 47)	1970 ± 100 (ref. 48)	2,060 ± 120 (ref. 47)

Values of Q_λ given here are derived from the matrix elements (see Fig. 3 legend) connecting the lowest-lying states in nuclei near $Z = 88$ and $N = 134$. The values for ^{220}Rn and ^{224}Ra are taken from the present work.

momentum of the state and π is its parity. (For ^{224}Ra the previously measured value of τ_{2^+} cannot be determined independently as the $2^+ \rightarrow 0^+$ transition is contaminated with the Ra X-rays.) In both cases the fitted matrix elements for the $2^+ \rightarrow 0^+$ E2 transition (^{220}Rn) and for the $4^+ \rightarrow 2^+$ E2 transition (^{224}Ra) were found to agree, within the experimental uncertainties, with the values obtained using the lifetime measurements.

The measured E1, E2 and E3 matrix elements for ^{220}Rn and ^{224}Ra are given in Table 1. The values of the intrinsic moments, Q_λ, are given in Fig. 3. These are determined from the experimental values of the reduced matrix element between two states having angular momenta I and I' induced to undergo a transition by the electromagnetic operator $E\lambda$, $\langle I'||E\lambda||I\rangle$, assuming the validity of the rotational model[22]. Here $\lambda = 1,2,3$ refers to E1, E2, E3 respectively. For the E2 and E3 matrix elements, the measured values are all consistent with the geometric predictions expected from a rotating, deformed distribution of electric charge, although these data do not distinguish whether the negative-parity states arise from the projection of a quadrupole-octupole deformed shape or from an octupole oscillation of a quadrupole shape[22]. Table 2 compares the experimental values of Q_λ derived from the matrix elements connecting the lowest states for nuclei near $Z = 88$ and $N = 134$ measured by Coulomb excitation. It is striking that while the E2 moment increases by a factor of 6 between ^{208}Pb and ^{236}U, the E3 moment changes by only 50% in the entire mass region. Nevertheless, the larger Q_3 values for ^{224}Ra and ^{226}Ra indicate an enhancement in octupole collectivity that is consistent with an onset of octupole deformation in this mass region. On the other hand, ^{220}Rn has similar octupole strength to ^{208}Pb, ^{230,232}Th and ^{236}U, consistent with it being an octu pole vibrator. In the case of a vibrator, the coupling of an octupole phonon to the ground state rotational band will give zero values for matrix elements such as $\langle 1^-||E3||4^+\rangle$, because an aligned octupole phonon would couple the 4^+ state to a 7^- state. Although the present experiment does not have sensitivity to this quantity, this effect has been observed for ^{148}Nd in the $Z \approx 56$, $N \approx 88$ octupole region[10], while for ^{226}Ra the intrinsic moment derived from the measured $\langle 1^-||E3||4^+\rangle$ is similar to that derived from the value of $\langle 0^+||E3||3^-\rangle$ (ref. 23). The deduced shapes of ^{220}Rn and ^{224}Ra are presented in Fig. 4. Here the values of quadrupole and octupole deformation β_2 and β_3 were extracted from the dependence of the measured Q_2 and Q_3 on the generalized nuclear shape[24].

The conclusions drawn from the present measurements are also consistent with suggestions from the systematic studies of energy levels[7] (relative alignment of the negative-parity band to the positive-parity band) that the even–even isotopes $^{218-222}$Rn and ^{220}Ra have vibrational behaviour while $^{222-228}$Ra have octupole-deformed character (see figures 12 and 13 in ref. 7). For odd-mass ^{219}Ra there is no evidence[25] for parity doubling, whereas for ^{221}Ra a parity doublet of states with $I = 5/2$ separated by 103.6 keV has been observed[26]. In the Ba–Nd region with $Z \approx 56$ and $N \approx 88$, where the octupole states arise from vibrational coupling to the ground-state band, the evidence for parity doubling of the ground state arising from reflection asymmetry is inconclusive[27,28]. This suggests that the parity doubling condition that leads to enhancement of the Schiff moment[29] is unlikely to be met in ^{219,221}Rn. On the other hand ^{223,225}Ra, having parity doublets separated by ~50 keV (ref. 21), will have large enhancement of their Schiff moments.

The values of Q_λ, deduced from the measured transition matrix elements, are plotted in Fig. 5 as a function of N. The anomalously low value of Q_1 for ^{224}Ra, measured here for the first time, has been noted elsewhere[8,13,30]. The measured Q_1 and Q_2 values are in good agreement with recent theoretical calculations of the generator-coordinate extension of the Gogny Hartree–Fock–Bogoliubov (HFB) self-consistent mean field theory[16], particularly using the D1M parameterization[40]. However, as remarked earlier, the trend of the experimental data is that the values of Q_3 decrease from a peak near ^{226}Ra with decreasing N (or A), which is in marked contrast to the predictions of the cluster model calculations[17]. It is also at variance with the Gogny HFB mean-field predictions of a maximum for ^{224}Ra (ref. 16). It should be noted, however, that relativistic mean field calculations[14] predict that the maximum value of Q_3 occurs for radium isotopes between $A = 226$ and 230, depending on the parameterization, and Skyrme Hartree–Fock calculations[15] predict that ^{226}Ra has the largest octupole deformation. Both predictions are consistent with our data. We cannot completely eliminate the possibility that there are unobserved couplings from the ground state to higher-lying 3^- states that should be added (without energy weighting) to the observed coupling to the

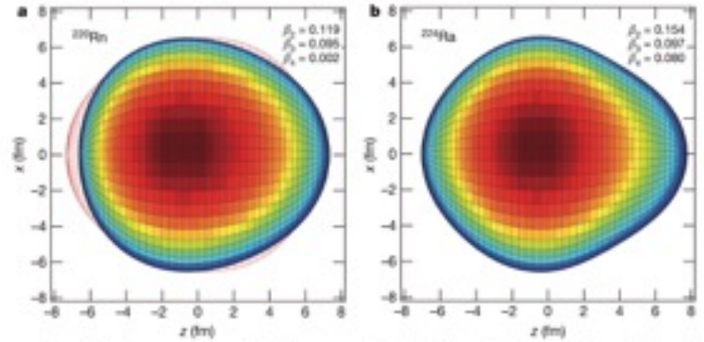

Figure 4 | Graphical representation of the shapes of ^{220}Rn and ^{224}Ra. **a**, ^{220}Rn; **b**, ^{224}Ra. Panel **a** depicts vibrational motion about symmetry between the surface shown and the red outline, whereas **b** depicts static deformation in the intrinsic frame. Theoretical values of β_4 are taken from ref. 10. The colour scale, blue to red, represents the y-values of the surface. The nuclear shape does not change under rotation about the z axis.

Podsumowanie

- Interpretacja energii obserwowanych kwantów gamma pozwala na badanie:
  - reakcji jądrowych
  - struktury jąder atomowych
- Bogactwo obserwowanych zjawisk i procesów zależy od naszej pomysłowości w projektowaniu eksperymentów